AD-A035 343 IOWA INST OF HYDRAULIC RESEARCH IOWA CITY F/G 13/2
MODEL STUDY OF THE INLET AND SUMP OF THE CLINTON FIRST AVENUE P--ETC(U)
NOV 76 C FARELL DACW25-76-C-0017
UNCLASSIFIED IIHR-196 NL

1 OF 2
AD
A035343

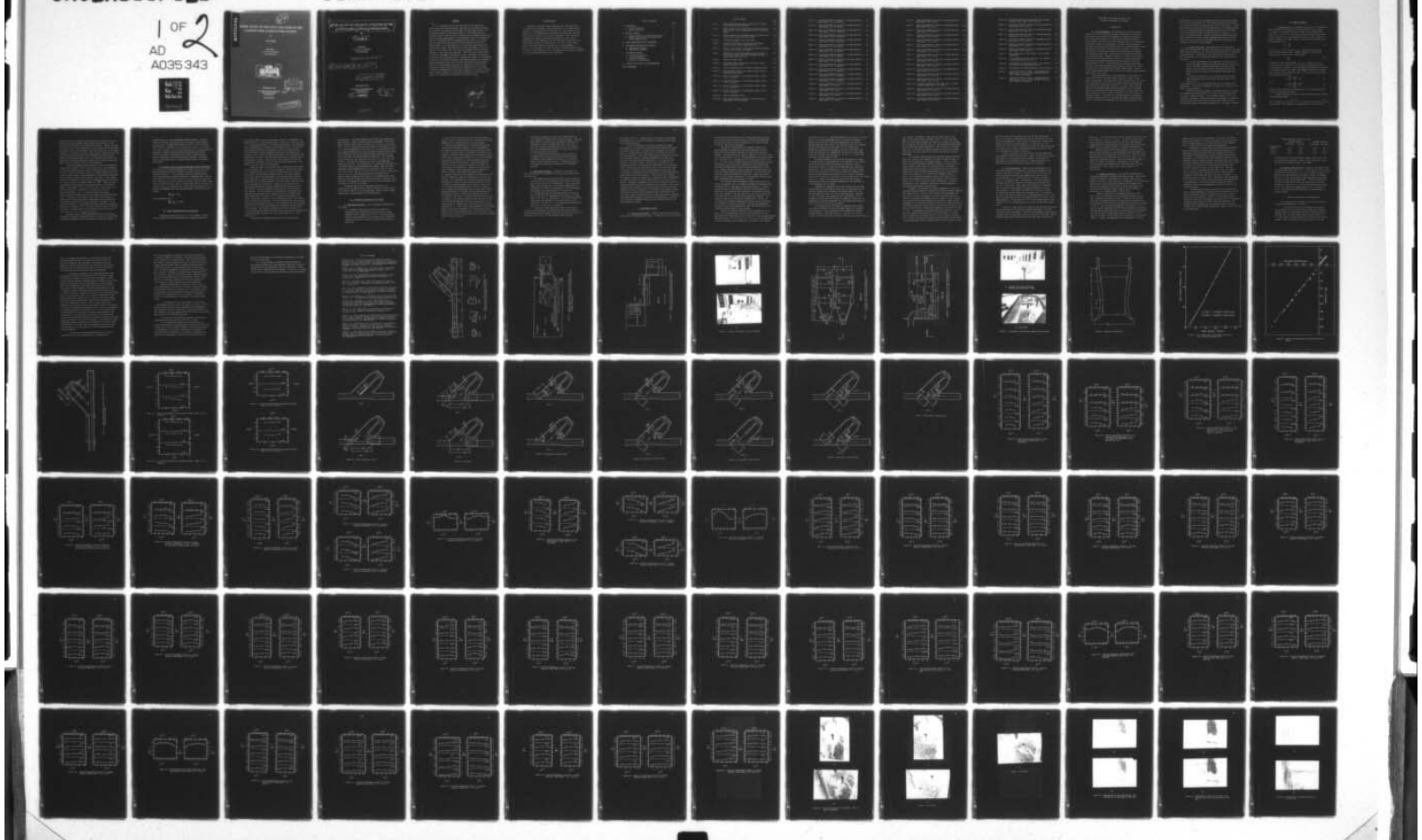

12

MODEL STUDY OF THE INLET AND SUMP OF THE CLINTON FIRST AVENUE PUMP STATION

by

Cesar Farell

Sponsored by
U.S. Army Corps of Engineers
Rock Island District

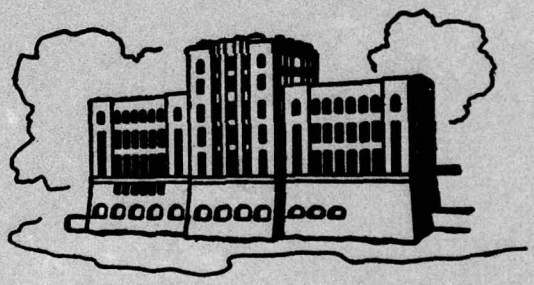

IIHR Report No. 196

Iowa Institute of Hydraulic Research
The University of Iowa
Iowa City, Iowa

November 1976

MODEL STUDY OF THE INLET AND SUMP OF THE CLINTON FIRST AVENUE PUMP STATION

by

Cesar Farell

Sponsored by
U.S. Army Corps of Engineers
Rock Island District

DACW-25-76-C-0017

DACW25-76-C-0017

IIHR-196

IIHR Report No. 196

Iowa Institute of Hydraulic Research
The University of Iowa
Iowa City, Iowa

November 1976

96 p.

ABSTRACT

A 1:7 - scale model of the inlet and sump of the Clinton First Avenue Pump Station was constructed, comprising the new approach channel to the station, the pump bays and forebay, the pump sumps and bells, and the approach conduit to the existing station. It was found that the 45-degree angle at which the flow is diverted from the approach channel into the two new pump sumps produces a large dead-water zone in the forebay and results in pronounced dips in the magnitude of the velocity in the pump bays and sumps, occurring toward the centerwall dividing the bay area. Captive eddies in the pump sumps due to this velocity nonuniformity were not detected, however, and neither were vortices originating at the free surface. On the other hand, thin vortices originating off the converging side walls of the sumps were visualized. The vortices were rather stable in position and somewhat intermittent in time. The pressure fluctuations on the side walls associated with the vortices were found to be considerable, but pressure fluctuations elsewhere on the sumps boundaries were negligible. Baffle arrangements using only few baffles and avoiding narrow passages where trash accumulations could result in obstruction of the flow were developed to improve the uniformity of the approach flows to the sumps. The baffle arrangements did not eliminate completely the side wall vortices, whose strength, frequency of occurrence, and duration of persistence were found to be related to the conditions of the approach flow.

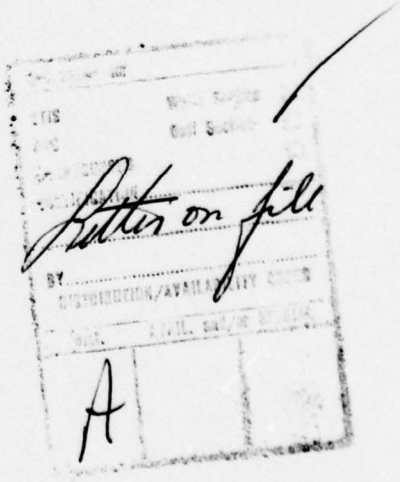

ACKNOWLEDGEMENTS

This model investigation was conducted for and sponsored by the U.S. Army Corps of Engineers, Rock Island District. The author wishes to express his appreciation for help given him in the construction and operation of the model by Messrs. Sam Doak, Don Logsdon, Dick Peterson and Mr. Doyle W. McCully of the Corps of Engineers. Their suggestions influenced the course of the study and improved the final results. Appreciation is also extended to Mr. Dale Harris and his shop staff for constructing the model in a short time; to Dr. John R. Glover and Mr. Arturo Sancholuz for their assistance with the instrumentation; to Messrs. S.-H. Chieh and C.-K. Lo who served as research assistants during the course of the study; and to Dr. J.F. Kennedy for many helpful suggestions and for critically reviewing the final manuscript.

TABLE OF CONTENTS

LIST OF FIGURES

MODEL STUDY OF THE INLET AND SUMP OF THE CLINTON FIRST AVENUE PUMP STATION

I. INTRODUCTION

A. General Background. The performance of a pump is affected markedly by the flow in the suction sump, particularly in the case of high specific speed pumps of the mixed-flow or axial-flow type due to their characteristic features -- high relative velocities, short impeller passages, few vanes, and little guiding action in the suction bell. The presence of swirl or circulation in the sump leads to rotation of the water in the intake pipe and may result in poor pump efficiency, accelerated wear of pump parts, and objectionable vibration. Furthermore, air-entraining vortices with a hollow core through which air is drawn into the pump bell may form. Vortex formation produces increased head loss through the pump, a symptom of which is the surging of the pumping system as vortices form and break, resulting in unstable performance of the pump and unwanted accelerations and decelerations of the flow. The entrainment of air, on the other hand, may adversely affect pump efficiency, with some estimates going as high as a 15% decrease in pump efficiency for a 1% entrained air by volume (Zanker 1968a). Finally, in multi-pump stations uneven distribution of the discharge among different pump units may also result.

Theoretical prediction of sump performance is not possible at present and for design purposes recourse generally is made to scale-model investigations. The experimental study reported herein is one such model investigation and was directed toward identifying and correcting any hydraulically objectionable features of the type briefly described above for the proposed forebay and sump configuration of the two-pump addition to the Clinton First Avenue Pump Station. Figure 1 shows the general plan view of the 1:7 model constructed at the Iowa Institute of Hydraulic Research. The flow to the two-pump addition is diverted at a 45-degree angle from an 8-ft. wide approach channel to the old pump station. The width of the pump bays just before the convergence of the

sump walls is 10.5 ft. For test purposes each of the two proposed pumps was to discharge 46,000 gpm (102.5 cfs) and the discharge from the pumps in the existing station (not modeled) also was to be 46,000 gpm. A ceiling was provided in the model for the upstream portion of the approach channel and for the downstream conduit withdrawing the discharge corresponding to the existing pump station (see channel sections in figure 1). The rest of the approach channel, forebay, and pump bays had operating water levels below their ceilings and were adequately ventilated so that the flows will occur in the free surface mode; therefore ceilings were not provided in the model for these segments.

B. Scope of the Study. The general aim of the study was to identify any objectionable features of the flow in the pump sumps that might affect pump efficiency and wear and to devise practical means of overcoming these deficiencies. Specifically, the following flow characteristics were investigated for the several operating conditions outlined later in the report:

1. Velocity distributions in the pump bays, the goal being to obtain reasonably uniform flows toward the pumps that would avoid, as far as possible, problems associated with swirling at the intake, vortex formation in and air entrainment into the pump bells, surging, and uneven load distribution between the two pumps.
2. Pressure fluctuations on the sump bottom below the pumps; these measurements later were made on the side walls near the bell as well.

Visual observations of the flow patterns were made to supplement these measurements. To this end, transparent side walls were installed in the model, as described later.

Design and testing of possible correctional measures to eliminate any undesirable feature uncovered as a result of the investigation was, of course, a primary objective. As noted later, however, due to the constraints imposed by a tight construction time-schedule, the solutions tried were only those which could be achieved with minimal changes in bay and sump geometry, preferably the addition of a few number of baffles.

II. MODELING CRITERIA

A. General Remarks on Similitude Requirements. The question of pump sump modeling principles has been dealt with by several authors (e.g. Paterson and Campbell 1968, Zanker 1968b, Denny and Young 1957, Denny 1956). A review of the relevant technical literature soon reveals, however, a number of unresolved problems of which one must be aware for proper interpretation of model results. Restricting our attention to undistorted models, let

$$L_r = \frac{L_m}{L_p} \tag{1}$$

where L_r is the length scale ratio, L_p is prototype length, and L_m the corresponding model length. Dynamic similarity of inertia and gravity forces requires that the Froude number,

$$F = \frac{V}{\sqrt{gL}} \tag{2}$$

be the same in model and prototype. In (2), V represents velocity, L length (vertical or horizontal if the model is undistorted), and g is the acceleration of gravity. Since most pump intake designs are such that a free surface exists at the sump, Froude number similarity is required for similarity of free surface behavior. The resulting velocity and discharge scaling relations are

$$V_r = \frac{V_m}{V_p} = \left(\frac{L_m}{L_p}\right)^{1/2} = L_r^{1/2} \tag{3}$$

and

$$Q_r = \frac{Q_m}{Q_p} = \frac{L_m^2 V_m}{L_p^2 V_p} = L_r^{5/2} \tag{4}$$

where Q denotes discharge and the subscripts m and p refer, respectively, to model and prototype quantities.

Dynamic similarity of viscous and inertia forces requires strictly that the Reynolds number

$$Re = VL/\nu \tag{5}$$

which represents the ratio of inertia to viscous forces, be equal for model and prototype. This condition is incompatible with (3) above, and if

Froude similarity is required, scale effects from viscous forces can be minimized by making the model Reynolds number large enough to insure fully developed turbulent flow conditions in the model. However, this may not ensure a fully accurate prediction of vortex formation and development, particularly if the vortex extends to the free surface and air entrainment through the vortex core takes place. While Reynolds number effects on free surface vortex formation and air core development have been recently examined by Daggett and Keulegan (1973), the information available is not sufficient to elucidate the problem, except that as expected no Reynolds number effects are present above a certain minimum Re.

The air entrainment characteristics of a flow are influenced by surface tension forces. This is true in particular of air entrainment by vortices, although the exact nature of the dependence is not precisely known. Daggett and Keulegan (1974), for example, found that for the range of values tested in their experiments on free-surface vortex formation no effect of surface tension seemed to be present. Other authors assume as a similarity criterion for air-entraining vortices the equality of the ratio, We/Re, of the Weber number, $We = \frac{\rho V^2 L}{\sigma}$ (where ρ is the mass density of the fluid and σ its surface tension), to the Reynolds number (Zanker 1968b, Collinson 1968, Kenn 1968). Since $We/Re = \mu V/\sigma$ a full-scale velocity law results if the same fluid is used in model and prototype. Such a scaling criterion has received partial support from other authors as well (Denny 1956, Denny and Young 1957). It should be noted, however, that a full scale velocity law would result in rather large model Froude numbers and consequently in considerable distortion of the flow conditions in the model. In the present investigation, in particular, the Froude number of the approach flow was of the order of 0.40. With model velocities equal to prototype velocities, the Froude number of the approach flow would have been of the order of 1.0 for a 1:7 length scale ratio.

Actually, the air entraining mechanism entails the development of surface disturbances (including vortices) for which the characteristic dimensionless parameters should be the Froude and Reynolds numbers. As

discussed above, for large enough model Reynolds numbers, one should expect scale effects from viscous forces to be small, except possibly in vortex cores. Although Froude number similarity results in surface tension forces in the model that are larger than those in the prototype by the factor $(Lp/Lm)^2$, due to the large magnitude of the Weber numbers encountered in prototype flows and unless very shallow flow sections result in the model, no significant scale effects (except possibly locally) from surface tension forces should be expected. This would seem to be especially true if no surface tension effects are observed in the model.

B. Modelling Criteria for the Clinton First Avenue Pump Station.

On the basis of the preceding discussion, the model of the Clinton First Avenue Pump Station was built following the Froude criterion to an undistorted scale of 1:7. This criterion, though not absolutely exact, is the best available for dynamic similarity of pump-sump flows. The geometric scale was chosen, after taking into account budget and laboratory space limitations, as large as possible to minimize possible Reynolds number effects on vortex formation. Usage of a Froude number scaling procedure, it should be noted, is in agreement with several available publications (e.g., Patterson and Campbell 1968; see also Wilson 1968). The velocity scale is then

$$\frac{Vm}{Vp} = \frac{1}{\sqrt{7}} = 0.378$$

and the discharge scale

$$\frac{Qm}{Qp} = \frac{1}{7^{5/2}} = 0.00771$$

III. MODEL CHARACTERISTICS AND CONSTRUCTION

An undistorted geometric scale $L_r = 1/7$ was adopted. Figure 1 shows the general plan view and sections of the approach channel and

the channel leading to the existing pumping station. All dimensions are model dimensions. A ceiling was provided in the model, as shown in figure 1, for the upstream portion of the approach channel and for the downstream conduit withdrawing the discharge to the existing station. For the rest of the approach channel and the pump bays, which had operating water levels below their celings, adequate ventilation was available in the prototype, and no ceiling was therefore provided. This facilitated visual observation of the flow. The long upstream reach of the approach channel was necessary in order to ensure correct inflow conditions to the forebay, pump bays, and sumps. Figure 2 shows the general disposition of the model on the first floor of the laboratory.

Water was supplied to the model from a constant-head tank through a 10-in. diameter pipe. A 9.6-ft-long rectangular closed conduit fitted with a coarse grid was used to effect the transition from the circular 10 in. pipe to the rectangular approach channel. The cross sectional area of this conduit was chosen equal to the prototype cross sectional area (scaled down to model dimensions) of the existing arch conduit upstream from the new approach channel. This arch conduit flows full when the two new pumps are in operation. Because of the relatively great length of approach channel available downstream from the outlet of the arch conduit, it was not necessary to model exactly the arch conduit's cross section. The flows from the two new pumps were siphoned from the pump sumps through geometrically scaled bells and 6-in. diameter pipes shown schematically in figures 2 and 3. These pipes discharged into a culvert fitted with a tailgate so that the downstream head on the siphons could be adjusted and controlled. The flow representing the existing pumping station was withdrawn by means of a 6-in. pipe directly from the bottom of the 10 ft by 6 ft (prototype dimensions) rectangular approach conduit to this station. This conduit was modeled over its entire length (31.5 ft in the prototype) and flows full when the new pumps operate simultaneously. A tailgate was also provided in the return flow culvert for the third outflow pipe.

The model was constructed from wood, and the inside painted

for protection. Joints were sealed using a silicon seal manufactured by Dow Chemical. Figure 4 shows two general photographic views of the model. Figures 5 and 6 show a horizontal and a vertical, respectively, cross section through the pump bays and forebay. Two rectangular 13 in. by 13 in. and two rectangular 13.5 in. by 6 in. lucite observation windows were installed, respectively, on the two outside converging vertical walls of the sumps and on the two end walls, to permit visualization of the flow in the sumps and into and around the pump bells. Two trapezoidal lucite windows were also installed on the floor of the sump just below the bells. The side well windows can be seen in the photographs in figures 4(b) and 7(a). The illumination of the right sump in figure 7(b) is provided through the corresponding floor window. Trash racks were installed as shown schematically by the dash line in figure 6. Each of these consisted of a grid of vertical bars, 3/8 in. deep and slightly less than 1/16 in. wide. The spacing between bars was about 5/32 in. Finally, figure 8 shows the cross section of the geometrically-scaled siphon bells and the transition from the bell profile to the 6-in. outflow pipe. The maximum bell diameter was 55 in. in the prototype, which corresponds to 7.86 in. in the model.

Noteworthy features of the sump design tested are the convergence of the sump side walls and the closeness of the bell rim to the side walls (about 1 in. in the prototype). There is also a slight upward slope in the sump floor in the flow direction.

IV. EXPERIMENTAL EQUIPMENT AND PROCEDURES

A. Experimental Equipment. The instrumentation employed was as follows:

1. Discharges through the intake pipe and siphons were measured by means of calibrated orifice meters and U-tube manometers with a resolution of 0.001 ft. The orifice meters were built and calibrated at the Institute using a calibration weighing tank (one of the scales can be seen, incidentally, in figure 4a).

2. Water surface elevations were measured with either point gages or simply a ruler affixed to the inside wall of the model, depending on the required accuracy of the measurement.

3. Velocities were measured with a miniature propeller-type current meter (propeller diameter 0.375 in.) manufactured by a British firm, Novar Electronics; the probe used is their type 403. The probe output is the number of revolutions in a fixed time interval and was measured and displayed by a digital counter with counting time intervals of 1, 10, and 100 seconds. The propeller was mounted on a vernier equipped point gage support to determine its position. The velocity measuring system can be seen in figure 7b, above the left sump. The current meter was calibrated in a towing tank; the velocity-output frequency relation obtained from the calibration is shown in figure 9, after Nakato and Kennedy (1976).

4. Pressure fluctuations were measured with Endevco model 8510 pressure transducers, rated for operation over a range of $\pm$15 psi gage. This transducer uses a miniature silicone pressure sensing chip on which a full piezoresistive Wheatstone bridge is bonded; the outside diameter of the casing is about 0.155 in. A strain gage balancing circuit, a Dana D.C. amplifier, and a Beckman type RS Dynograph recorder completed the instrumentation necessary for recording the pressure fluctuations. The pressure (recorder) output was calibrated statically in a cylindrical steel tank. A typical calibration curve is shown in figure 10. The conversion factors to be used with the last set of recordings made are 1.268 in. H_2O per milimeter of recording paper for transducer No. 0 and 1.185 in. H_2O per mm for transducer No. 1. These factors varied somewhat over the several months of the study; accordingly the calibration was checked before each set of recordings was made. The conversion factors given here can be used in conjunction with the pressure recordings shown in figures 41 and 42.

The pressure transducers initially were installed on the floor transparent windows under the pump bells axes. They were later moved to a position on the transparent windows on the convergent side walls, somewhat under and to the side of each bell; the exact positions were 3-7/8 in. from the end wall of the sump measured along the side wall and 3-1/8 in. from the sump floor at this point.

5. Flow visualization was achieved by means of food dye introduced into the flow at the desired locations through a hypodermic needle mounted on the end of a long tube and supplied from an elevated reservoir. Confetti sprinkled on the surface were also used occasionally for visualization purposes.

B. Experimental Procedure. According to the intial test plan, the model was to be operated for the following prototype pumping conditions:

1. Both pumps operating with sump water levels at elevations 580.0 ft and 576.5 ft, equivalent to flow depths at the pump bays of 10.5 ft and 7.0 ft, respectively. (The corresponding depths above the sump floor at the pump centerline were 0.3 ft lower, 10.2 ft and 6.7 ft respectively). The corresponding model depths were, respectively, 18 in. and 12 in.

2. One pump operating with sump water levels at elevations 578.5 ft and 574.5 ft, equivalent to flow depths at the pump bays of 9 ft and 5 ft, respectively. (The corresponding water depths above the sump floor at the pump centerline were respectively 8.7 ft and 4.7 ft.) The corresponding model depths were 15.4 in. and 8.5 in., respectively.

3. Conditions 2. duplicated except using the other pump.

For all tests each pump was to discharge when operating 46,000 gpm and the discharge from the pumps in the existing station also was to be 46,000 gpm at all times. The corresponding model discharge

per pump was 0.791 cfs. Maximum inflow to the model with both pumps operating was then 2.372 cfs (including the discharge from the pumps in the existing station).

Start-up and operation of the model proceeded as follows. The tailgate in the return flow culvert was lowered about half way and the siphon valves closed, the intake valve was opened, and the water level in the model then rose slowly until it was above the level of the siphon pipelines. The siphon valves then were opened and the inflow into the model increased to maintain approximately the same level so that all pipelines would be purged of air. The inflow was then adjusted to the desired value. By adjusting the settings of the corresponding valves, the outflows were then brought to their desired values, attempting at the same time to attain the correct water level in the model. Relatively small final adjustments in the water level in the model were possible without changing the outflows by adjusting the water levels in the return culverts, a useful feature for attaining the required steady state conditions in a minimum of time. Approximately one hour was required to achieve steady flow for a given set of conditions. Thereupon, measurements were made of the desired velocity distributions and/or the pressure fluctuations were recorded. Since considerable time was necessary to carry out the velocity distribution measurements and since, furthermore, the recording of the pressure fluctuations had to be coupled with simultaneous visual observation of the flow in both sumps, as discussed later, velocity and pressure fluctuation measurements were generally carried out at different times. Any drift of the electronic equipment associated with temperature changes also was minimized in this way.

V. EXPERIMENTAL RESULTS

A. Velocity Distributions. Figure 11 shows the cross sections where velocity measurements were taken. In addition, a few velocity distri-

butions around the siphon bells also were measured along a circular arc on a plane 1.92 in. below the plane of the bell rim (about half way between the bell rim and the sump bottom) at a radial distance of 8.85 in. from the bell centerline.

The velocity distributions over sections D and E in the approach channel were measured to define the approach flow and to verify that correct inflow conditions into the forebay area were obtained. The distributions are shown in figures 12.1, 12.2, 13.1 and 13.2 for model depths of 12 in. (two-pump operation, total model inflow 2.372 cfs) and 8.5 in. (one-pump operation, total model inflow 1.582 cfs). In these and the following figures showing the measured velocity distributions, x_m and x_p denote, respectively, model and prototype horizontal distances across the bay sections measured from the left walls (looking downstream), V_m and V_p model and prototype velocities, and y the (model) depth below the free surface. For the velocity distributions aroung the syphon bells (along the circular arcs defined above) s_m and s_p denote, respectively, circumferential distances along each arc measured from the mid-point of the arc.

The different baffle arrangements tested with the aim of improving the approach flow to the pumps and minimizing undesirable flow disturbances in the pump sumps are sketched in figure 14. They are presented roughly in chronological order and are discussed below in that order. The dimensions and, especially, the positioning of each baffle were decided in each case after a few trial runs in which only a few key points of the velocity distributions were measured. The results of these trial runs are not included herein. The aim at all times was to minimize constructional changes, using in particular as few baffles as possible, and later to try baffling arrangements that would avoid narrow passages where major flow blockage and trash accumulation could develop in the prototype.

Figures 15 through 18 show the velocity distributions in the model of the original design, without any training walls, for two-pump operation at model depths of 18 in. and 12 in., and one-pump operation with model depths of 15.4 in. and 8.5 in. Note that the openings underneath the two beams across the pump bays (see figure 6) have heights

of 10-9/32 in. and 12 in., and that therefore for the larger flow depths some of the velocity measurements fall in the wake of the beams. Measuring cross sections A and B are downstream of the 10-9/32-in. opening; measuring cross section C is downstream of the 12-in. opening. The mean flow velocities for sections A, B, and C (obtained by dividing the discharge for each pump, 0.791 cfs, by the wetted area of the cross section) are, respectively, for the 12 in. model depth, 0.655 fps, 0.527 fps, and 0.504 fps; and for the 8.5 in. model depth, 0.925 fps, 0.744 fps, and 0.710 fps.

Noteworthy features of the velocity distributions in figures 15 through 18 are the pronounced dips in the magnitude of the velocity occurring toward the center wall dividing the bay area. This is particularly evident in the case of one-pump operations, figures 18.1 through 18.4. The large differences in velocity depicted in figures 18.2 for section B and 18.3 for section C seem to be somewhat attenuated by the converging walls, as figure 18.1 for section A indicates. (Note, however, that only 3 points per level were measured for the narrower section A.) Figure 18.4, which shows the velocity distributions around the bell, does not show much improvement in the uniformity of the distributions near the pumps.

Comparison of figures 15 and 16 with figures 17 and 18 shows clearly that the critical depths in the sense of exhibiting less uniform distributions are (as expected) the smaller ones, 18 in. for two pump operations and 8.5 in. for one-pump operations. Therefore, in view of the tight time schedule of this investigation, it was decided to restrict attention to these two depths in relation to the development of a baffle arrangement that would improve the characteristics of the flow into the two new sumps.

As indicated earlier, the baffle arrangements tested used as few baffles as possible in order to minimize changes in the geometry of the forebay. A first modification was to extend the centerwall as shown for case 1 (see figure 14) but without the 2 in. opening. A strong lateral surging motion developed, which was not present with the

2 in. opening. Incidentally, there was only minor surging in the sumps for the model without any baffles: about 0.2 in. in each pump bay with the two pumps operating, and about 0.4 in. when only one pump was in operation; in the latter case, the surging seemed slightly higher for the right pump (looking downstream). The effect of the centerwall (with the 2 in. opening to eliminate surging) is to shift the minimum velocities in the left sump from the right to the left wall (looking downstream).

For the model without baffles the nonuniform velocity distributions are a result of the inability of the flow to make the sharp, 45 degree turn as required by the boundary geometry. (This is clearly seen in the flow visualization pictures in figure 37, and will be discussed somewhat further later on.) Preliminary tests to determine whether better flow uniformity could be achieved by forcing the flow toward the low velocity regions were carried out for the two-pump operation and a depth of 12 in. with baffle arrangements numbers 2, 3, and 4. In all cases the orientation, length, and position of the baffles were adjusted to achieve the best possible results (shown in figures 20, 21, and 22) with each baffle configuration. The baffle arrangement of case 3 produced a particularly marked improvement in the velocity distributions (see figure 21).

Because of the possibility of trash accumulations in the somewhat narrow passages between the baffles and the walls producing objectionable obstructions to the flow, other training wall arrangements then were tried. In case 5 one baffle, 4 in. high, was placed along the bottom of the channel and forebay as shown in figure 14, with the other two (vertical) baffles placed against the side walls. Again, a marked improvement in the velocity distribution resulted (see figures 23 and 24). The baffle arrangement of case 6 also was tried (figures 25 and 26), but did not produce velocity distributions comparable in uniformity to those of case 3. Arrangements with a baffle along the bottom as in case 5 then were examined in more detail by varying the length, the height, and the position of this baffle (cases 7, 8 and 9, figures 27 through 30). Finally, it was concluded that the vertical baffle in the left bay (looking downstream) could be dispensed with by using two baffles along

the bottom, one along the centerline of the left bay (looking downstream), the other one longitudinal but off the centerline of the right bay (looking downstream). Cases 12 and 13 represent the configurations judged to be optimal for bottom baffles 3 in. high and 4 in. high, respectively. The velocity distributions for these two cases at sections A, B, and C, and the velocity distributions around the bells for case 12, are presented in figures 33 through 36.

Vertical baffles off the right side wall (looking downstream) of the approach channel also were tried. Again, as with the full center-wall solution, a strong surging motion resulted, and therefore no measurements were performed in this case. Three bottom baffles also were tried, but the third baffle was found to be ineffective.

B. Flow Visualization. Figure 37 shows photographs of flow visualization tests in the forebay for the baffle arrangement of case 12, using food dye as a marker. For photos a) and c) the tip of the needle injecting the dye was held somewhat higher than the top of the bottom baffles (3 in. high in this case), whereas for photos b) and d) it was somewhat lower. The inability of the flow to make the 45 degree angle turn to conform to the boundary without separating from it is clearly seen. This leads to the formation of a dead water zone to the left of the forebay, as shown in particular by the dye area in photo e). The action of the baffles is seen to be to divert the bottom flow into the sumps and to dissipate some of the energy of the flow in the approach channel (for the two-pump operation and a 12-in. depth, the model mean velocity in the approach channel is about 2.1 fps, corresponding to a Froude number of 0.37; for the one-pump operation and a depth of 8.5 in., the mean velocity is 1.95 fps and the Froude number 0.41).

Figure 37 e) shows clearly the reason for the increased velocities over the left wall of the left sump (looking downstream) in the model without any baffle arrangements. The flow in the approach channel actually overshoots the left sump. Most of the left sump flow (in the model without baffles) comes from the forebay area of the right sump (always looking

downstream). This flow cannot turn sharply around the center wall (see the dye pattern in figure 37 e) and as a consequence the velocities in the left sump are larger toward the left wall. Flow from the forebay area of the right sump into the left sump still occurs at low depths for the conditions of figure 37 e (baffle arrangement 13).

Figures 38 and 39 show visualizations of the flow into the bells, with dye injection in the centerplane of the sump (figure 38) and very near the converging side wall (figure 39). The latter figure shows that close to the wall the flow "rolls up" and tends to form a region of concentrated vorticity. Figure 40 depicts more clearly the core of the vortex thus formed; visualization in this figure is by the dissolved air released into the vortex core due to the low pressures there. This vortex is more fully discussed in the next section.

C. Pressure Fluctuations. The pressure transducers were originally installed on the sump bottom under the bell. Only minimal pressure fluctuations, associated with the rather small surging present in the sump, could be detected. Furthermore, flow visualization tests did not disclose any vortex formation off the sump floor as described for example by Quick (1970) or Nakato and Kennedy (1976). No air-entraining vortices formed either at the free surface as described, e.g., by Zanker (1968) or Denny (1956).

However, further flow visualizations uncovered a fairly thin vortex core originating at the converging side walls near the bell, as depicted in figures 39 and 40. Figure 40, which clearly shows this vortex made visible by the dissolved air released by the low pressures in the vortex core, was taken with the baffle arrangement of case 12. With this baffle arrangement the occurrence of the air core was rather intermittent and the core was difficult to photograph. With the model without baffles the air core was much less intermittent and could be seen to be remarkably stable in position. The frequency of occurrence of the vortex and the duration of its persistence after it formed was diminished by the improvement in the pump

approach flow by the baffle arrangements. But while of a fleeting nature with the baffles in place, the strength of the vortex did not seem to decrease markedly in the sense that the air core seemed to form, at times, and to have the same general appearance.

Confirmation for these visual observations was obtained with pressure recordings by installing the pressure transducers at the approximate location where the air core originated from the wall. The pressure recordings shown in figures 41 and 42 were obtained in this manner. It should be noted that although the vortex core was remarkably stable in position whenever the vortex formed, its position fluctuated somewhat and the transducer, which was rather small, could not register all instances of vortex formation (see figure 40), especially because the vortex core was rather thin. (The core seen in figure 40 is actually the band swept by the air filament during the exposure time, which had to be kept relatively long to produce a photo that would clearly show the air filament.) It should also be noted, however, that simultaneous visual observation of the vortex air core and of the pressure recordings disclosed that significant parts of the record intervals showing only small or negligible fluctuations corresponded with instances in which no air core was observed.

The differences between the records for the left and right pumps (looking downstream) in figures 41 and 42 could be due in part to the positioning of the two transducers relative to the small regions of vortex formation. Because of the important effect of the relative positions of transducers and vortex cores on the pressure records, no major analysis of these records was undertaken. The minimum negative pressures that were obtained, during a 3-minute interval, for the model without baffles and in cases 12 and 13 are given in the table below:

Minimum Pressures recorded (in. H_2O)

	Two-pump operation		One-pump operation	
	Right pump	left pump	Right pump	left pump
Model without baffles	-30.5	-27.5	-33.5	-31.3
Case 12	-29.4	-21.8	-25.3	-27.5
Case 13	-27.3	-21.8	-10.2	-26.5

Conversion factors for the records of figures 41 and 42 are 1.268 in. H_2O per mm for transducer number 0 (right pump) and 1.185 in. H_2O per mm for transducer number 1 (left pump).

D. Surging in the Pump Sumps. Surging for the model without any baffling was small, about 0.2 in. in each sump with the two pumps operating and a flow depth of 12 in. in the forebay, and about 0.4 in. when only one pump operated and the depth of flow in the forebay was 8.5 in. In the latter case, the surging seemed slightly higher for the right pump (looking downstream). The baffle arrangements of cases 13 and 14 did not change the surging for the two-pump operation at a depth of 12 in. For the one-pump operations (depth 8.5 in.) the surging was somewhat smaller, 0.3 in., instead of 0.4 in. All these values are fairly small and were measured to within 5 percent.

VI. SUMMARY, CONCLUSIONS, AND RECOMMENDATIONS

The conclusions of this study, including a brief summary of supporting arguments, are as follows:

1. The layout of the bays and forebay of the proposed two new pumps for the Clinton First Avenue Pump Station produced approach flows to the pump sumps with rather nonuniform velocity distributions. The nonuniformity arises from the inability of the flow to make the sharp 45 degree turn required by the boundary geometry. Only a small amount of surging occurred in the pump

bays for the proposed configuration. Very minimal pressure fluctuations could be detected on the sump floor under the bell and no vortices formed off the sump floor. Air-entraining vortices forming at the free surface did not occur either, but thin vortices originating off each converging side wall were clearly detected by flow visualizations and pressure fluctuation measurements.

2. A definite improvement in the pump-approach flows could be obtained by suitable baffle configurations. The baffle arrangements referred to herein as cases 12 and 13 would seem best suited to the constraints imposed of minimum changes in forebay, bay, and sump geometry and avoidance of baffle arrangements with narrow passages where trash accumulations and accompanying obstruction of the flow could develop in the prototype. The velocity distributions for case 13 (figures 35 and 36) seem just slightly better than those for case 12 (figures 33 and 34). Comparison of figure 18.1 (for the model without baffles) with figures 34.1 and 36.1, all three corresponding to one-pump operations and a depth of 8.5 in., gives an idea of the improvement in the velocity distributions resulting from introduction of the two baffle arrangements 12 and 13. This can also be seen from a comparison of the velocity distributions around the bell, in particular of figures 18.4 (model without baffles) and 34.4 (case 12) corresponding to one-pump operations and a depth of 8.5 in. It is noted here that the measurements of the velocity distribution around the bell as described earlier in the report are very sensitive to orientation and position of the probe with respect to the oncoming flow, due to the large velocity gradients in this area of measurement. This problem is further complicated because the direction of the approach flow for each point of measurement is not known, and the measurements are therefore somewhat unreliable. For this reason only a few distributions of this type were measured.

3. The pressure fluctuation measurements and the flow visualizations of the vortices forming off the converging side

walls near the pump bells show that these vortices are affected in strength, frequency of occurrence, and duration of persistence by the conditions of the approach flow. The vortices are remarkably stable in position whenever they occur; they still move about somewhat, however, and more than one transducer would be needed to research their nature, a study beyond the scope of the present work. The baffle arrangements investigated herein did not eliminate them completely. Actually, the maximum vortex strength detected over a period of time was reduced only slightly, although frequency of occurrence and persistence were significantly affected. Examination of the relevant literature shows that the conditions of vortex formation in pump sumps are still little understood.

Regarding possible adverse effects of these vortices on pump performance, the air coming out of solution could indeed affect the performance as much as air entrained by a free surface vortex, but the amount of air involved in the process described herein is probably, with intermittency and all, very small. Nevertheless, no data on this problem seem to be available (see however Zanker 1968a).

4. An opportunity to test scale effects in general and on vortex formation in particular as discussed in section II of this report would be available if the prototype could be instrumented. This possibility should be explored as it could provide answers to some important similitude problems and pave the way for more accurate model predictions of prototype sump flows.

In the light of the foregoing conclusions, the principal recommendations derived from this study are as follows:

a) The flow-training baffles improve significantly the velocity distributions in the pump-approach flows and should be used to this effect in the prototype. However, the question of whether this improvement in the velocity distributions is necessary to obtain satisfactory performance of the pumps (in particular, the question of the improvement in pump efficiency and wear brought

about by the improvement in the velocity distributions) was beyond the scope of this study.

b) If the prototype is operated initially without any flow-training baffles and if pump operation difficulties related to the approach flow are encountered under these conditions, further testing could be conducted in the prototype. In this case, the model results could be used to guide the selection of corrective measures.

LIST OF REFERENCES

Collinson, A.E. 1968 Discussion of "Some Hydraulic Modeling Techniques," by K.J. Zanker, Symposium on Model Testing of Hydraulic Machinery and Associated Structures, The Institution of Mechanical Engineers, Proceedings 1967-68, Vol. 182, Part 3M.

Daggett, L.L. and Keulegan, G.H. 1974 "Similitude in Free-Surface Vortex Formation," Journal of the Hydraulic Division, ASCE, Vol. 100, No. HY 11, Proc. Paper 10941.

Denny, D.F. 1956 "An experimental study of air entraining vortices in pump sumps," The Insititution of Mechanical Engineers, Proceedings, Vol. 170, No. 2.

Denny, D.F. and Young, G.A.J. 1957 "The Prevention of Vortices and Swirl at Intakes," Transactions 7th Conference of IAHR, Lisbon, Vol. 1, Paper No. C1.

Kenn, M.J. 1968 Discussion of "Some Hydraulic Modeling Techniques," by K.J. Zanker, Symposium on Model Testing of Hydraulic Machinery, and Associated Structures, The Institution of Mechanical Engineers, Proceedings 1967-68, Vol. 182, Part 3M.

Nakato, T. and Kennedy, J.F., 1976 "Model study of the Lake Chicot Pumping Plant," Iowa Institute of Hydraulic Research Report No. 188.

Paterson, I.S. and Cambell, G. 1968 "Pump Intake Design Investigations," Symposium on Model Testing of Hydraulic Machinery and Associated Structures, The Institution of Mechanical Engineers, Proceedings 1967-68, Vol. 182, Part 3M.

Quick, M.C. 1970 "Efficiency of air-entraining vortex formation at water intake," Journal of the Hydraulics Division, ASCE, Vol. 96, No. HY7.

Wilson, E.H. 1968 Discussion of "Some Hydraulic Modeling Techniques," by K.J. Zanker, Symposium on Model Testing of Hydraulic Machinery and Associated Structures, The Institution of Mechanical Engineers, Proceedings 1967-68, Vol. 182, Part 3M.

Zanker, K.J. 1968a Author's reply to discussion of "Some Hydraulic Modeling Techniques", Symposium on Model Testing of Hydraulic Machinery and Associated Structures, The Institution of Mechanical Engineers, Proceedings 1967-68, Vol. 182, Part 3M.

Zanker, K.J. 1968b "Some Hydraulic Modeling Techniques", Symposium on Model Testing of Hydraulic Machinery and Associated Structures, The Institution of Mechanical Engineers, Proceedings 1967-68, Vol. 182, Part 3M.

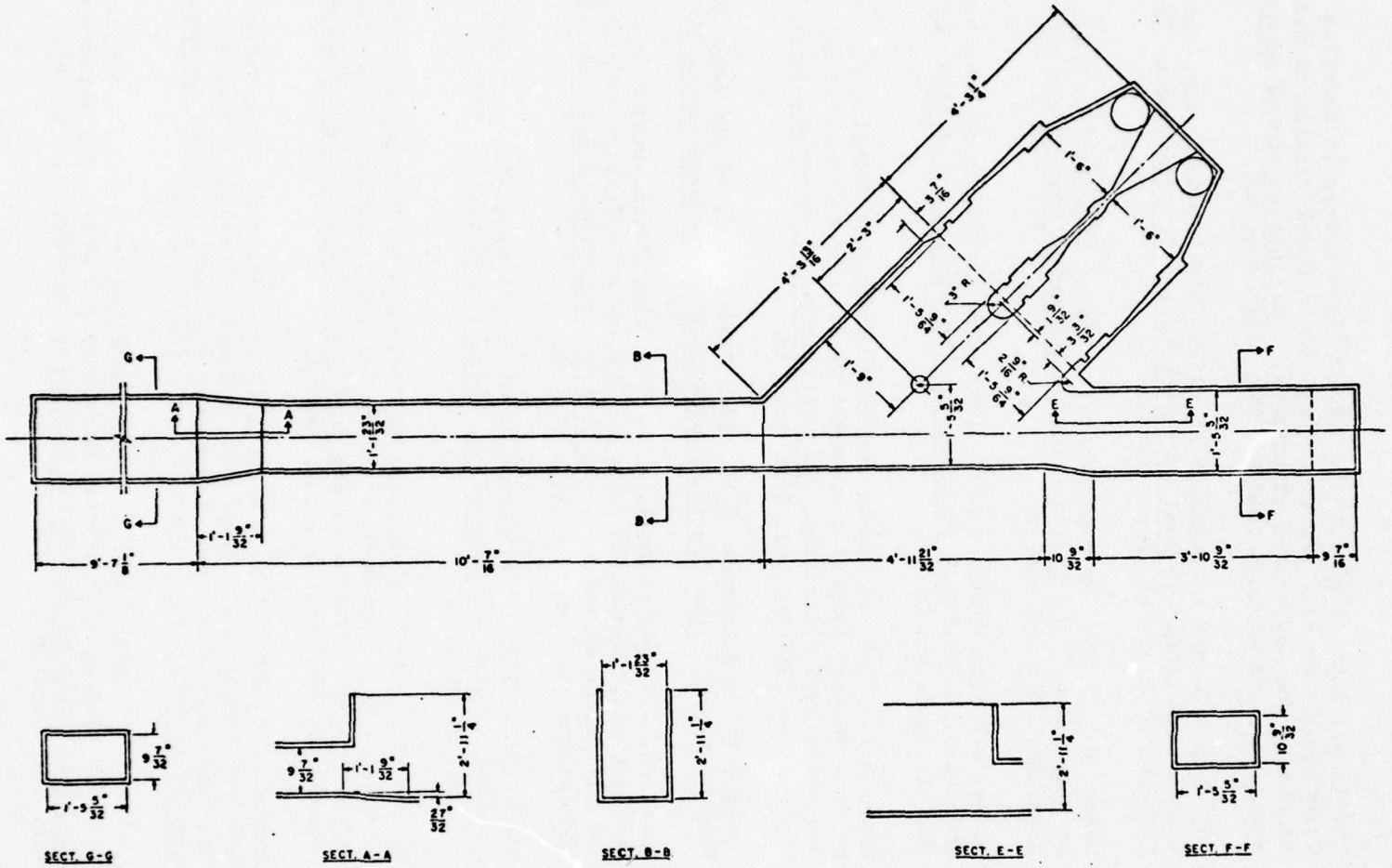

Figure 1. General plan view and channel sections of the Clinton First Avenue Pump Station Model

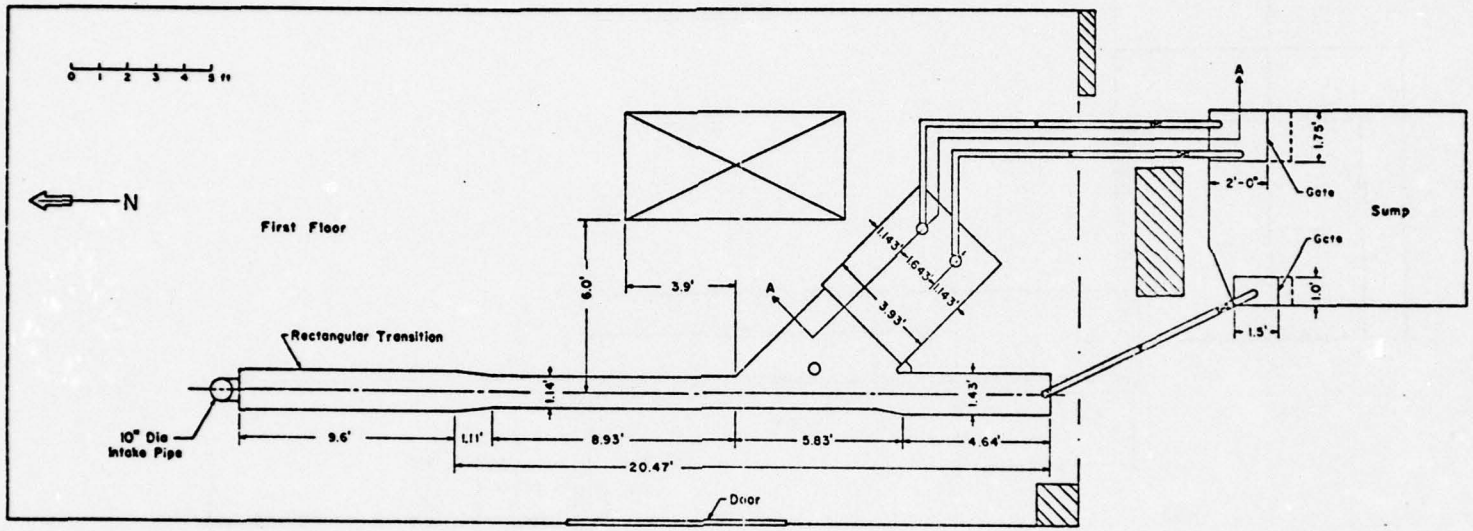

Figure 2. General layout of the Clinton First Avenue Pump Station Model on first floor of laboratory (section is shown in figure 3)

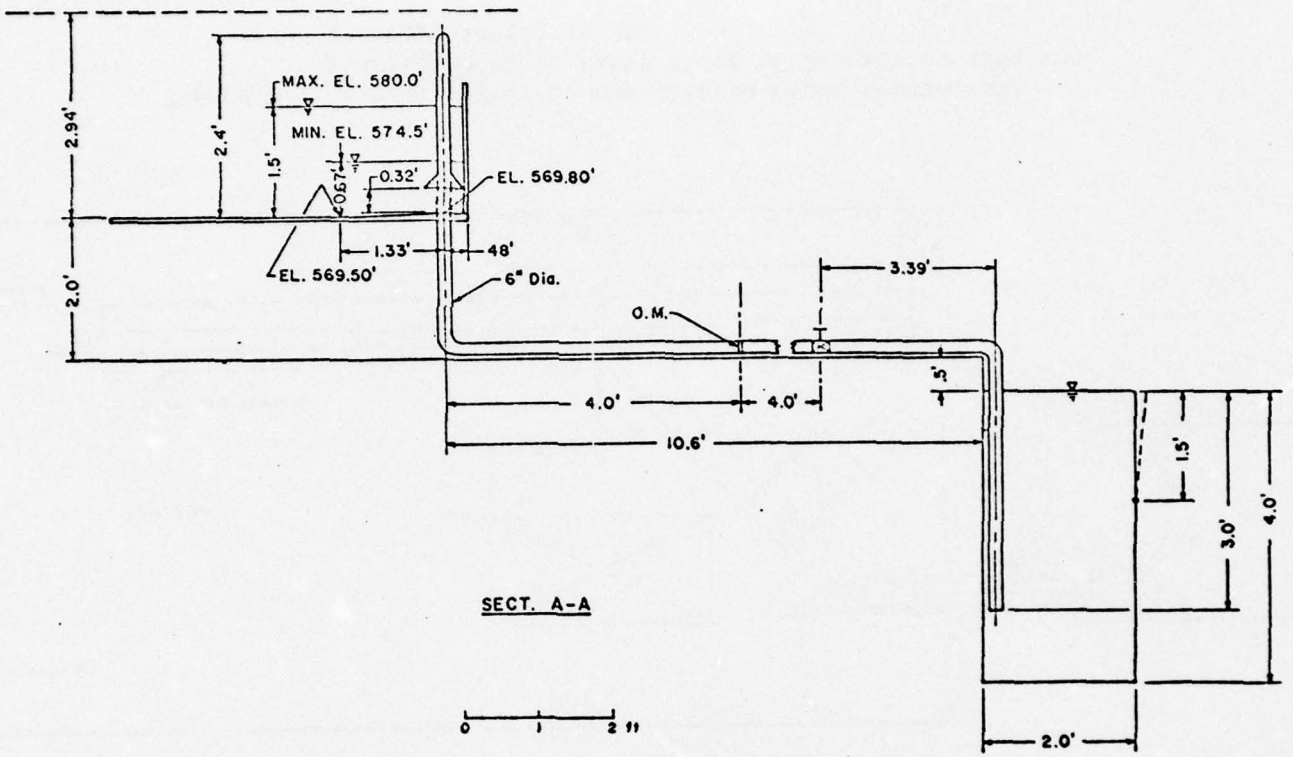

Figure 3. Partial section view of general layout and syphon of the Clinton First Avenue Pump Station Model

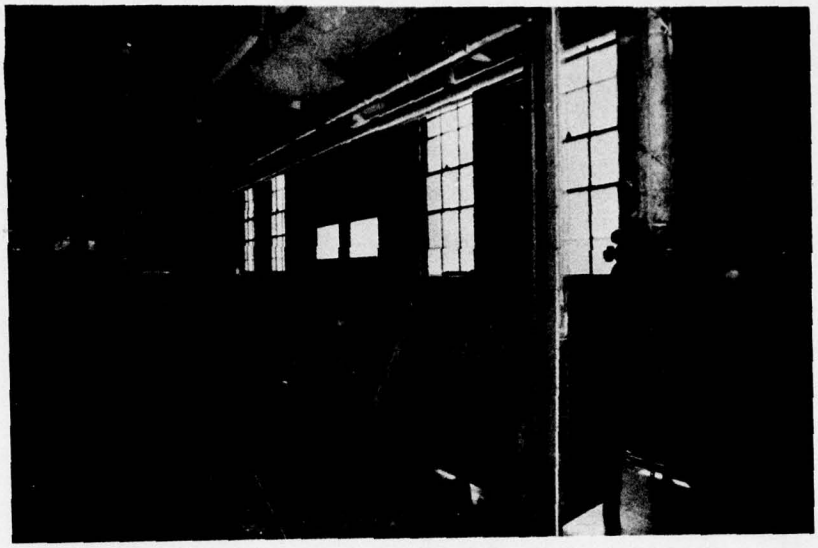

(a)

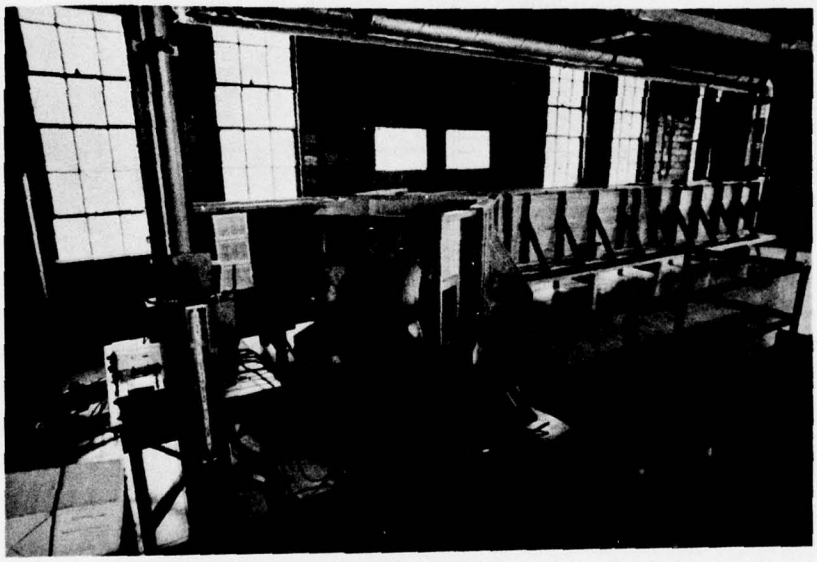

(b)

Figure 4. General photographic views of the model

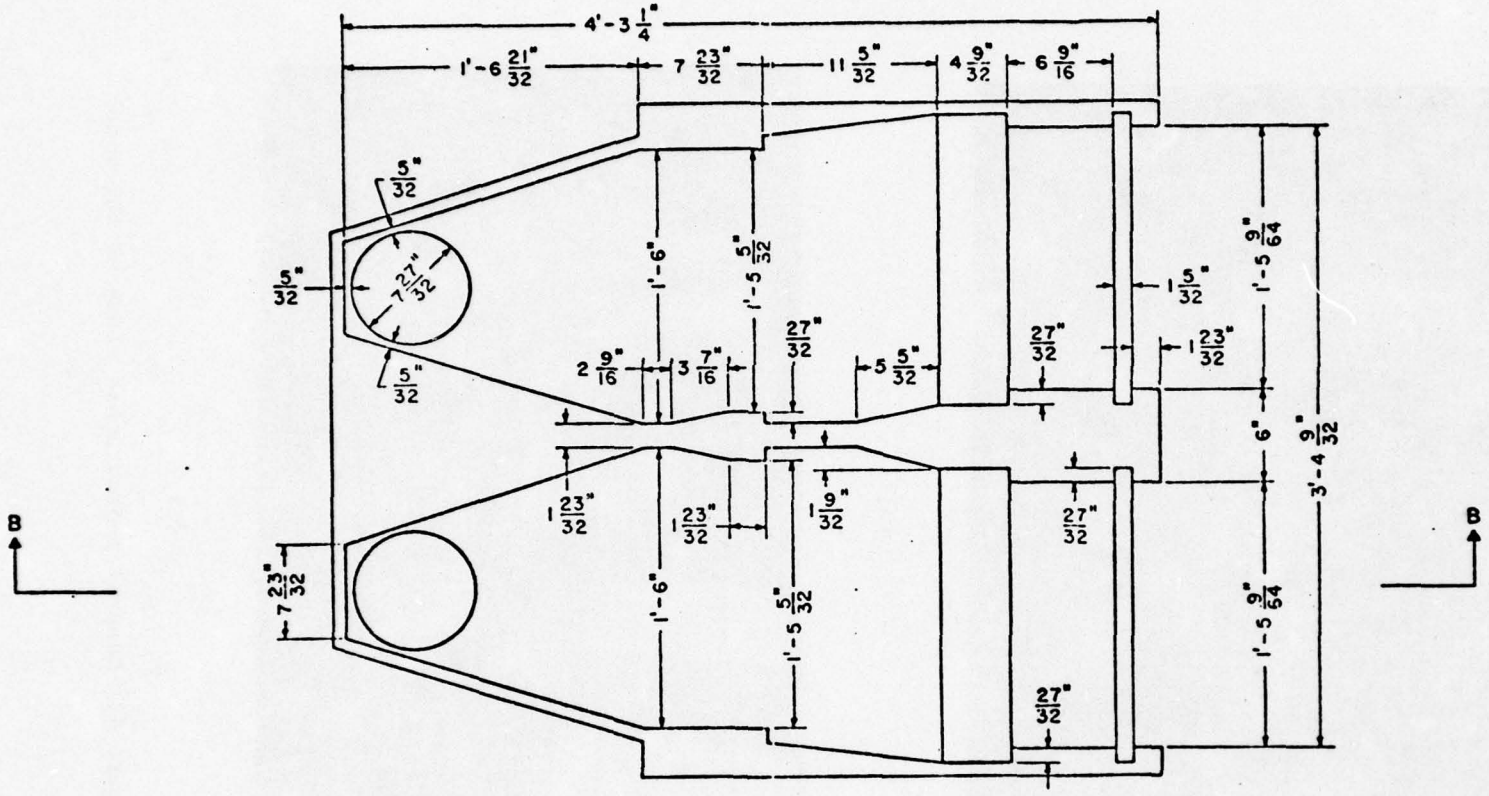

SECT. A-A

Figure 5. Horizontal cross section of pump bays and forebay (vertical cross section shown in figure 6)

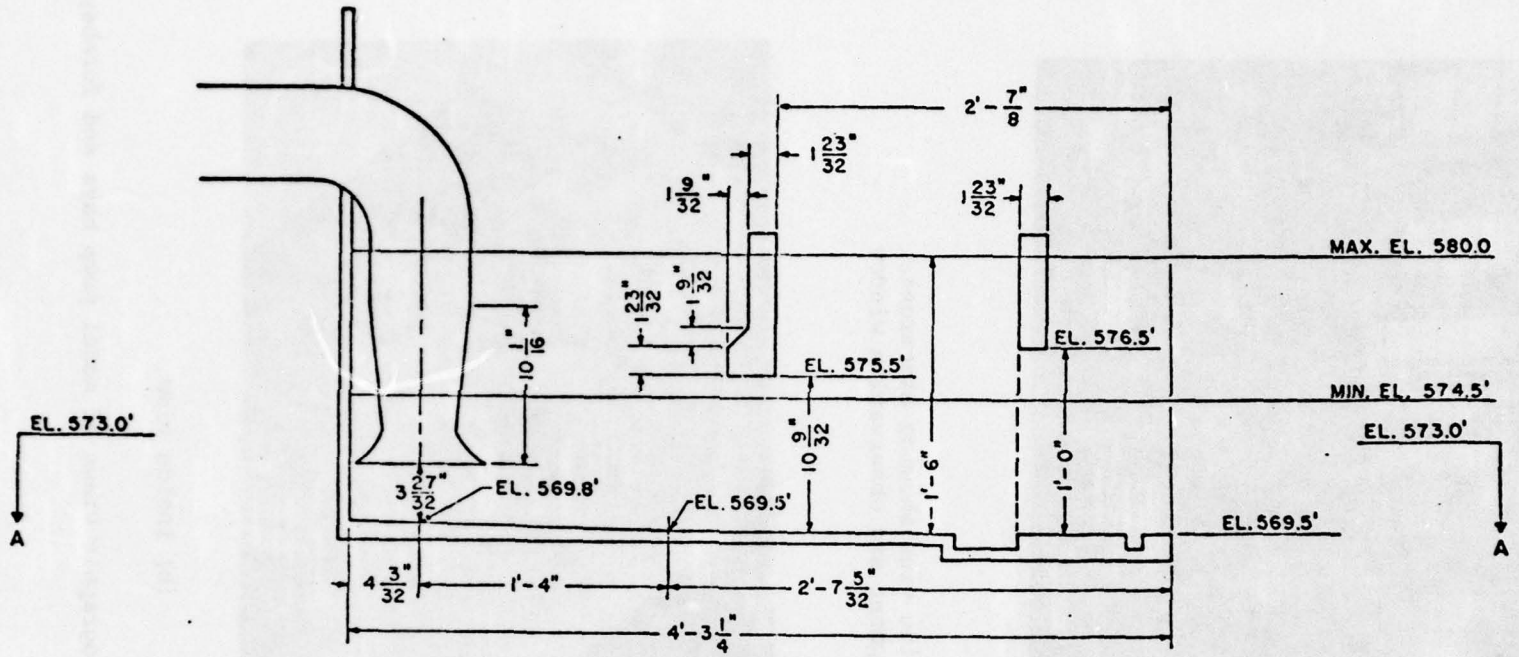

SECT. B-B

Figure 6. Vertical cross section of pump bays and forebay (horizontal cross section shown in figure 5)

(a) outside view showing electronic equipment and observation window

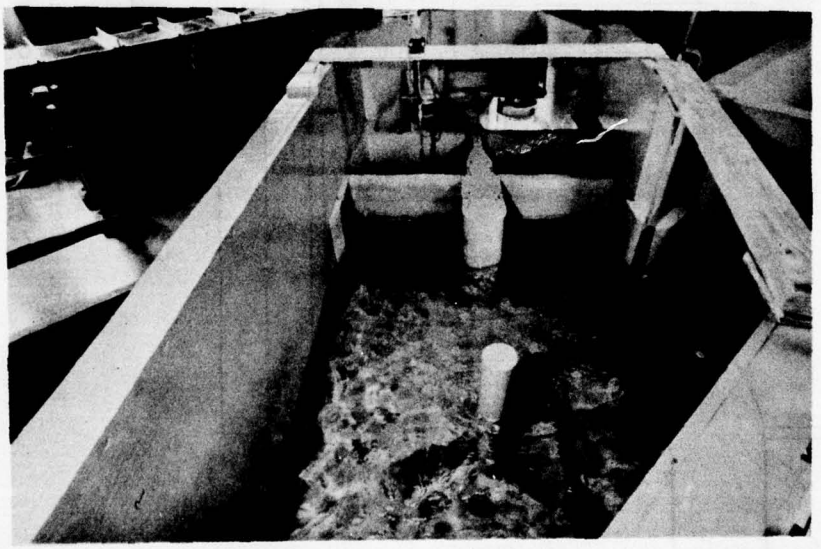

(b) inside view

Figure 7. Photographic views of model pump bays and forebays

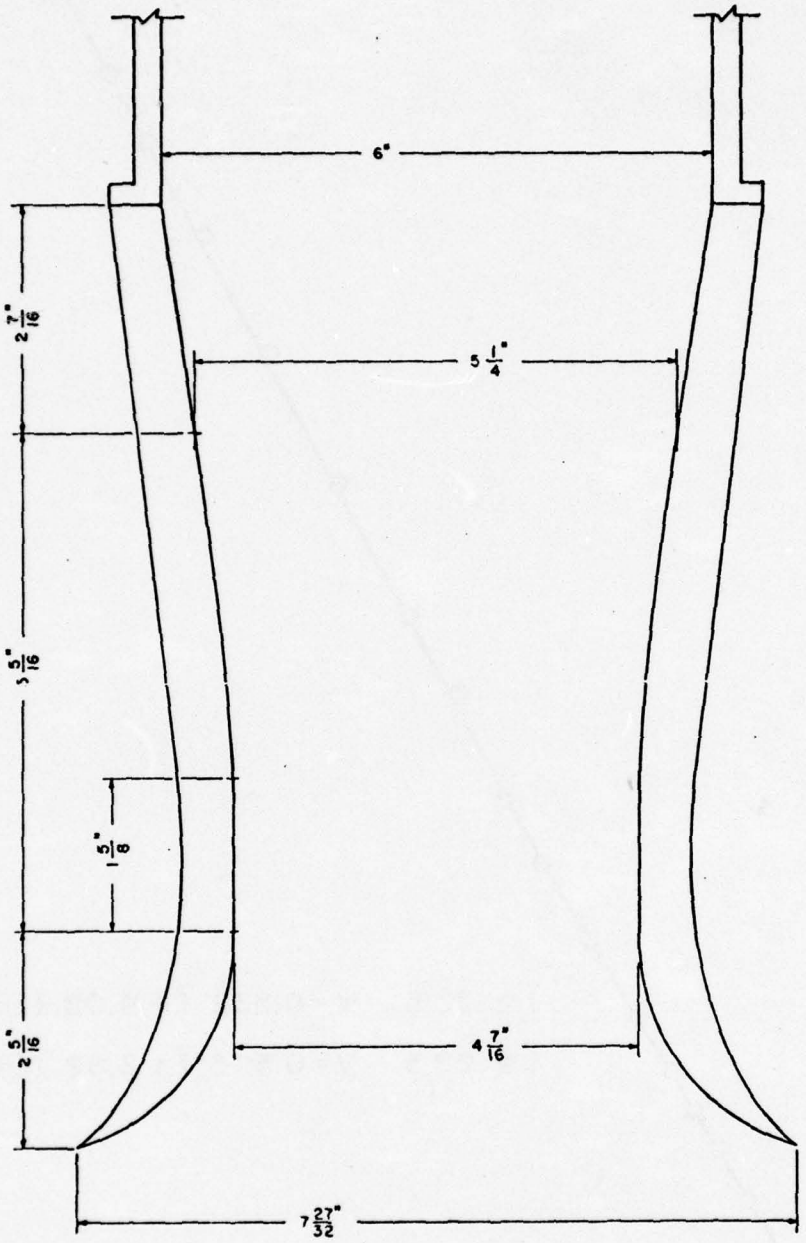

Figure 8. Section of syphon bells

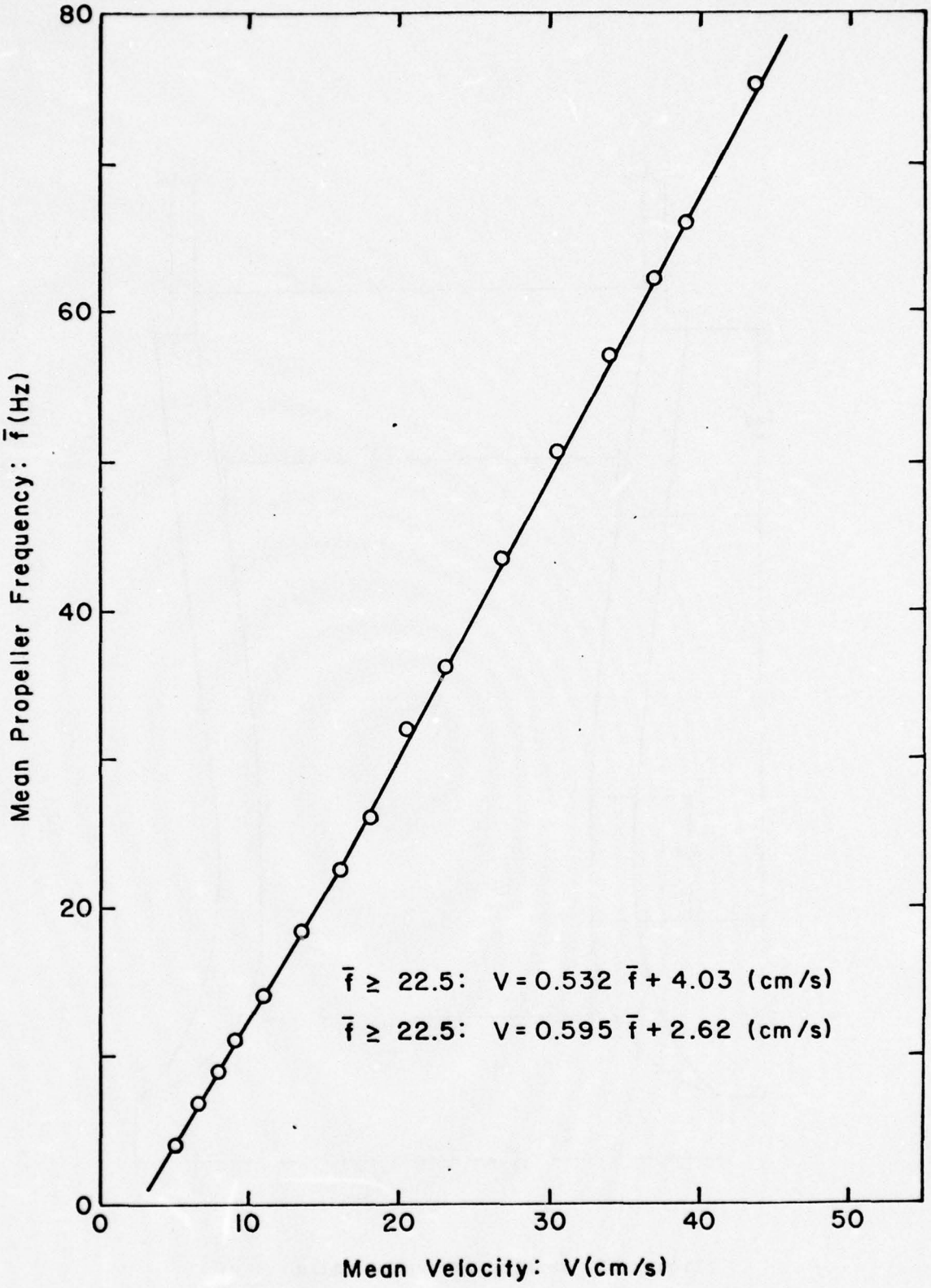

Figure 9. Calibration curve of miniature current meter (after Nakato and Kennedy 1976)

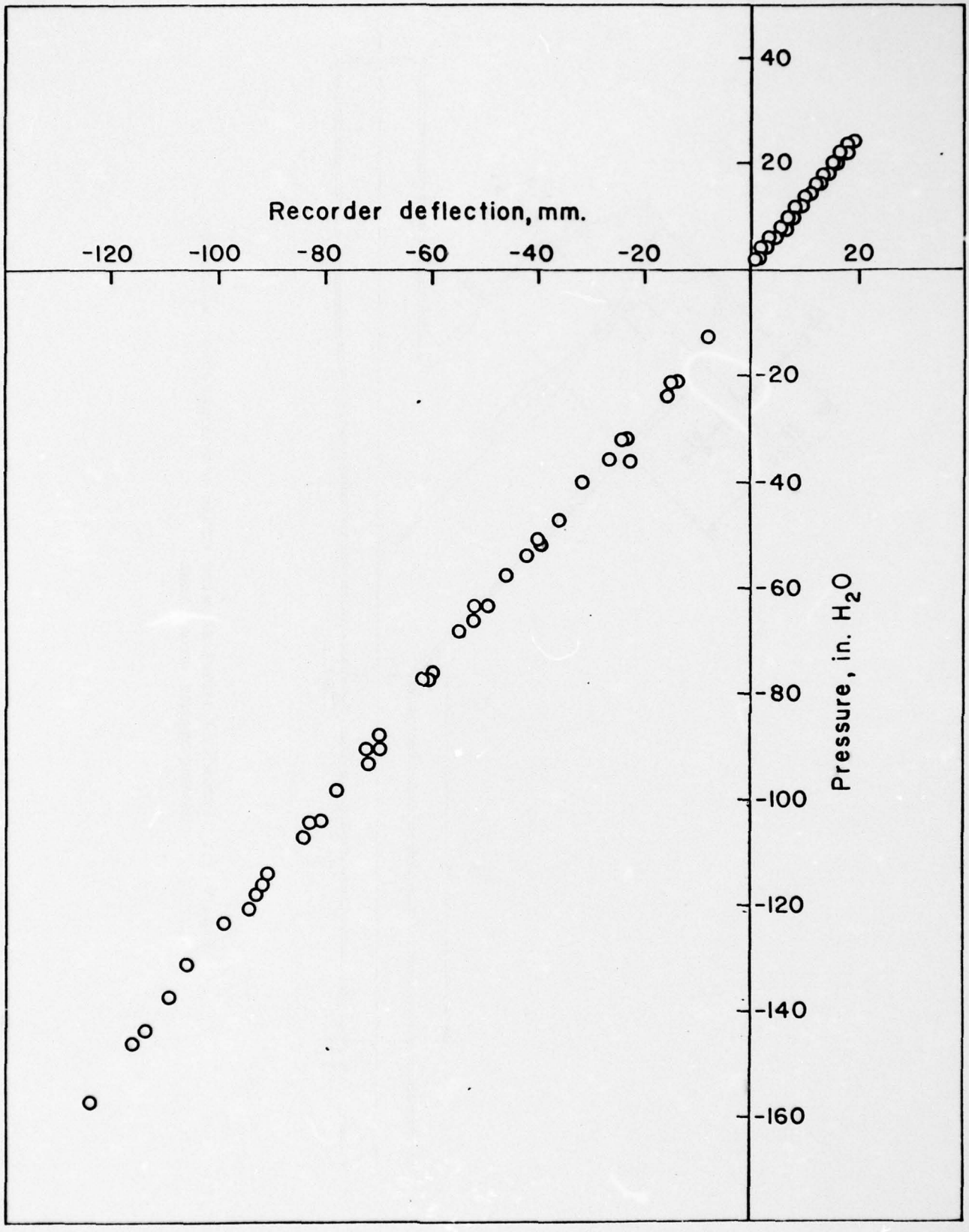

Figure 10. Typical calibration curve of pressure measuring system

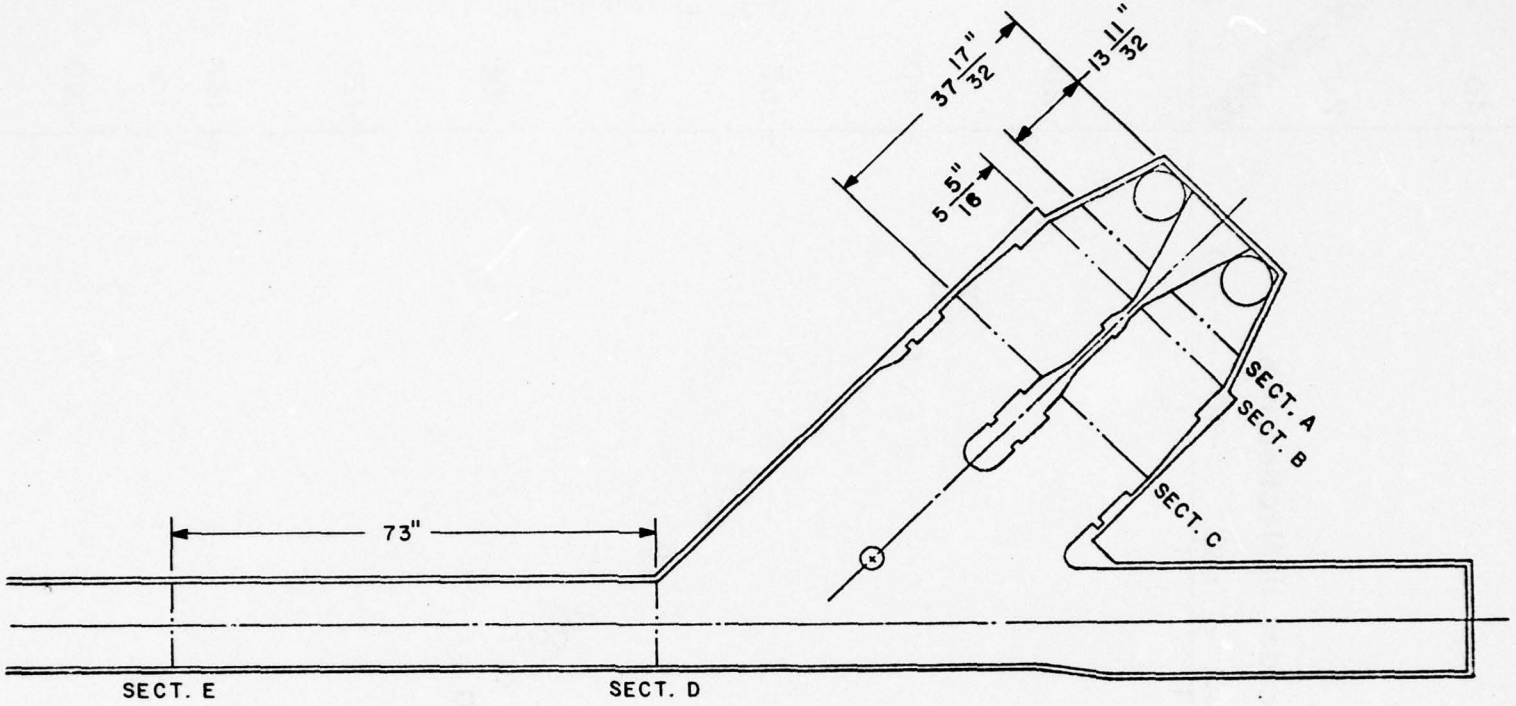

Figure 11. Sketch of model showing cross sections where velocity measurements were taken

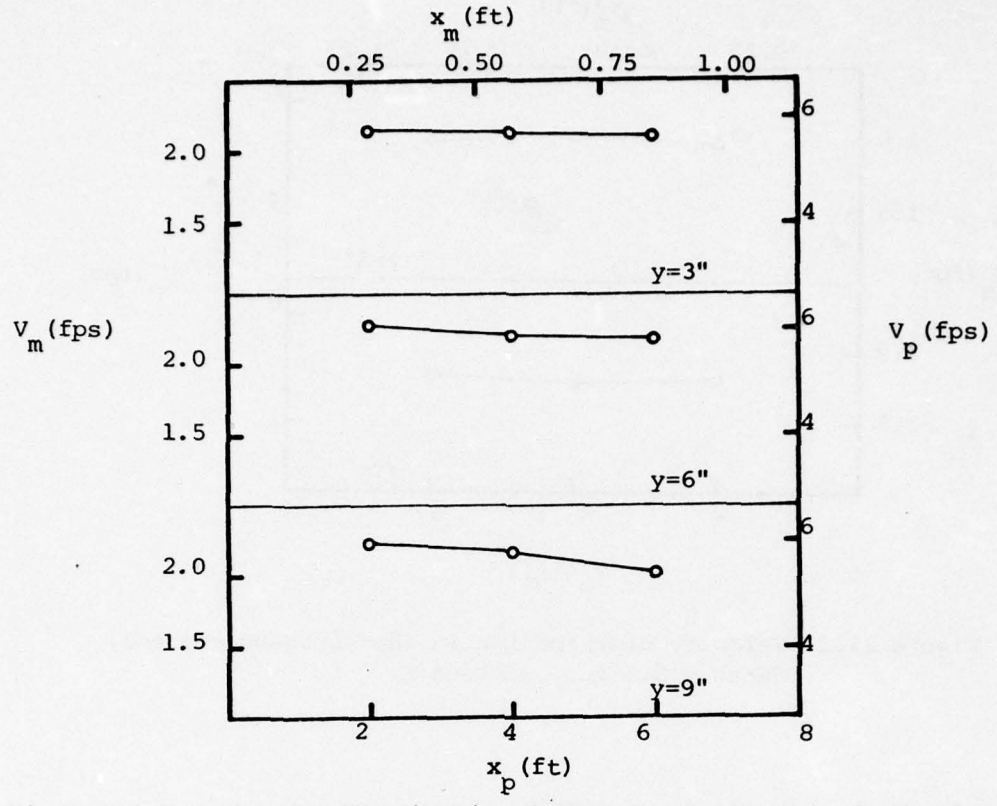

Figure 12.1 Velocity distribution in the approach channel, depth = 12 in., section E.

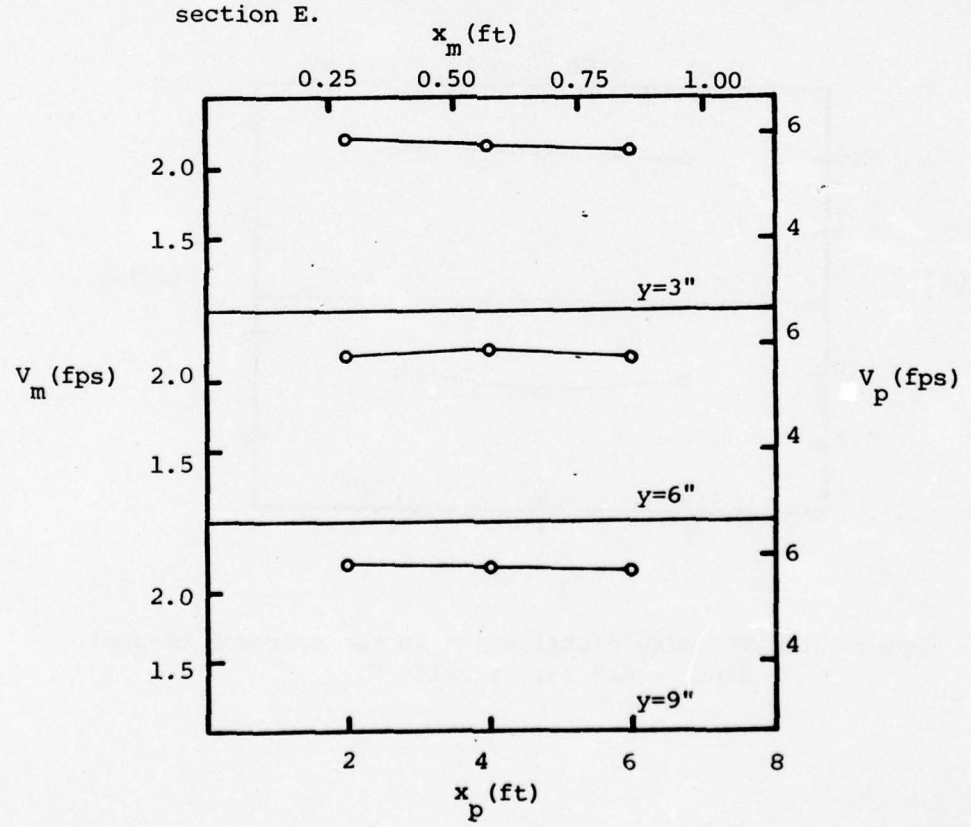

Figure 12.2 Velocity distribution in the approach channel, depth = 12 in., section D.

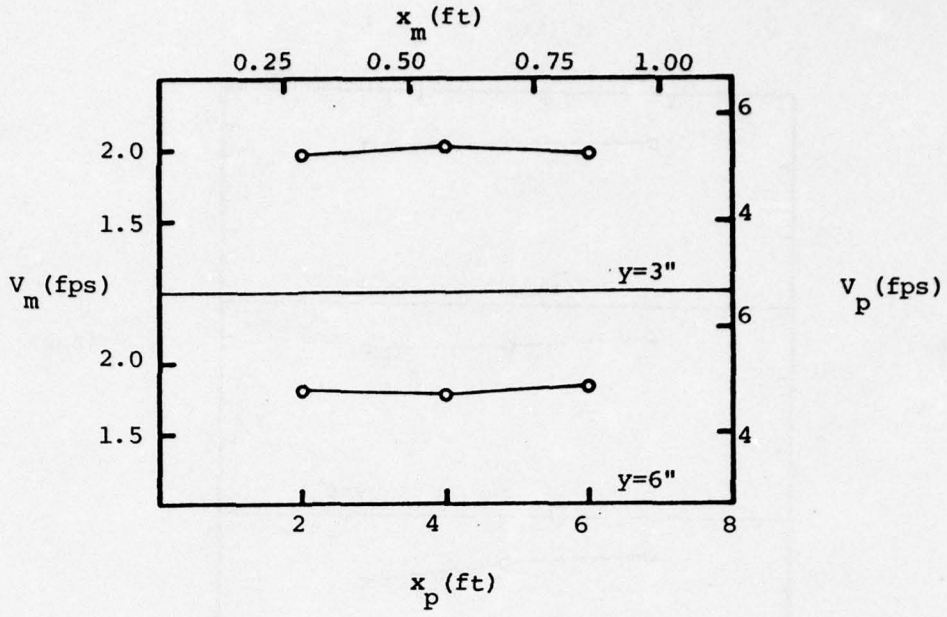

Figure 13.1 Velocity distribution in the approach channel, depth = 8.5 in., section E.

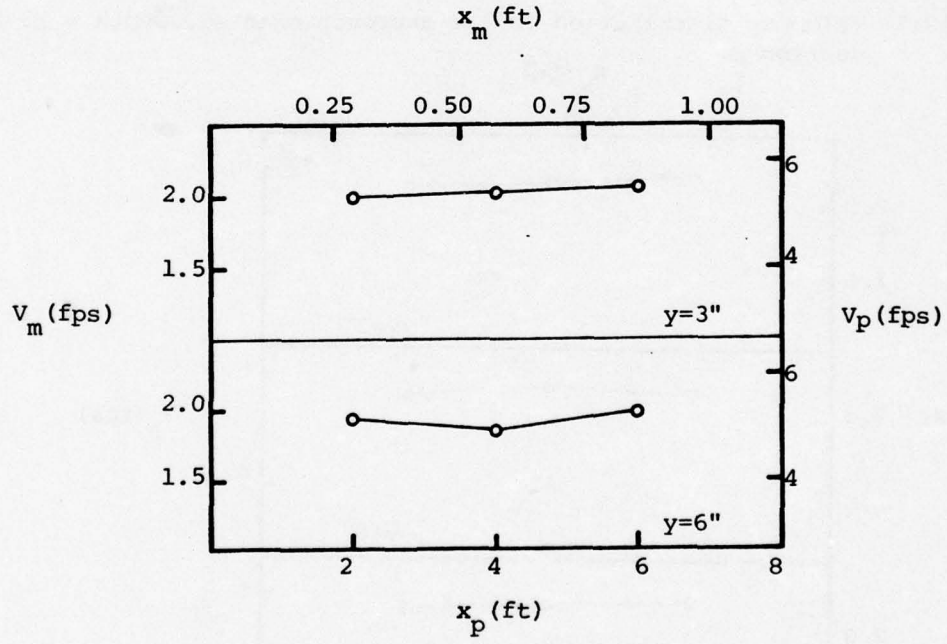

Figure 13.2 Velocity distribution in the approach channel, depth = 8.5 in., section D.

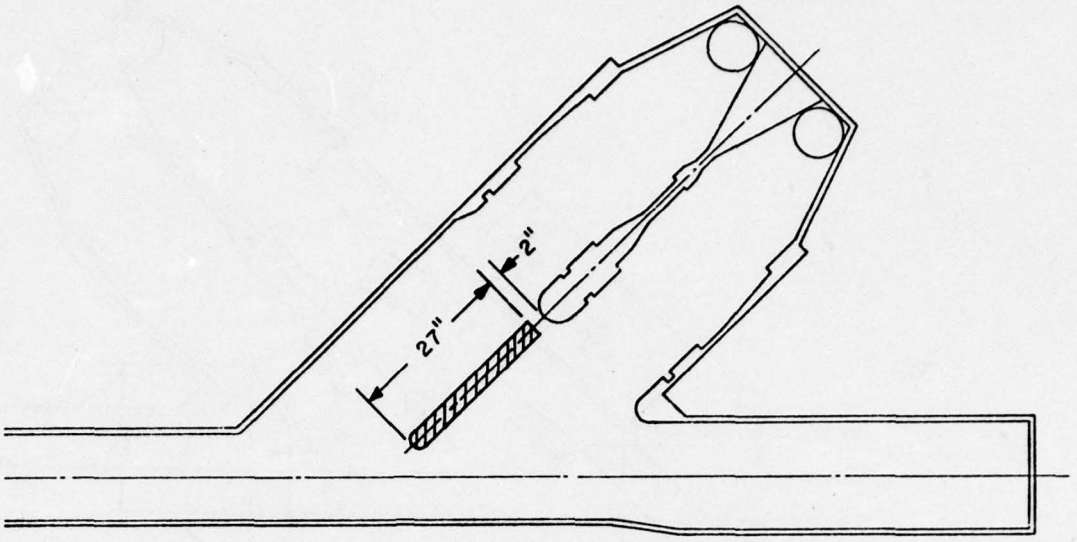

Case 1

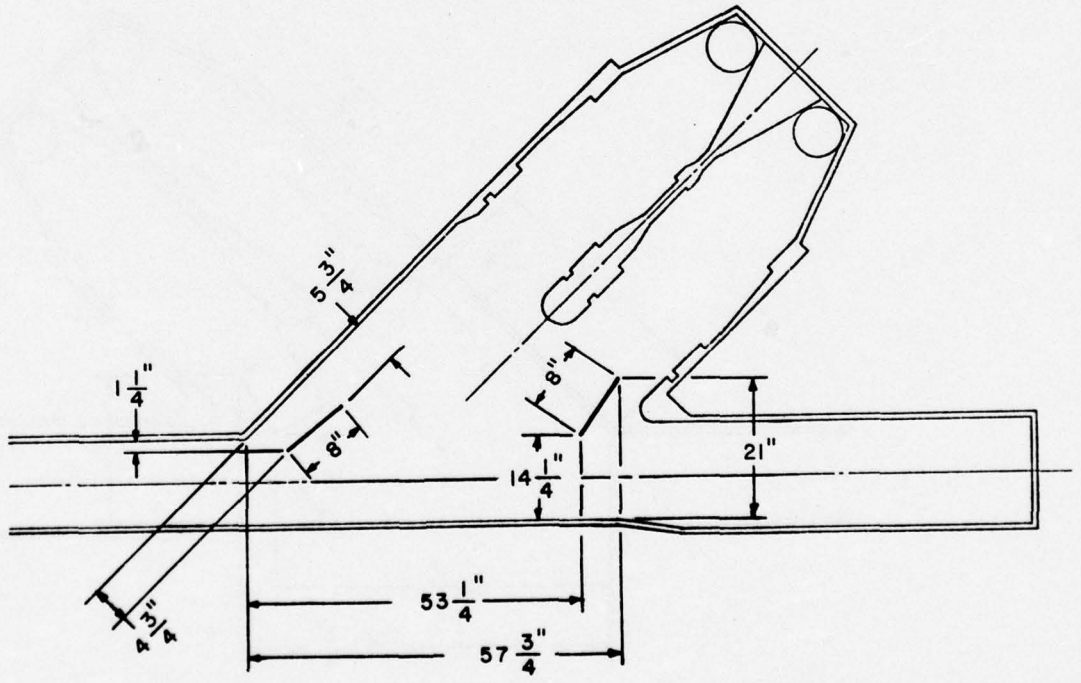

Case 2

Figure 14. Baffle arrangements tested

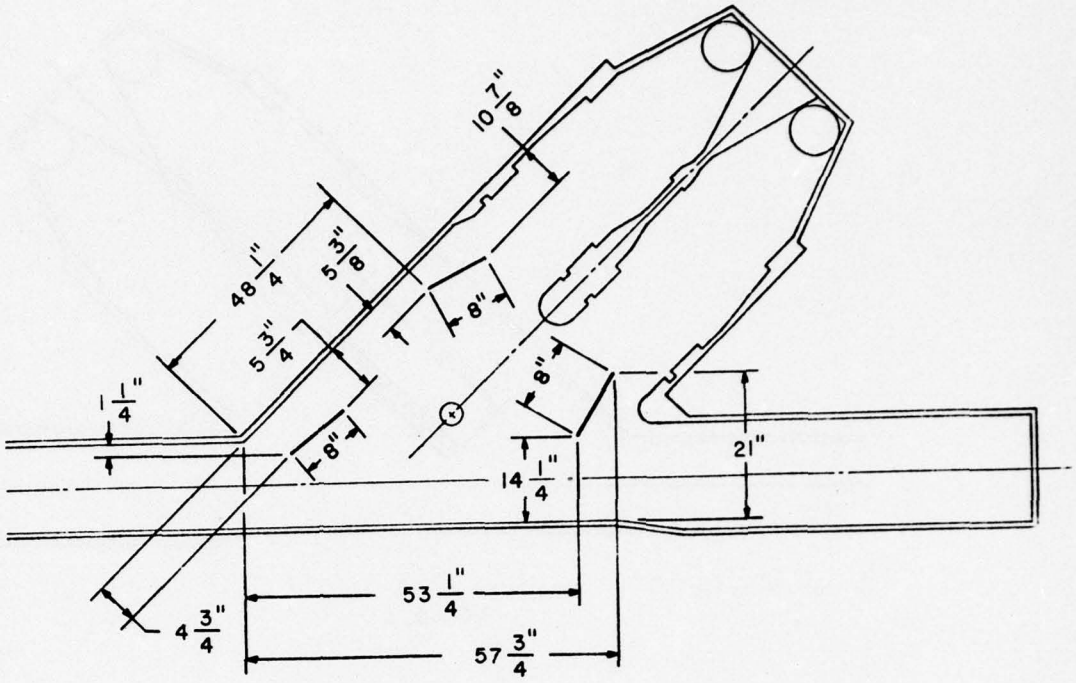

Case 3

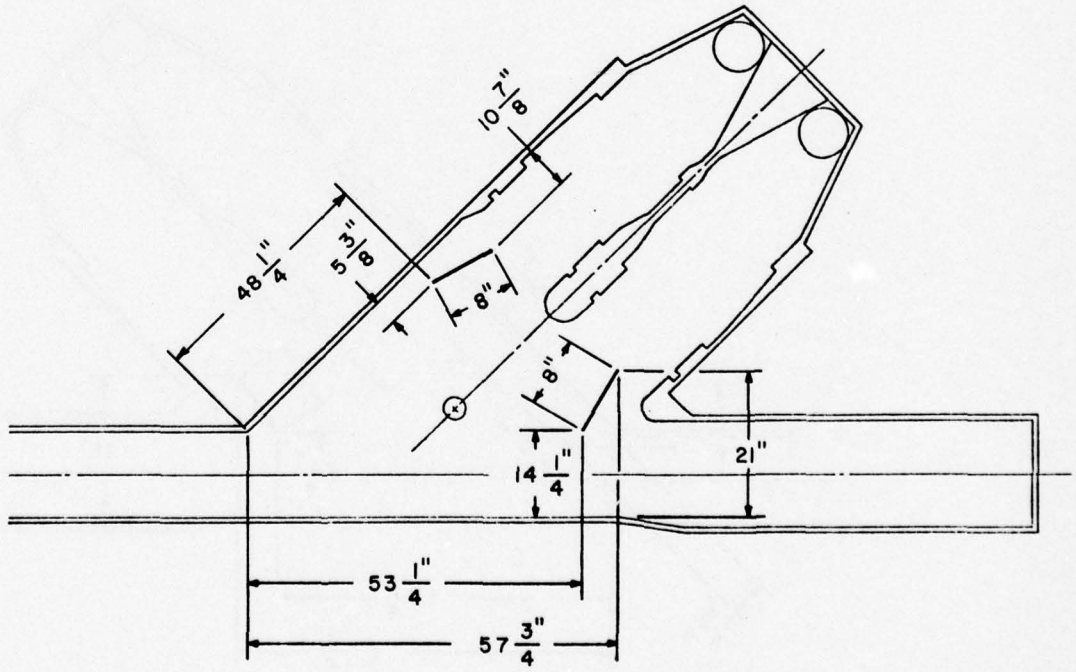

Case 4

Figure 14 (continued)

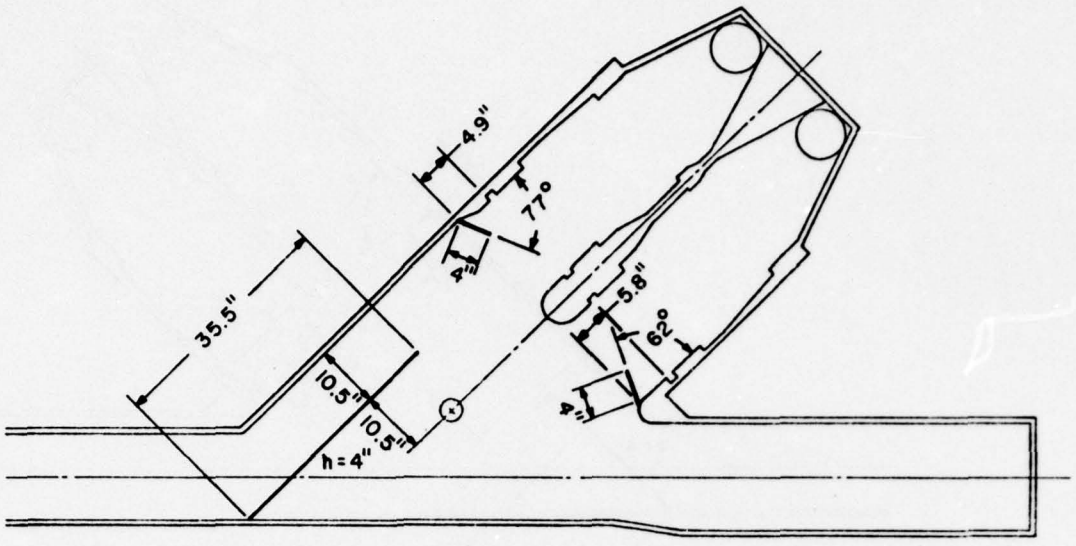

Case 5

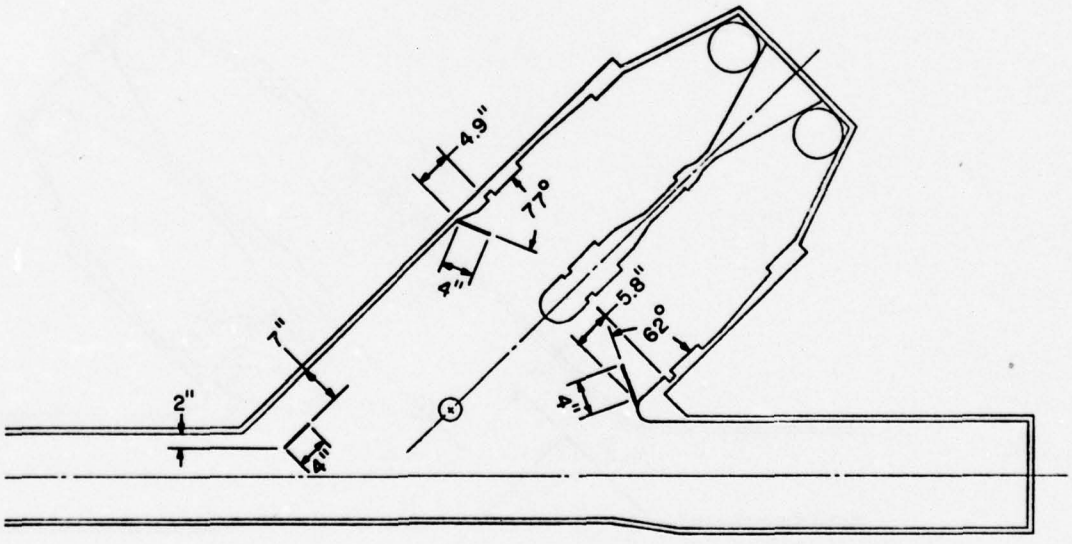

Case 6

Figure 14 (continued). h = baffle height

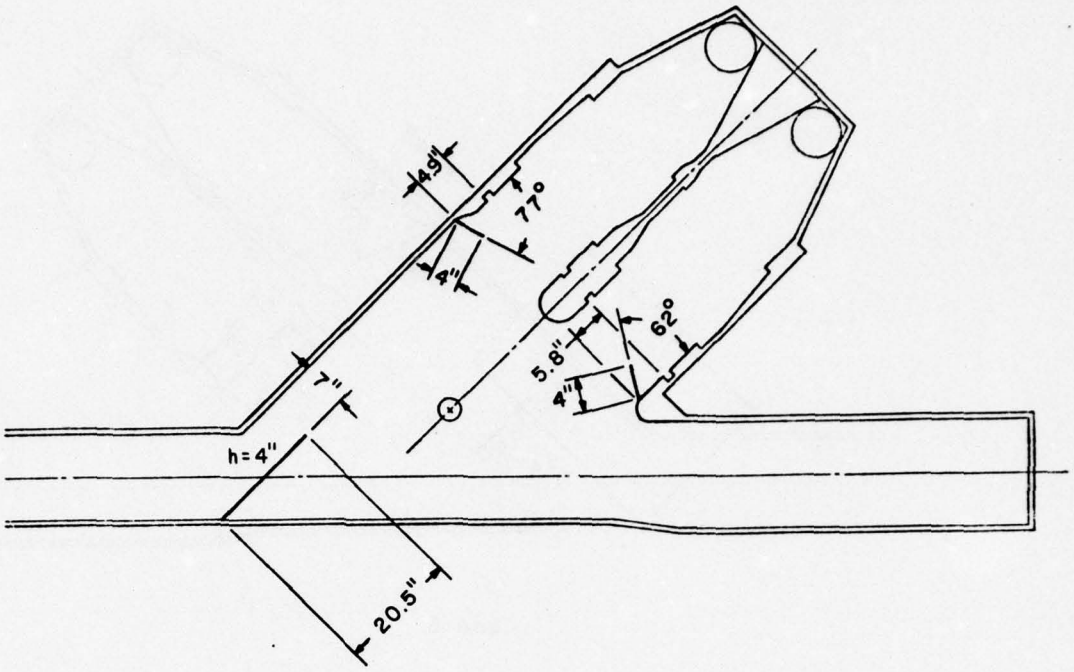

Case 7

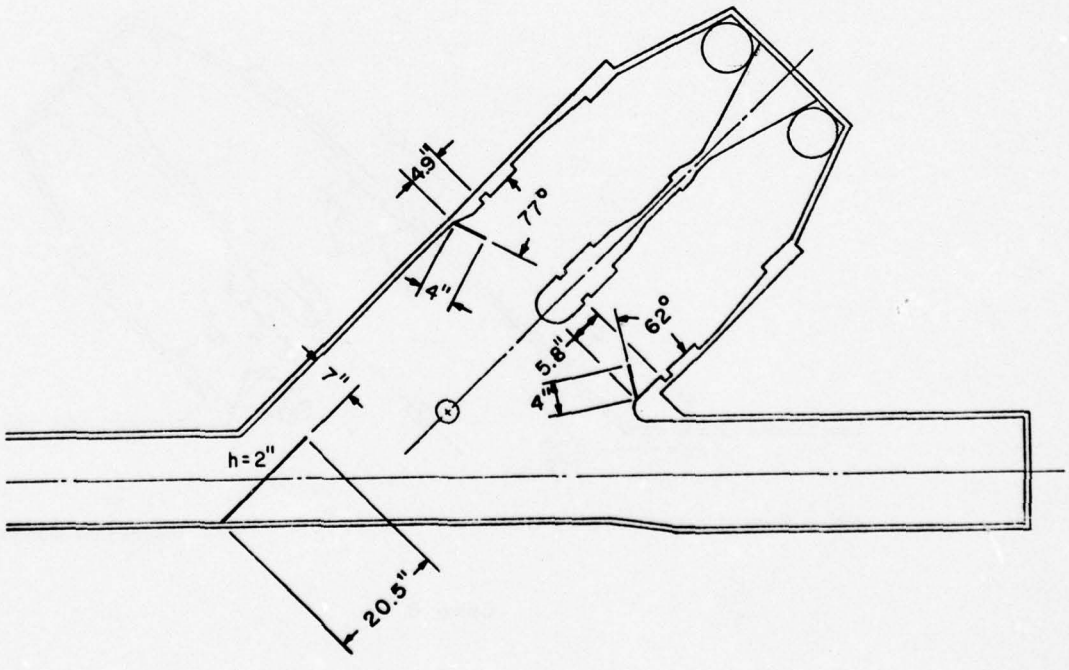

Case 8

Figure 14 (continued). h = baffle height

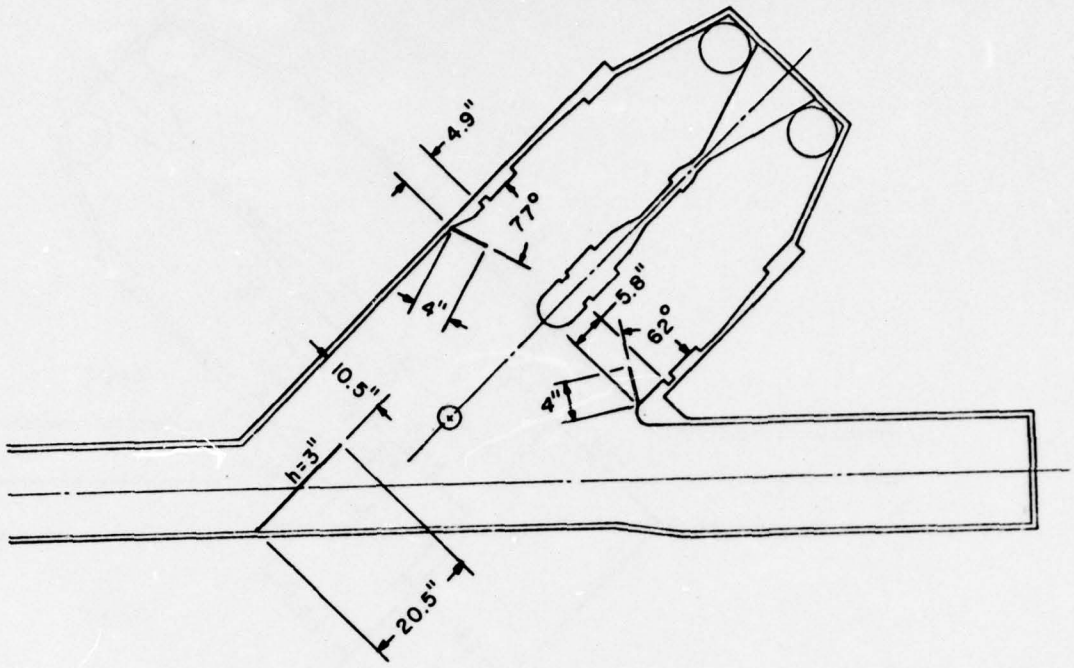

Case 9

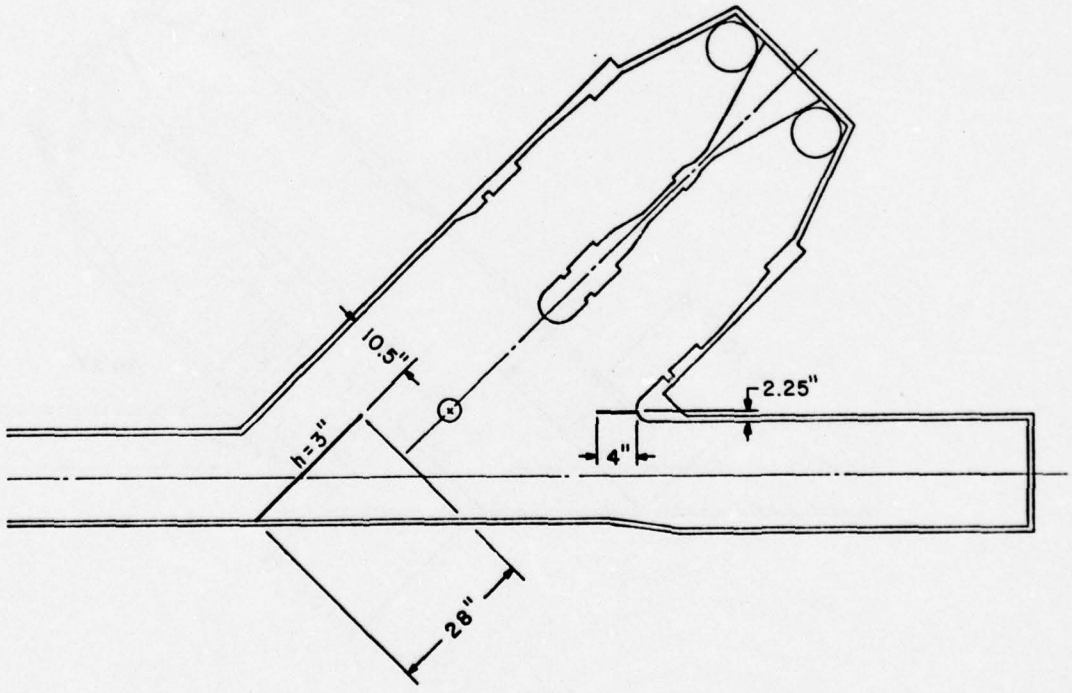

Case 10

Figure 14 (continued). h = baffle height

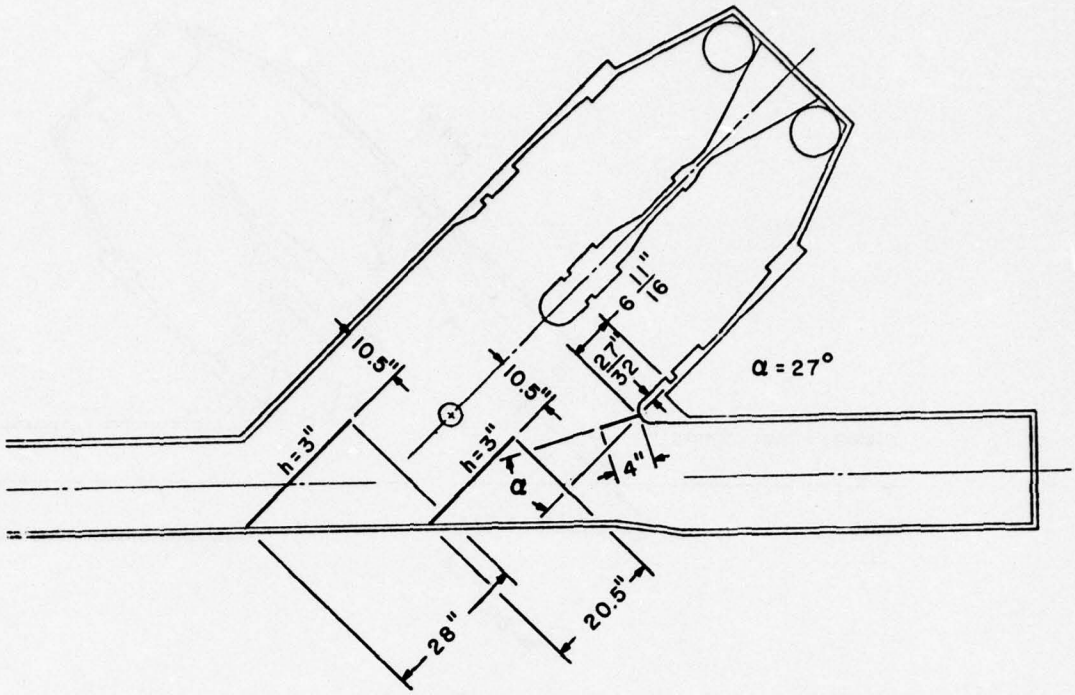

Case 11

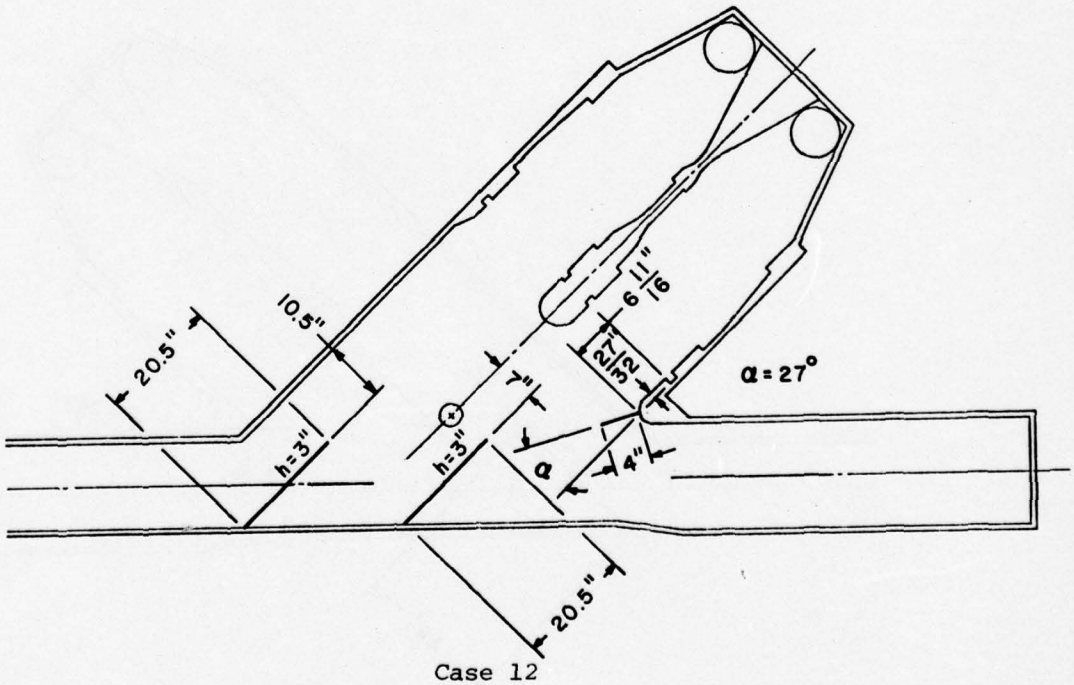

Case 12

Figure 14 (continued). h = baffle height

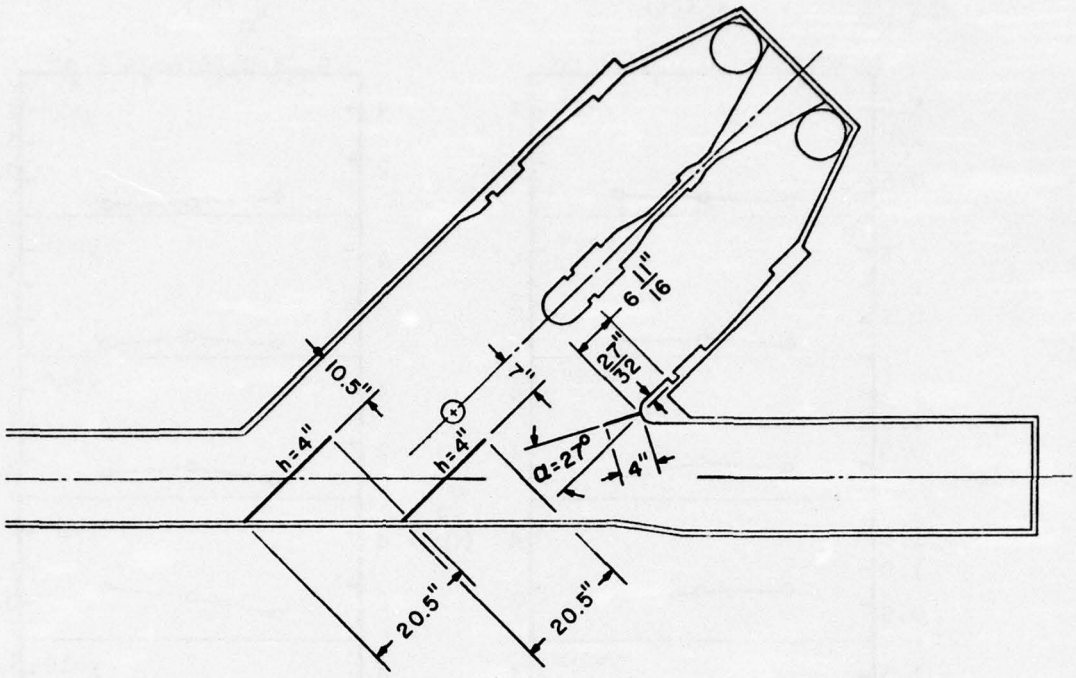

Case 13

Figure 14 (continued). h = baffle height

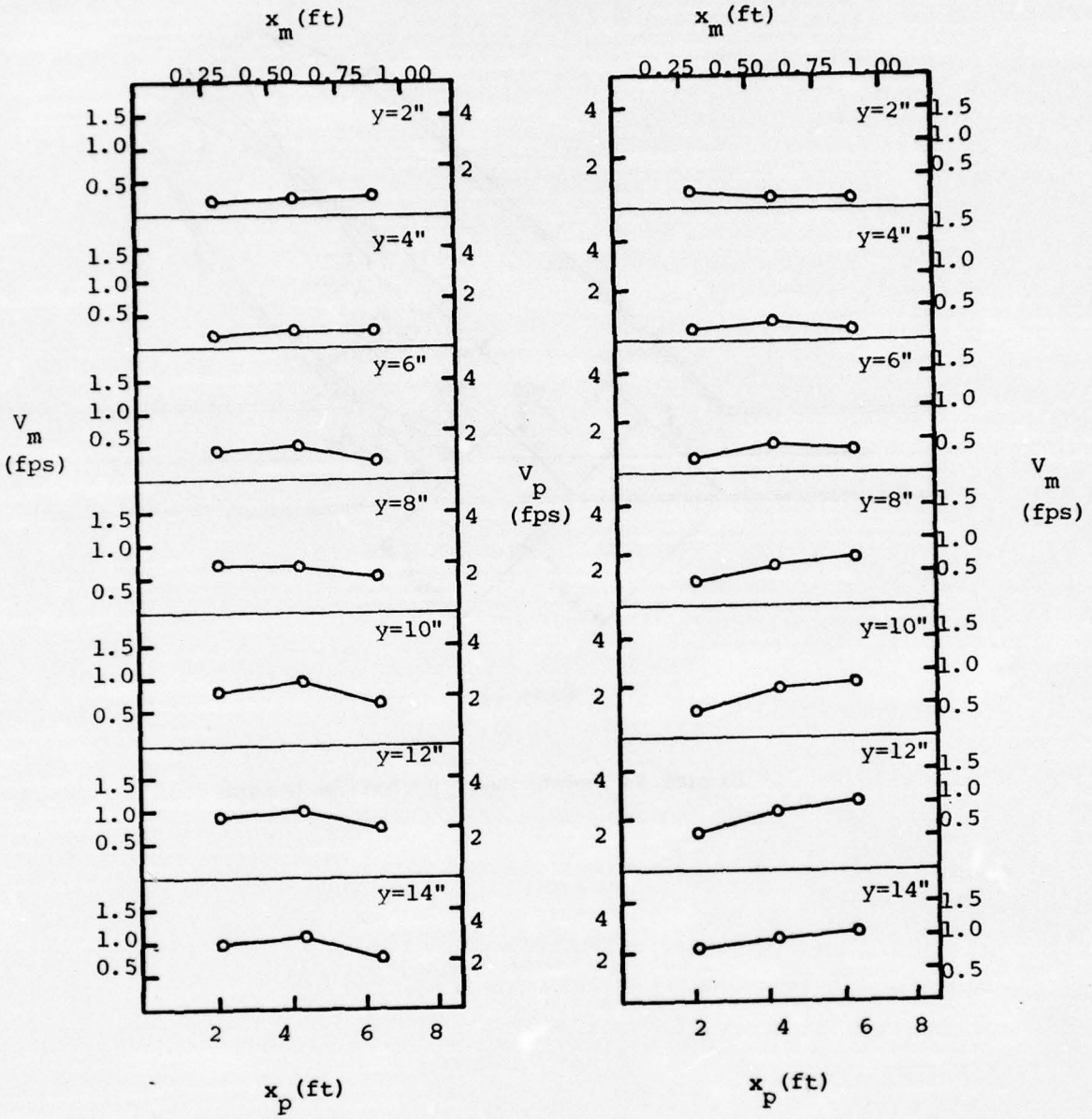

Figure 15.1 Velocity distribution (section A, two-pump operation, model depth = 18", no baffles)

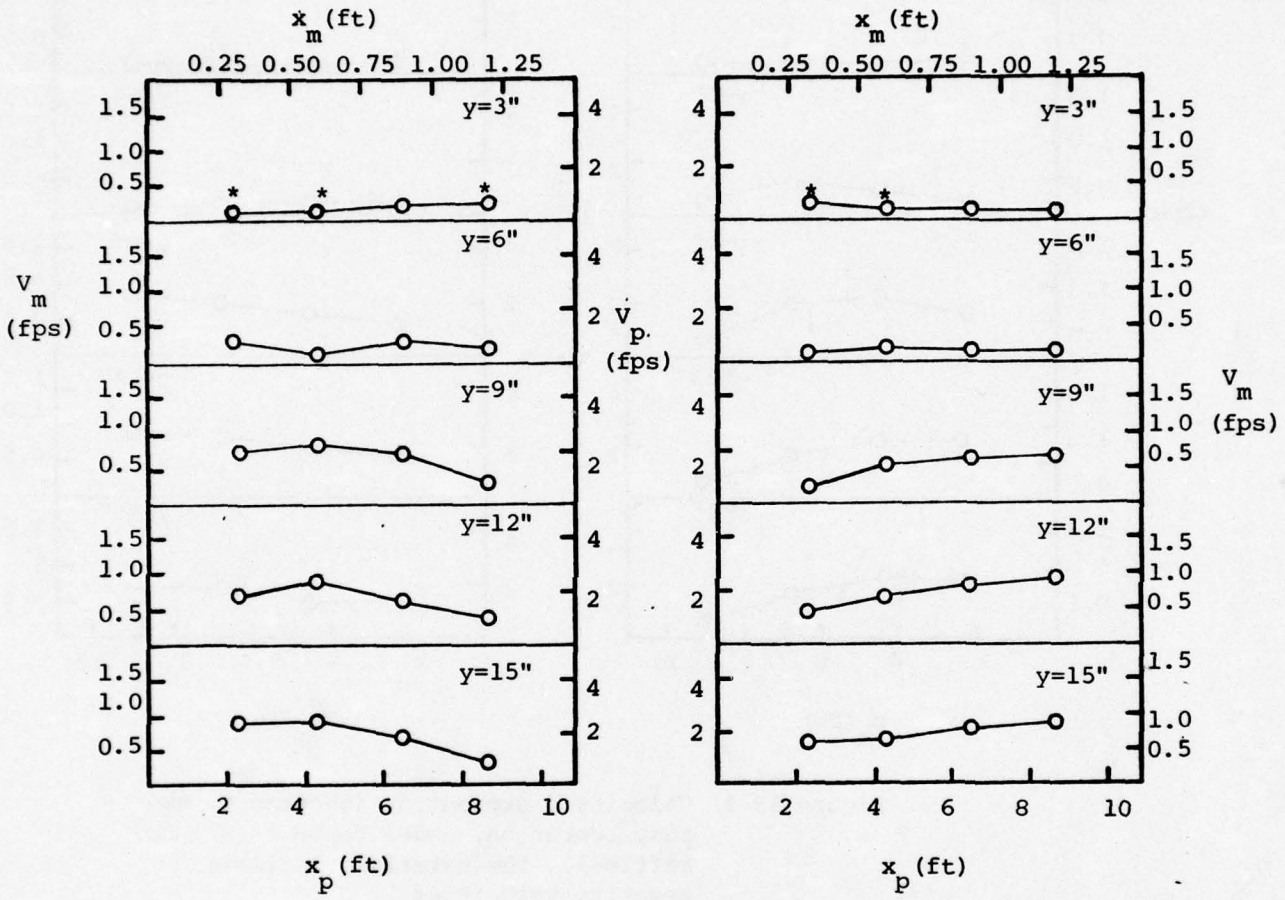

Figure 15.2 Velocity distribution (section B, two-pump operation, model depth = 18", no baffles). The asterisks indicate negative velocities

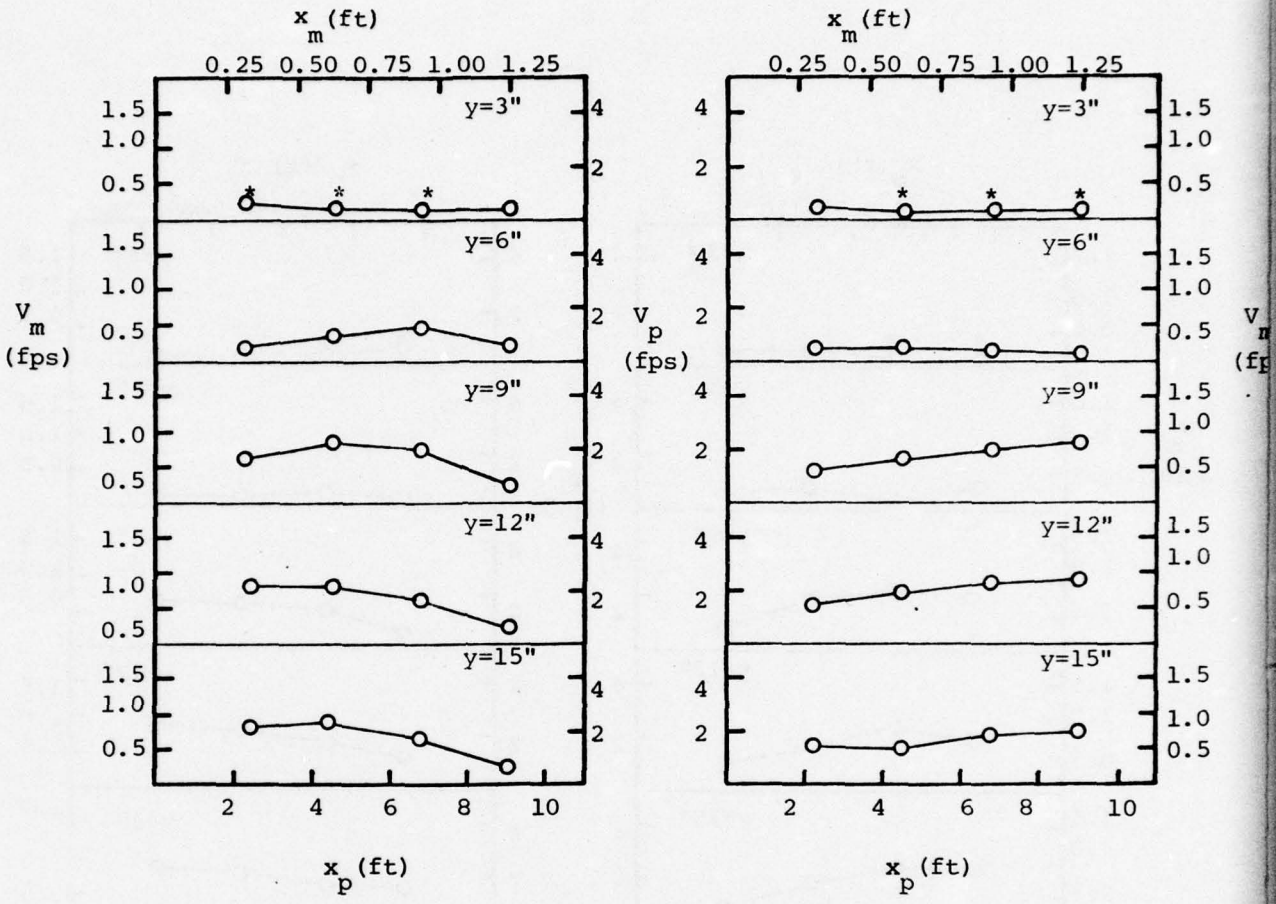

Figure 15.3 Velocity distribution (section C, two-pump operation, model depth = 18", no baffles). The asterisks indicate negative velocities

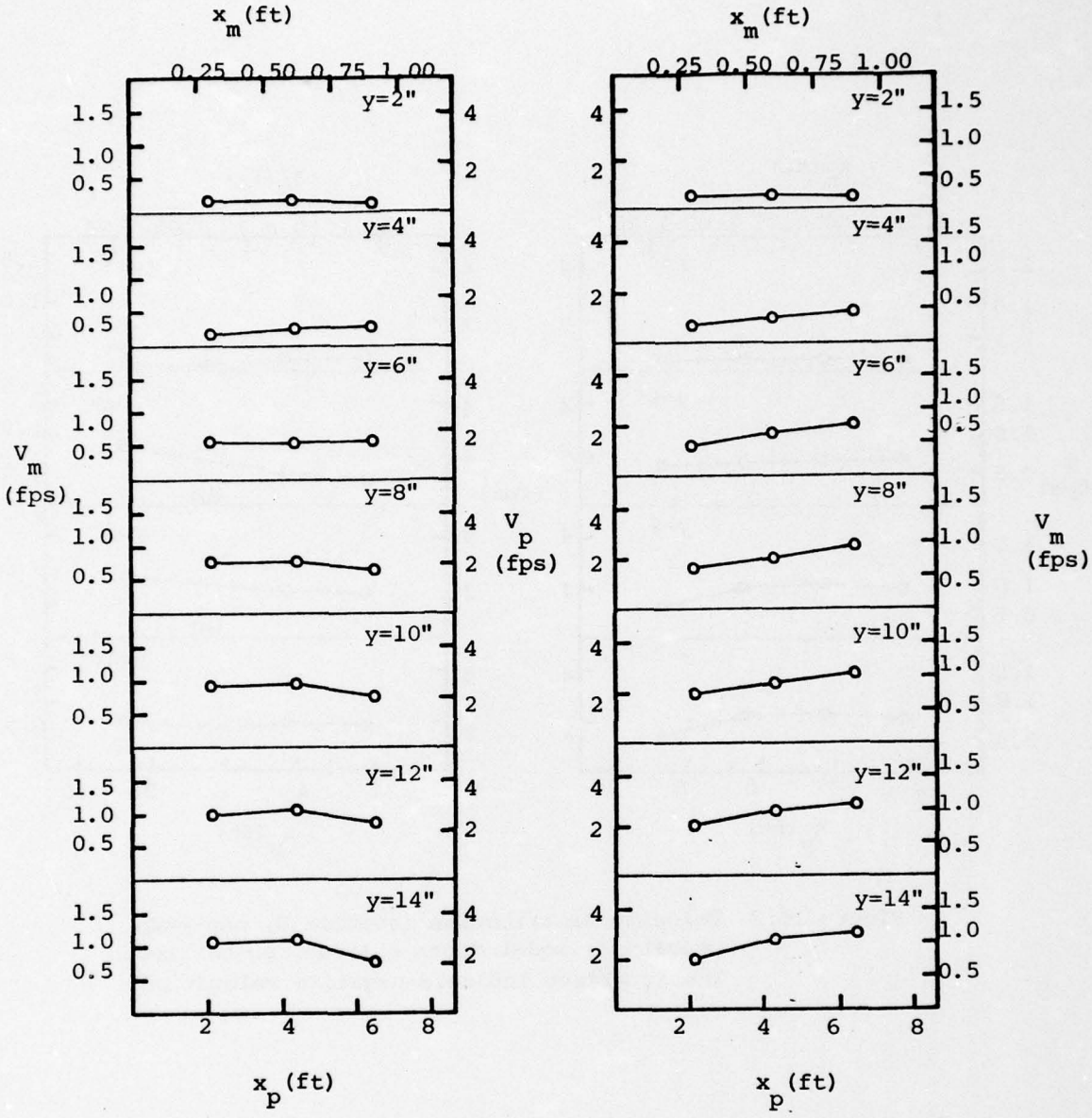

Figure 16.1 Velocity distribution (section A, one-pump operation, model depth = 18", no baffles)

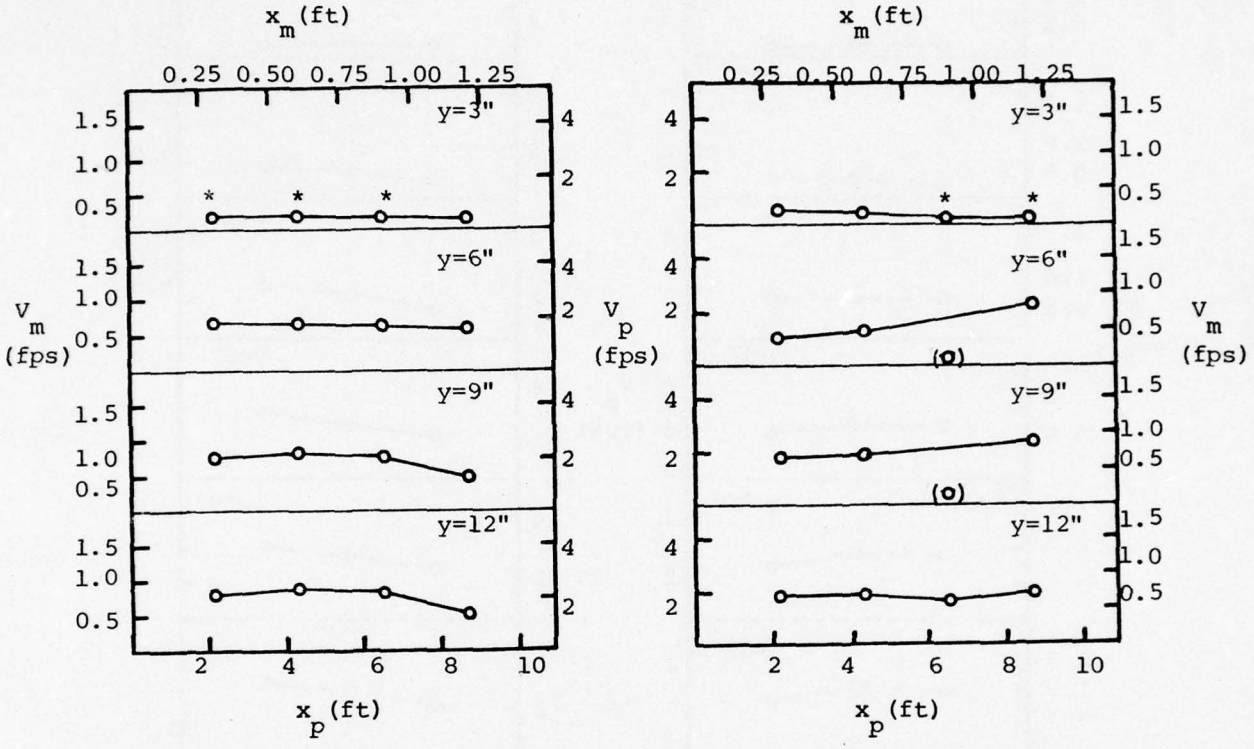

Figure 16.2 Velocity distribution (section B, one-pump operation, model depth = 15.4", no baffles). The asterisks indicate negative velocities

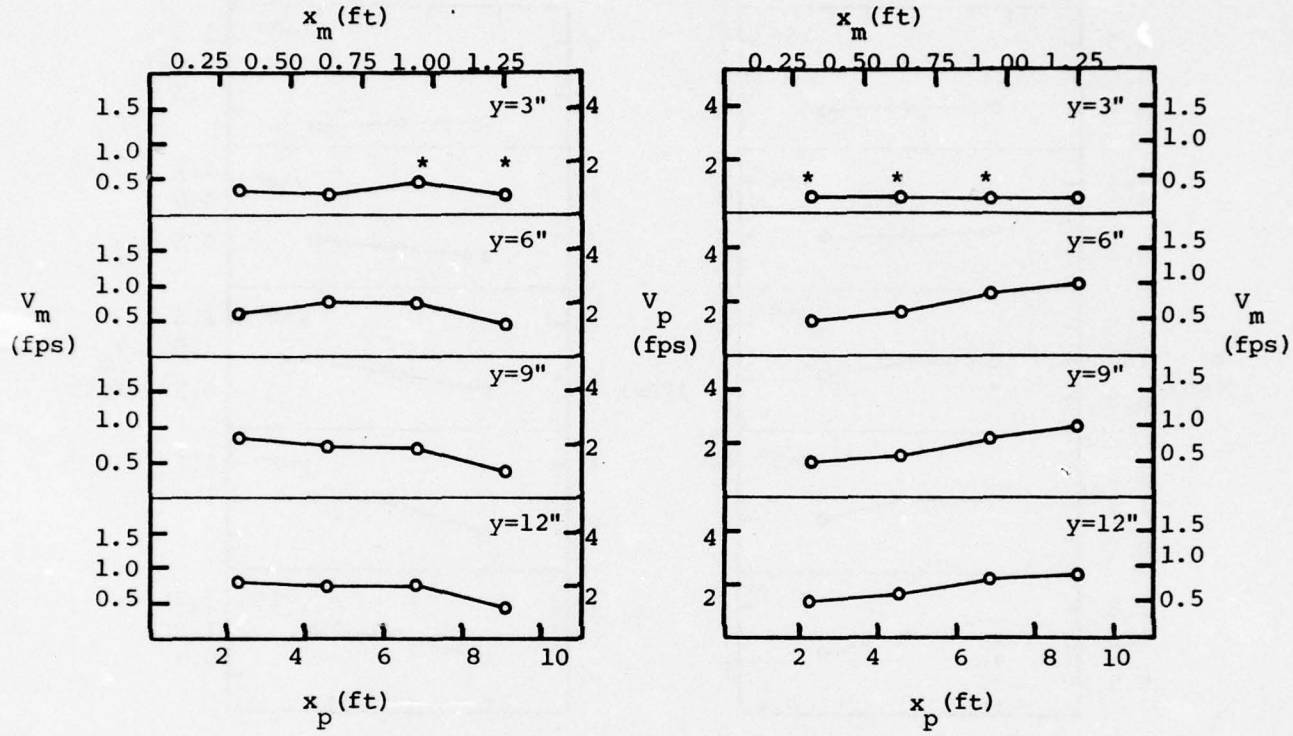

Figure 16.3 Velocity distribution (section C, one-pump operation, model depth = 15.4", no baffles). The asterisks indicate negative velocities

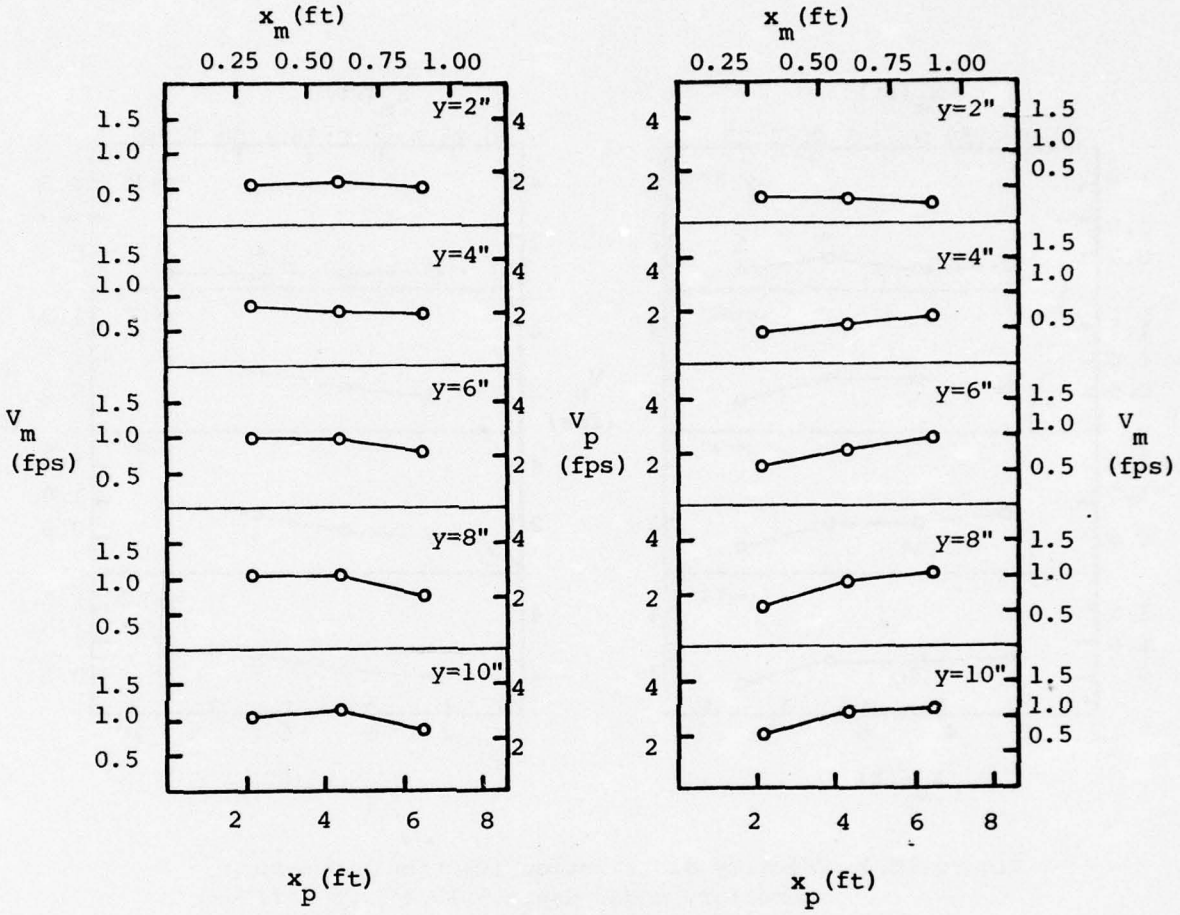

Figure 17.1 Velocity distribution (section A, two-pump operation, model depth = 12", no baffles)

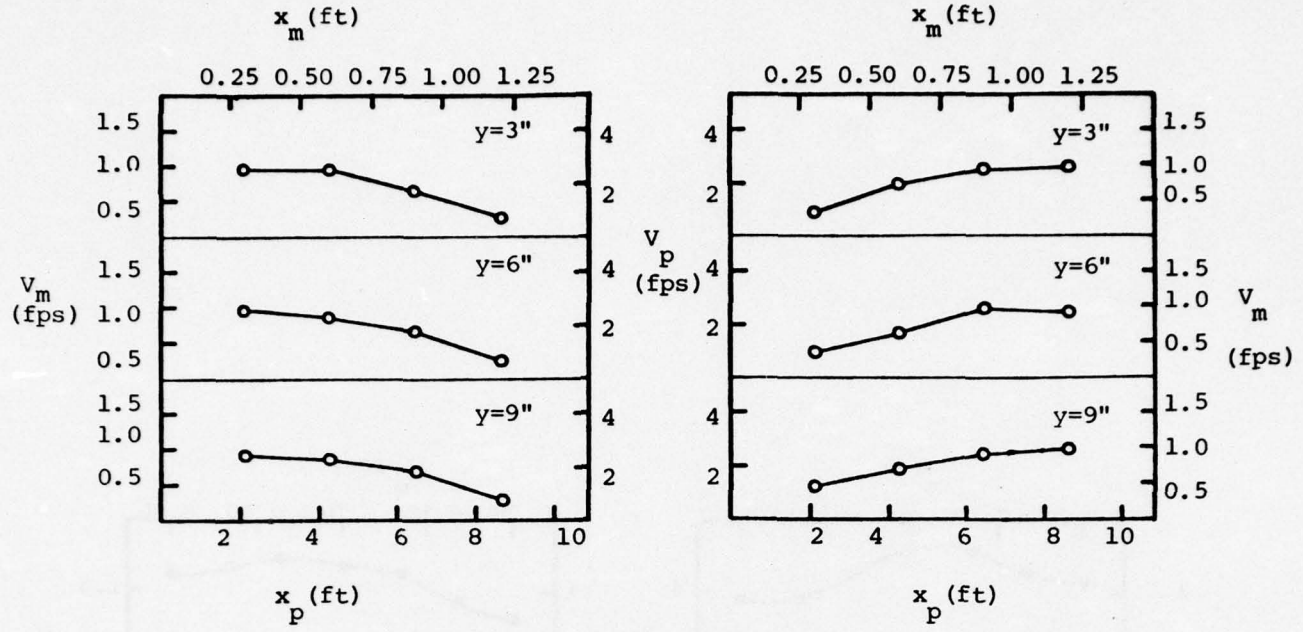

Figure 17.2 Velocity distribution (section B, two-pump operation, model depth = 12", no baffles)

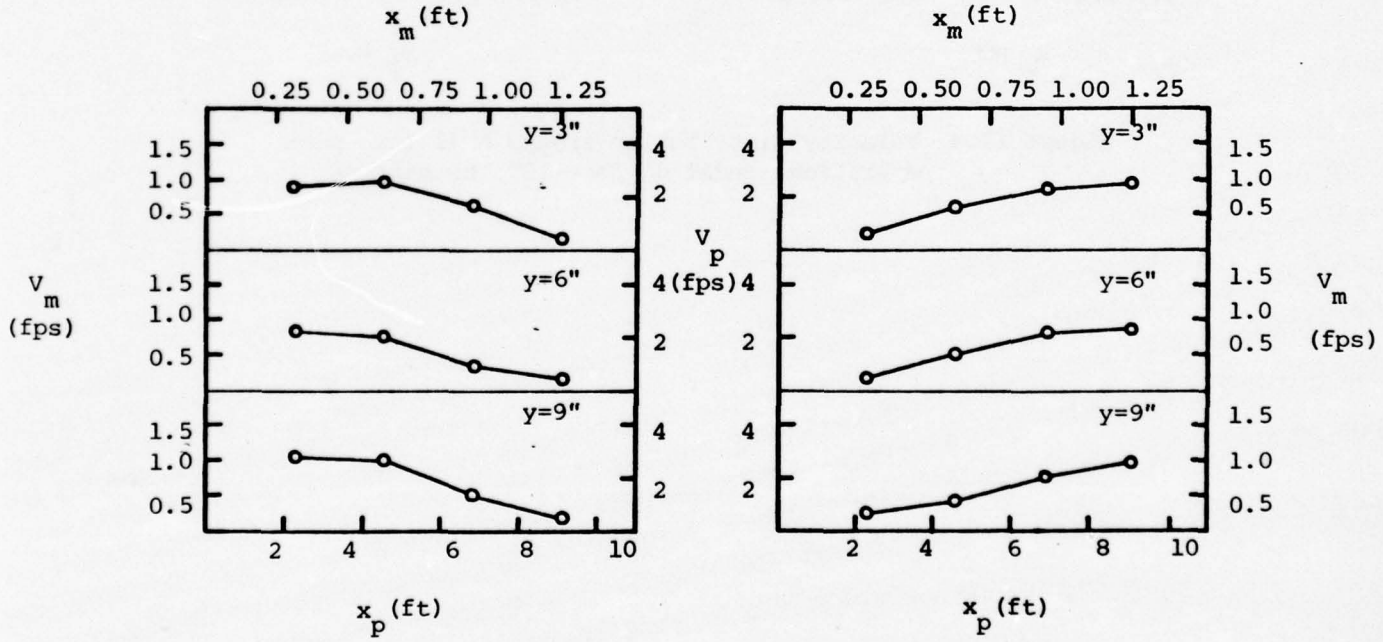

Figure 17.3 Velocity distribution (section C, two-pump operation, model depth = 12", no baffles)

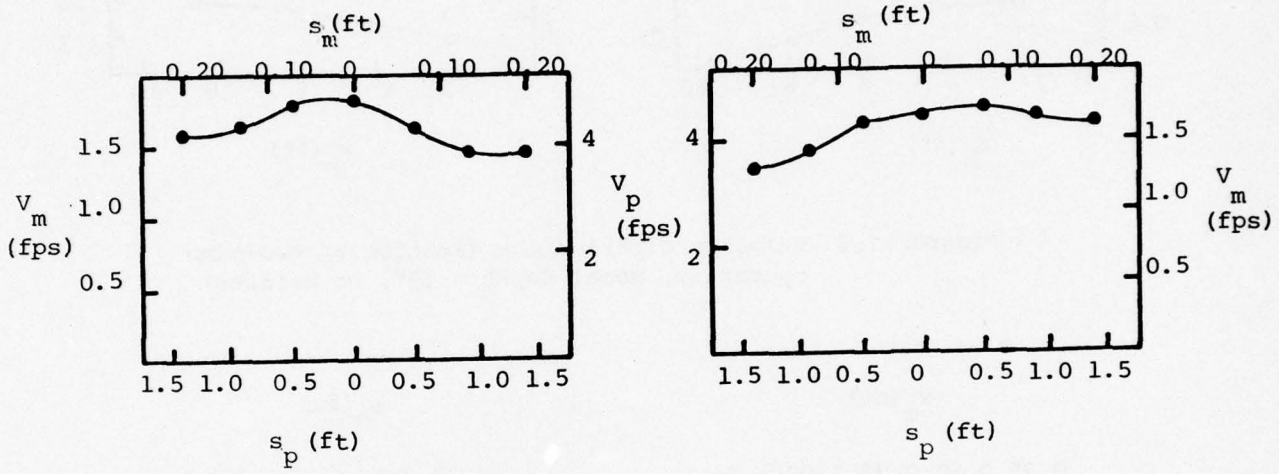

Figure 17.4 Velocity distribution around bell (two-pump operation, model depth = 12", no baffles)

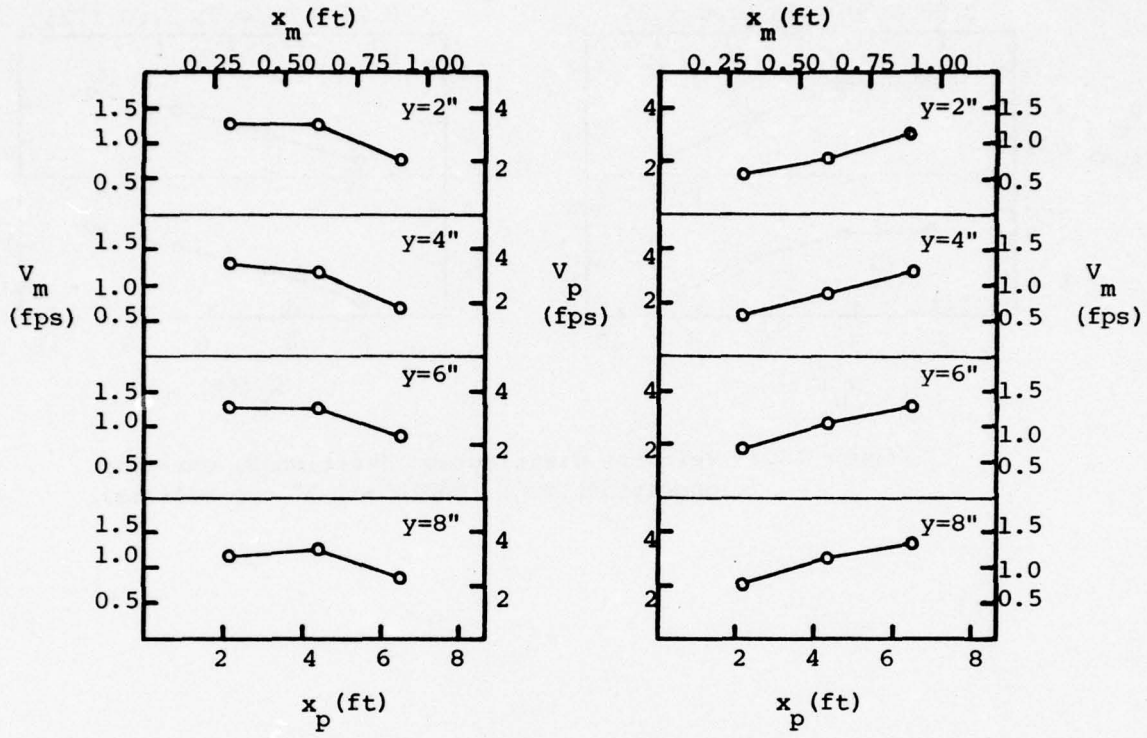

Figure 18.1 Velocity distribution (section A, one-pump operation, model depth = 8.5", no baffles)

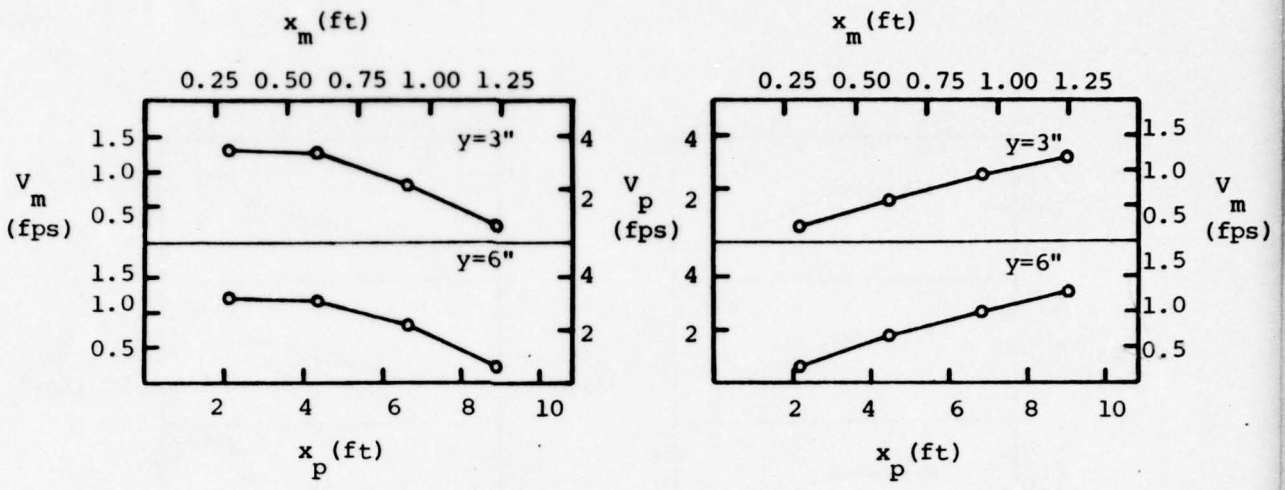

Figure 18.2 Velocity distribution (section B, one-pump operation, model depth = 8.5", no baffles)

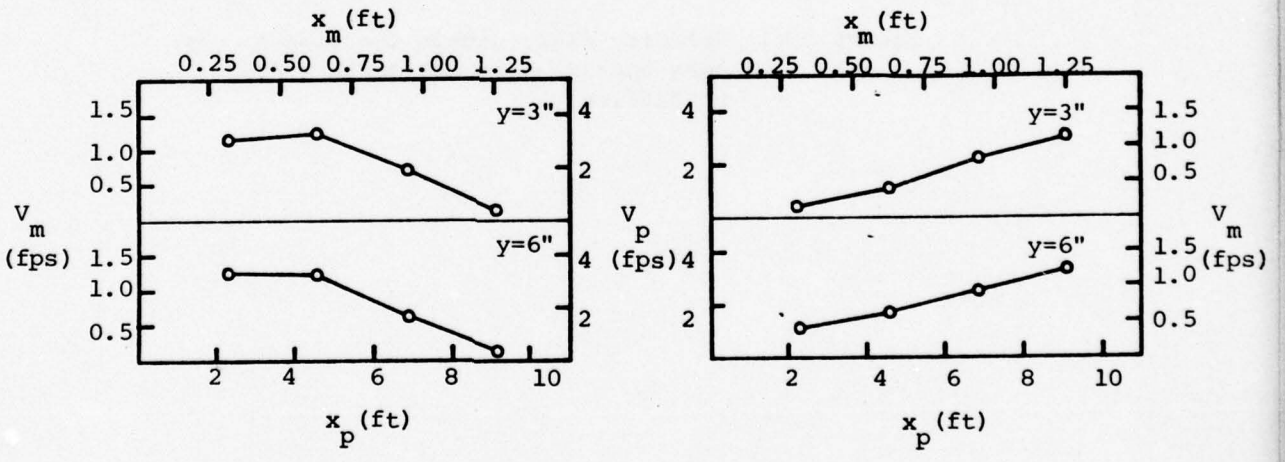

Figure 18.3 Velocity distribution (section C, one-pump operation, model depth = 8.5", no baffles)

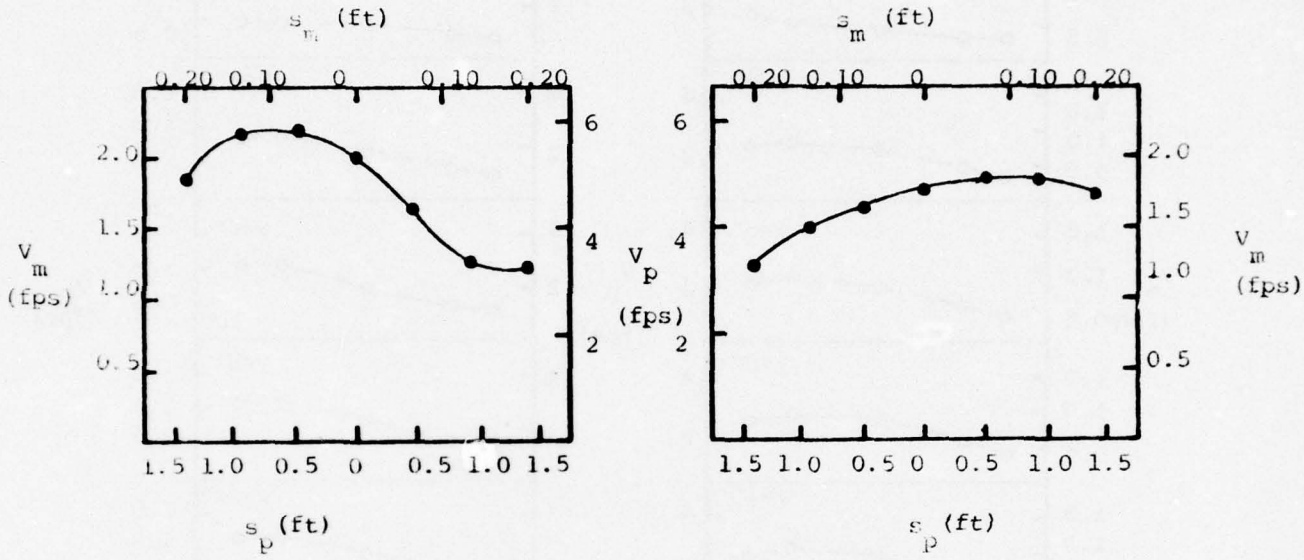

Figure 18.4 Velocity distribution around bell (one-pump operation, model depth = 8.5", no baffles)

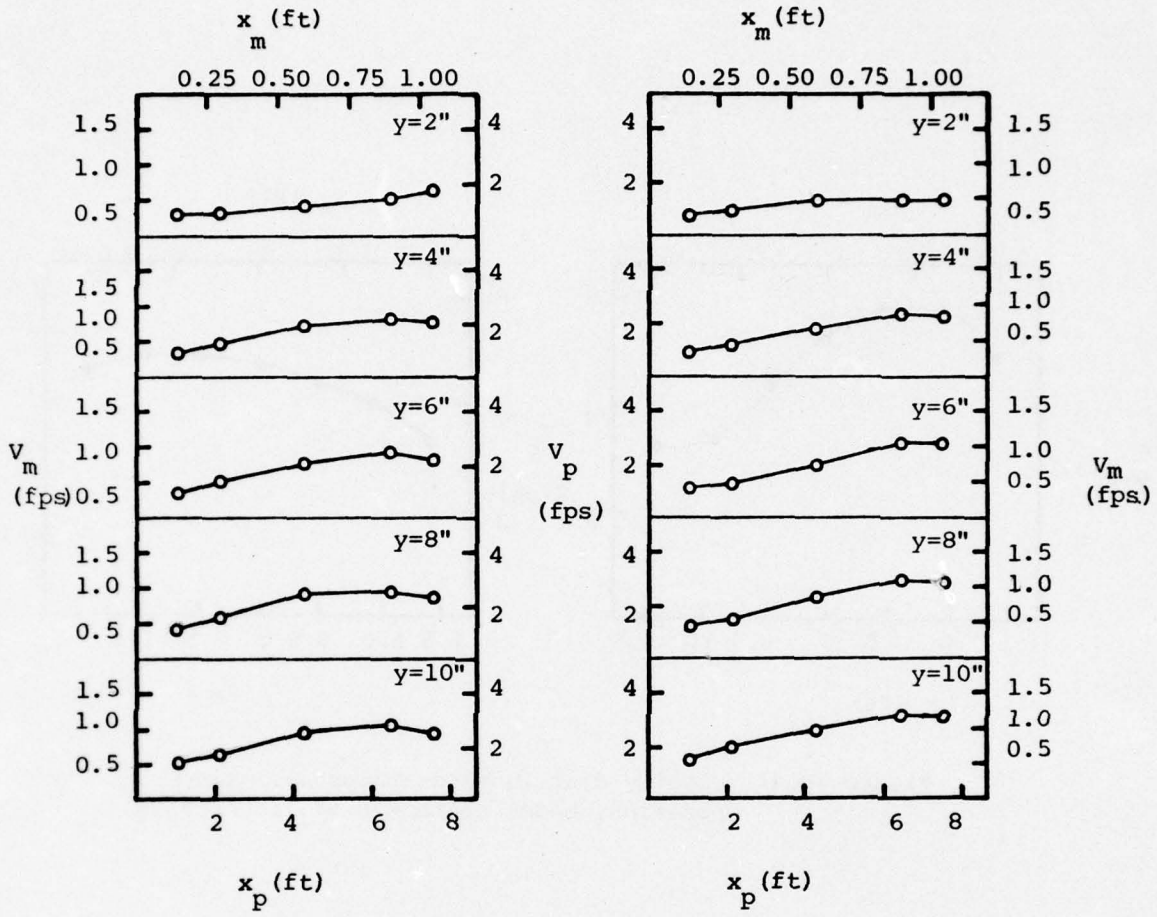

Figure 19. Velocity distribution (section A, two-pump operation, model depth = 12", case 1)

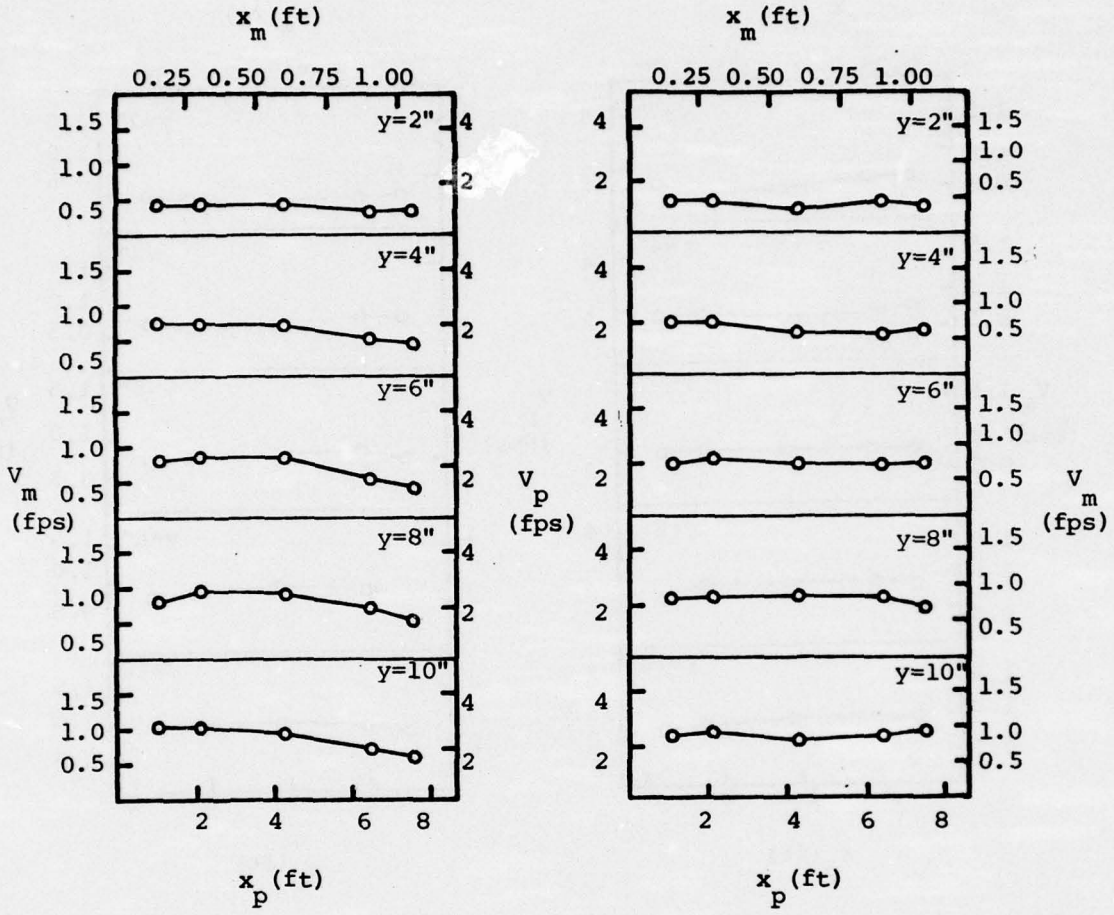

Figure 20. Velocity distribution (section A, two-pump operation, model depth = 12", case 2)

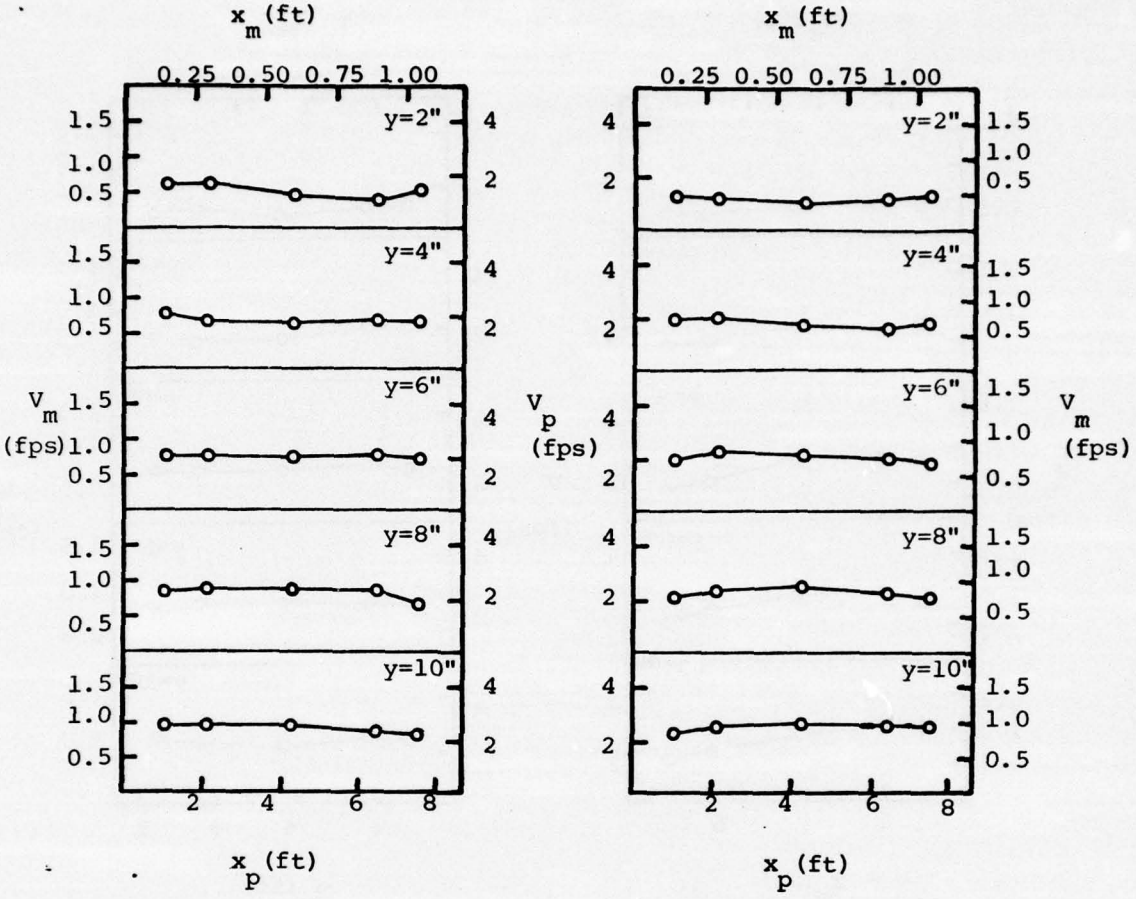

Figure 21. Velocity distribution (section A, two-pump operation, model depth = 12", case 3)

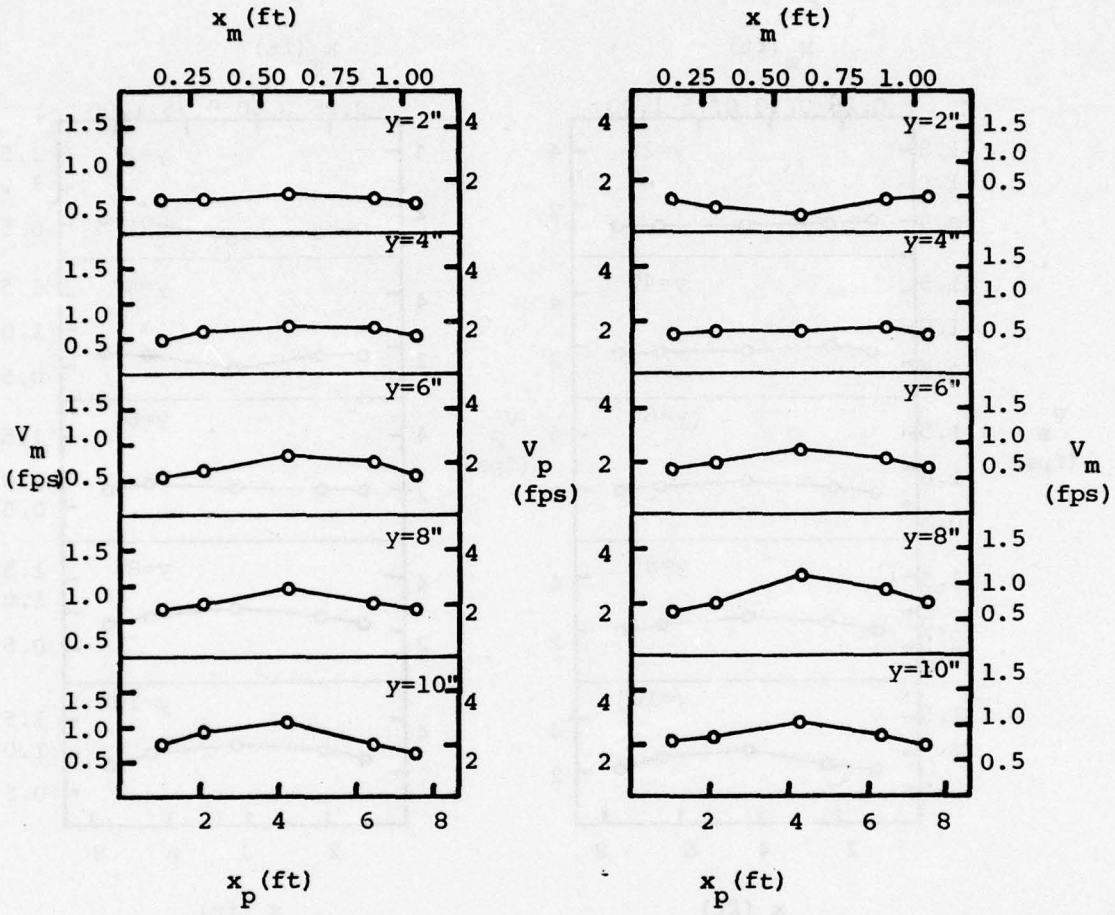

Figure 22. Velocity distribution (section A, two-pump operation, model depth = 12", case 4)

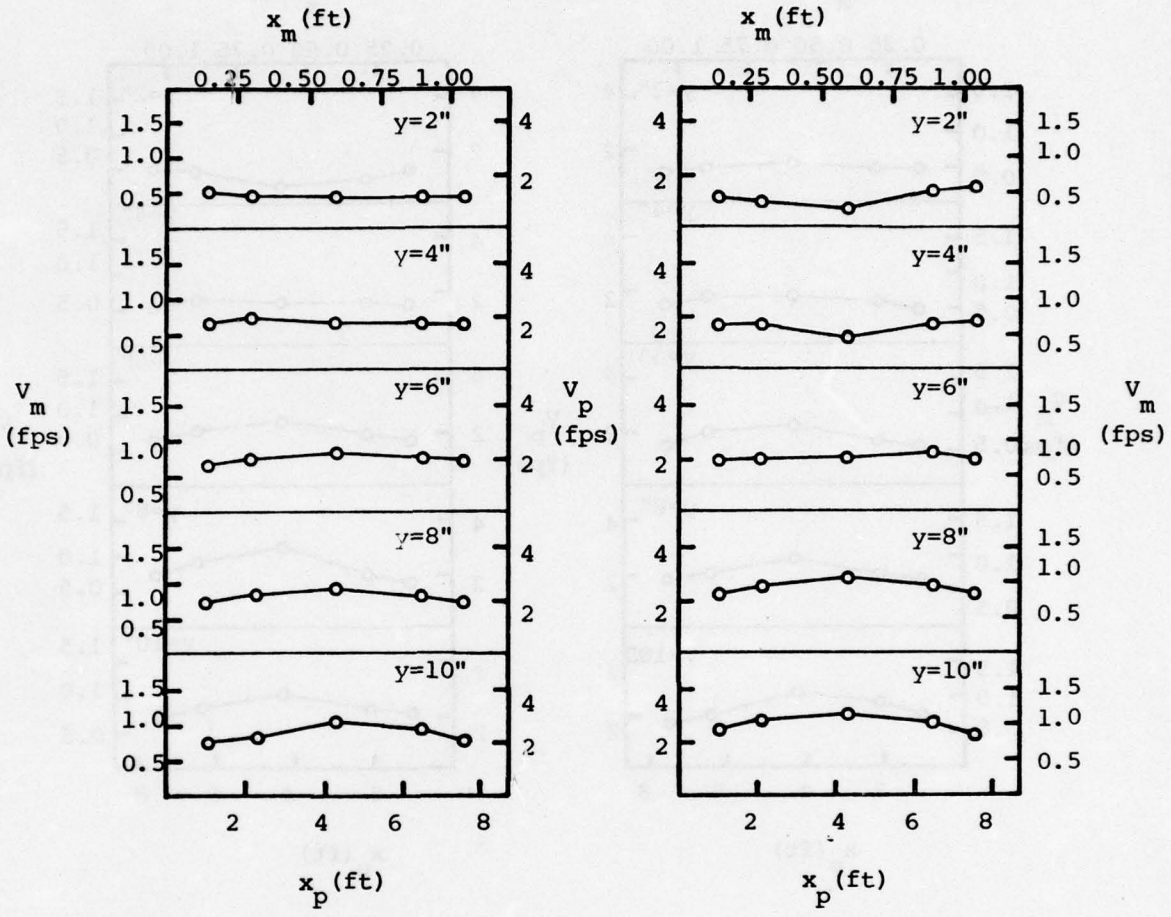

Figure 23. Velocity distribution (section A, two-pump operation, model depth = 12", case 5)

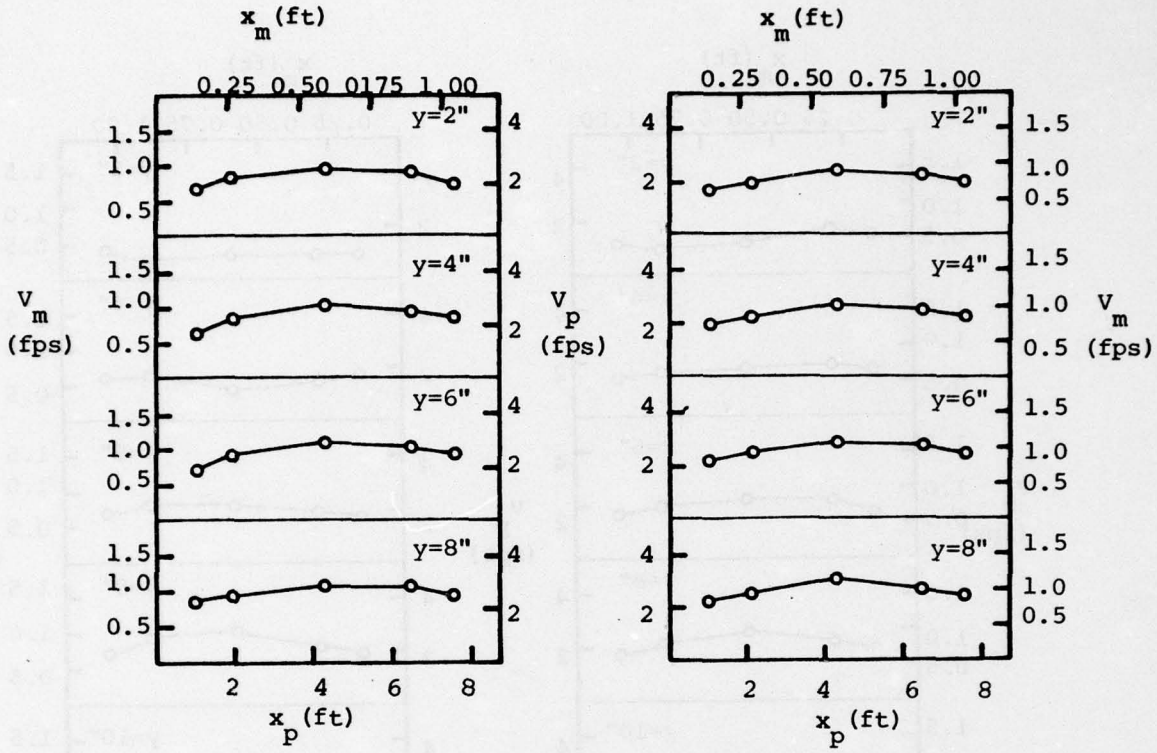

Figure 24. Velocity distribution (section A, one-pump operation, model depth = 8.5", case 5)

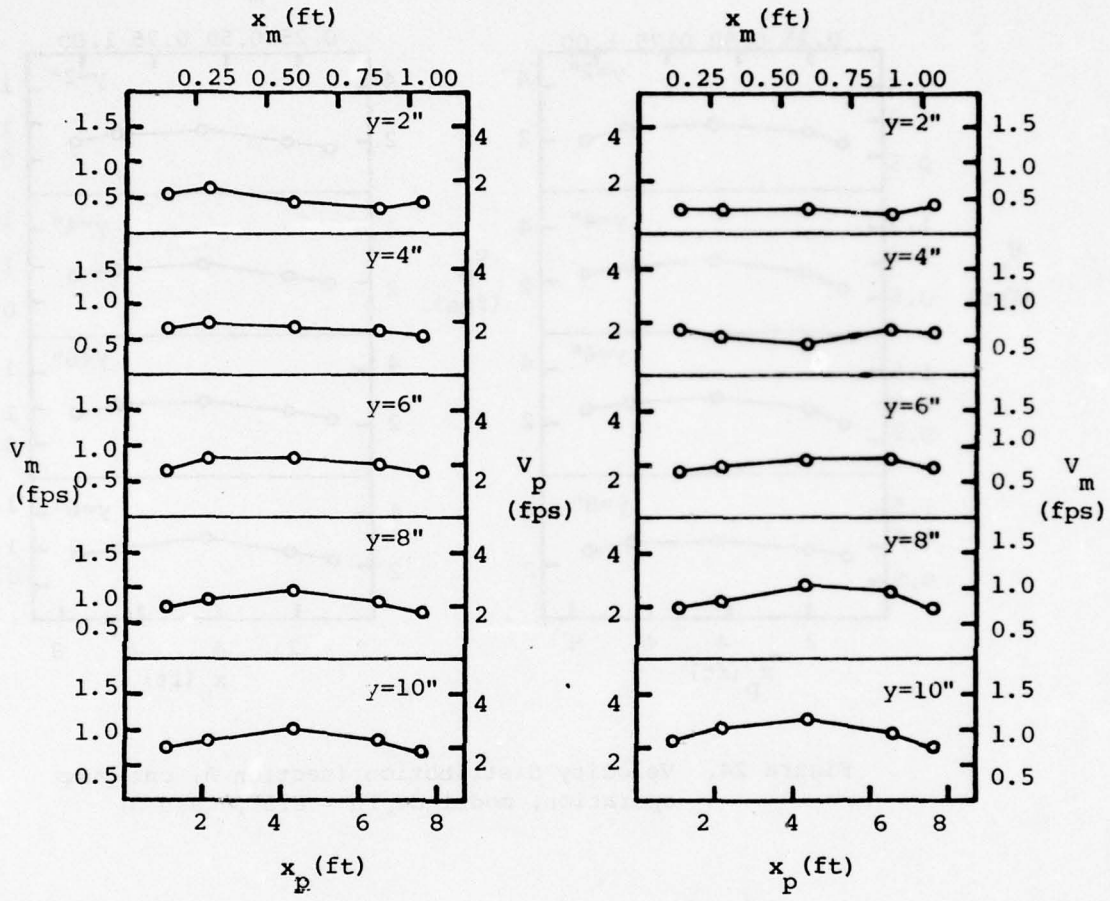

Figure 25. Velocity distribution (section A, two-pump operation, model depth = 8.5", case 6)

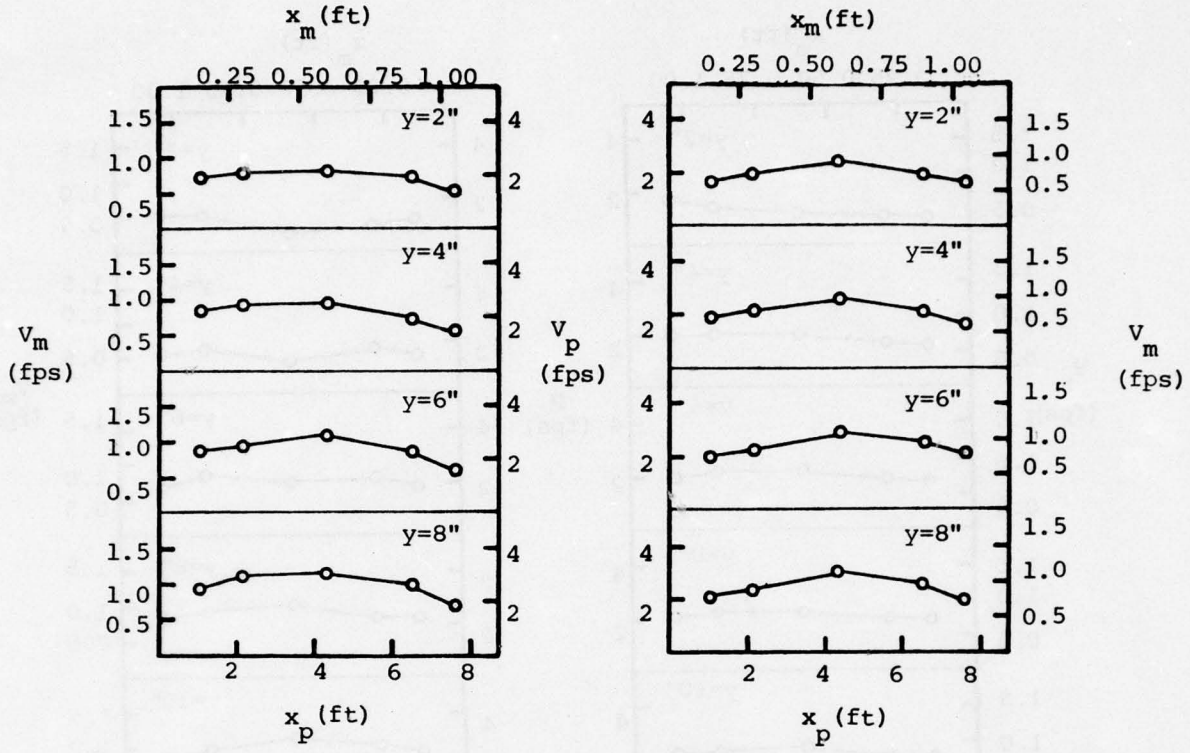

Figure 26. Velocity distribution (section A, one-pump operation, model depth = 8.5", case 6)

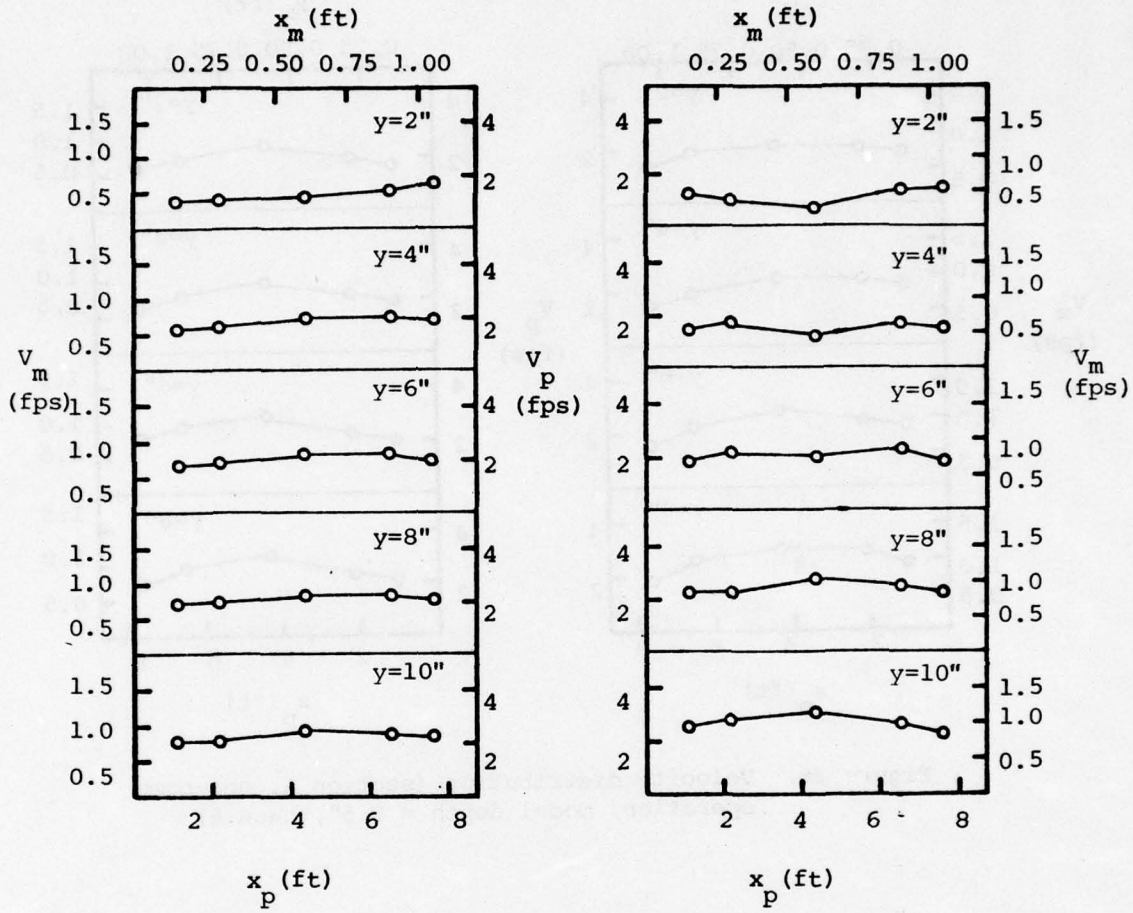

Figure 27. Velocity distribution (section A, two-pump operation, model depth = 12", case 7)

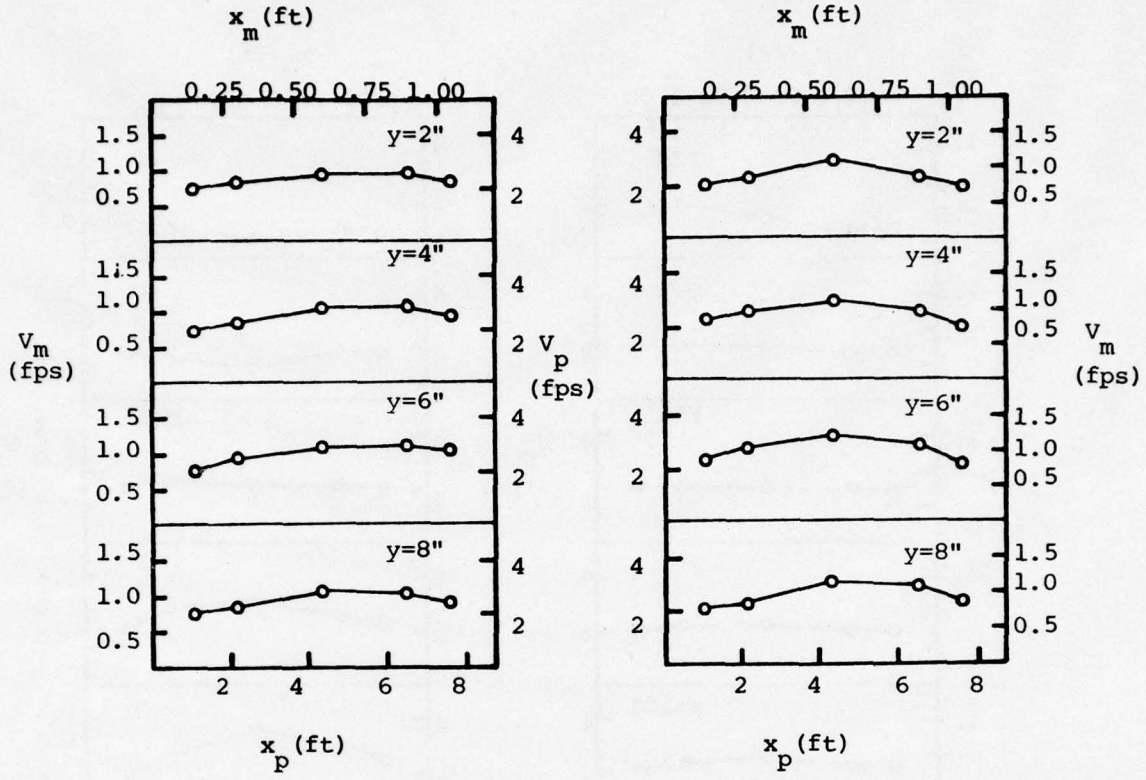

Figure 28. Velocity distribution (section A, one-pump operation, model depth = 8.4", case 7)

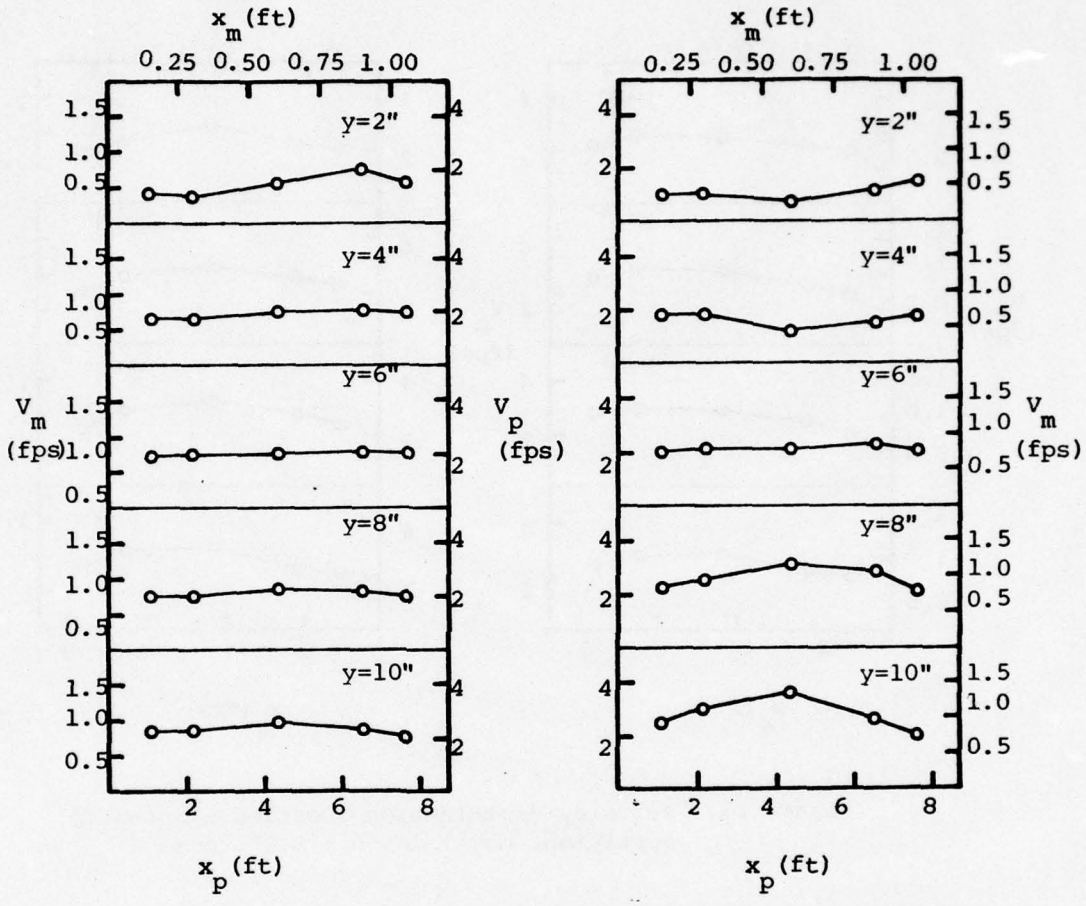

Figure 29. Velocity distribution (section A, two-pump operation, model depth = 12", case 8)

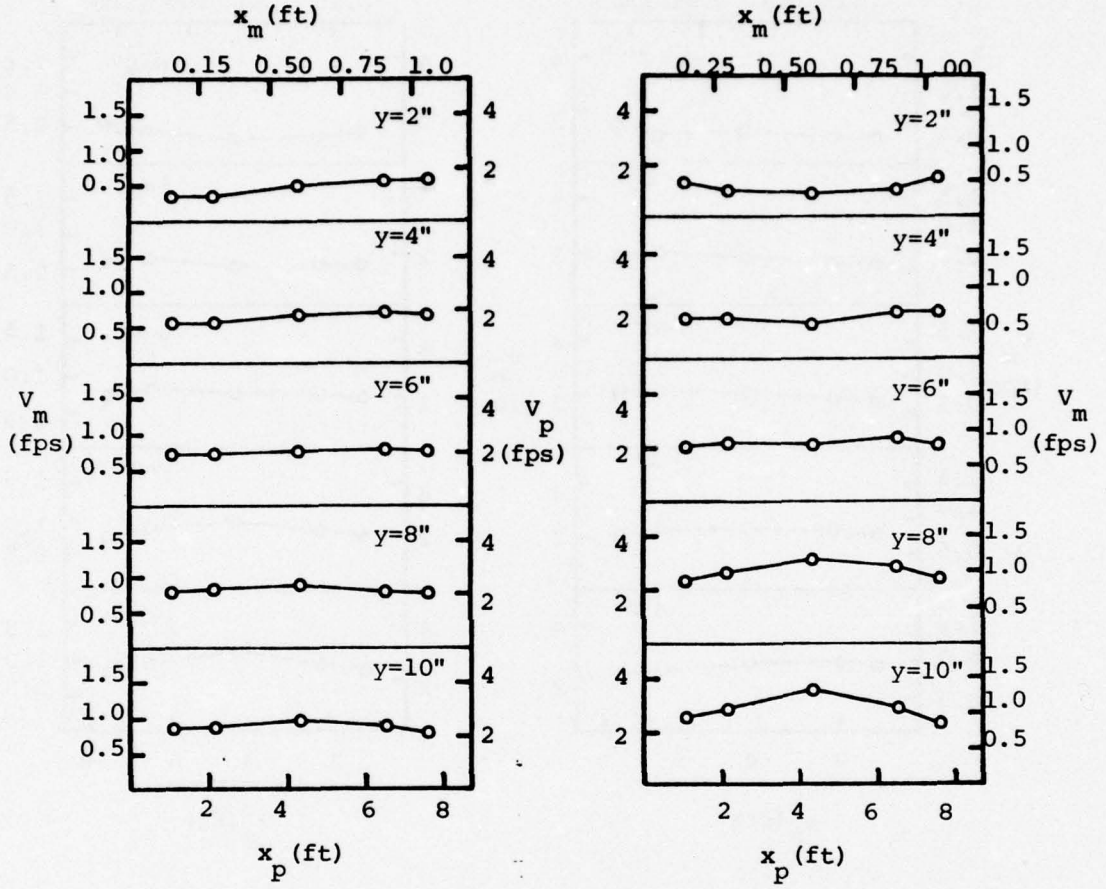

Figure 30. Velocity distribution (section A, two-pump operation, model depth = 12", case 9)

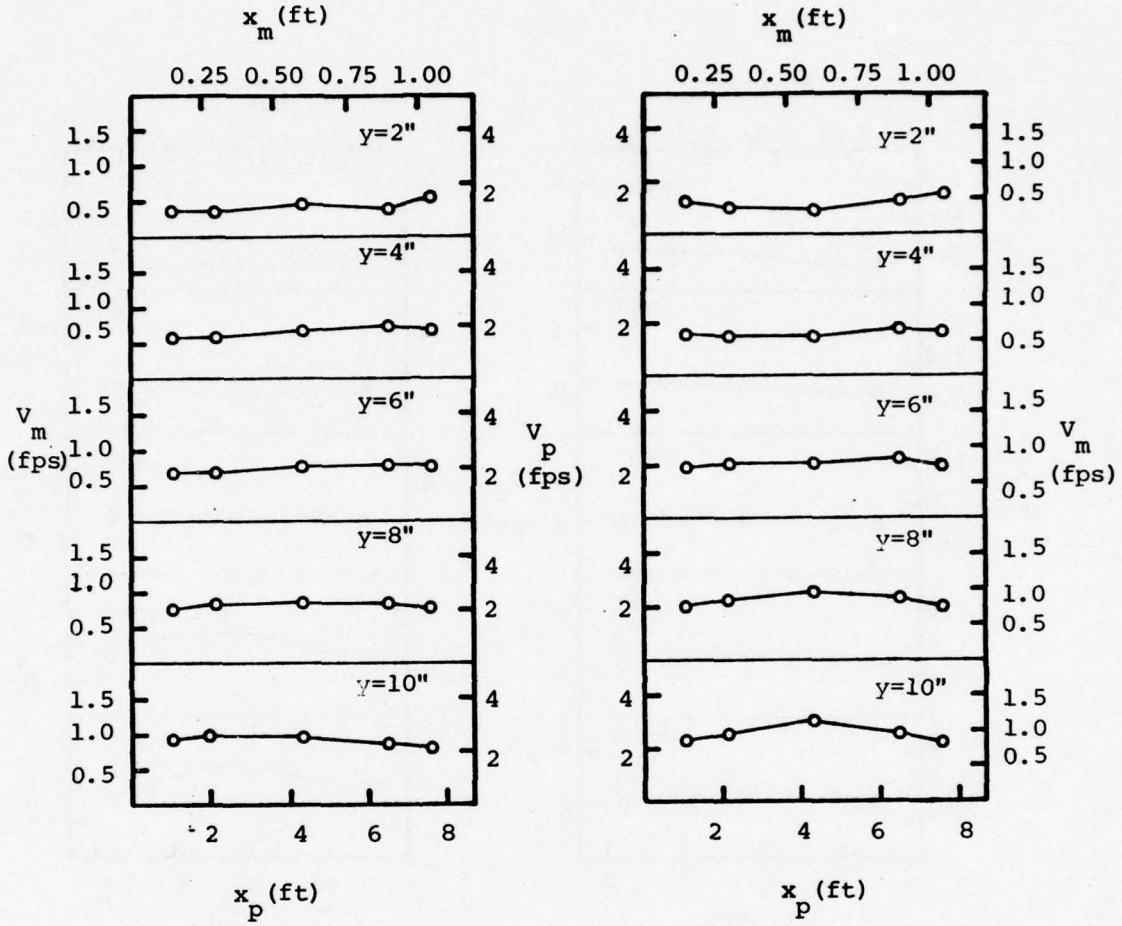

Figure 31. Velocity distribution (section A, two-pump operation, model depth = 12", case 10)

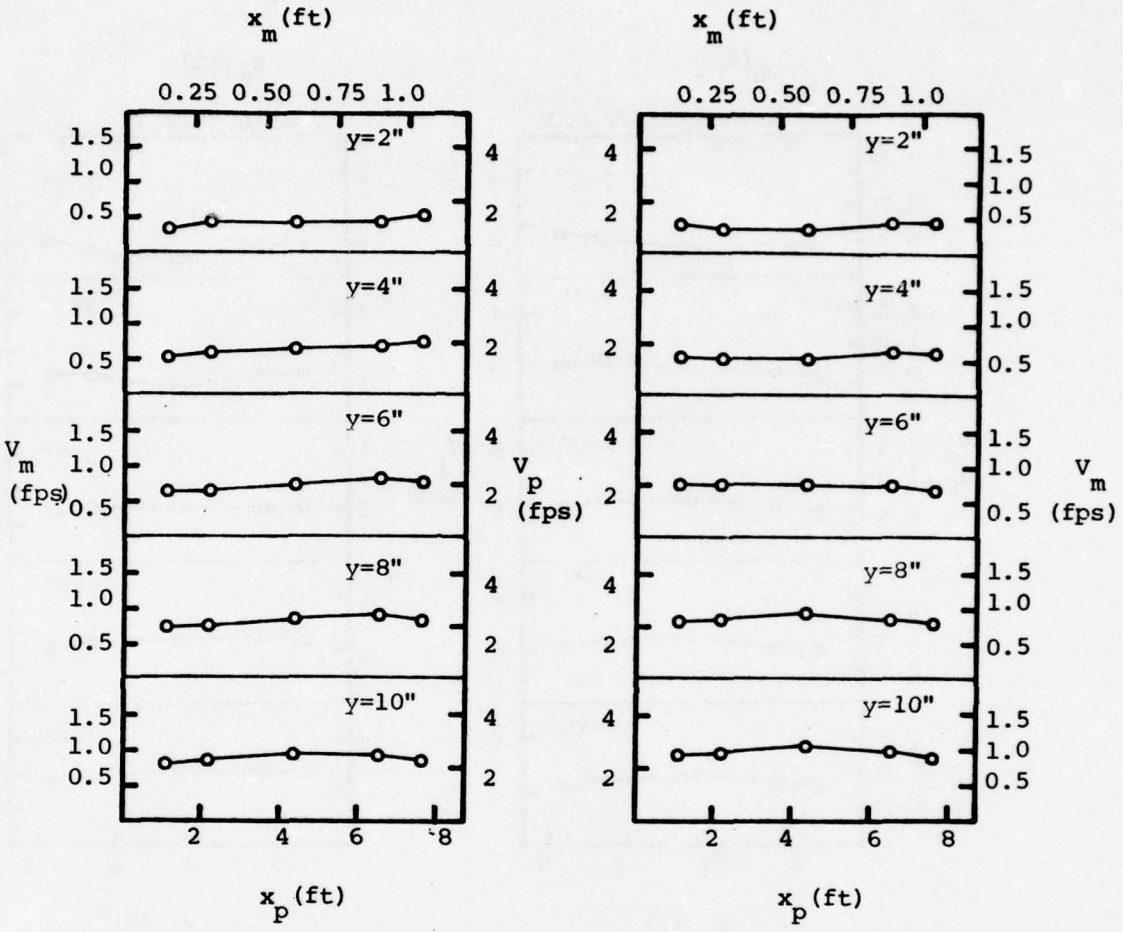

Figure 32. Velocity distribution (section A, two-pump operation, model depth = 12", case 11)

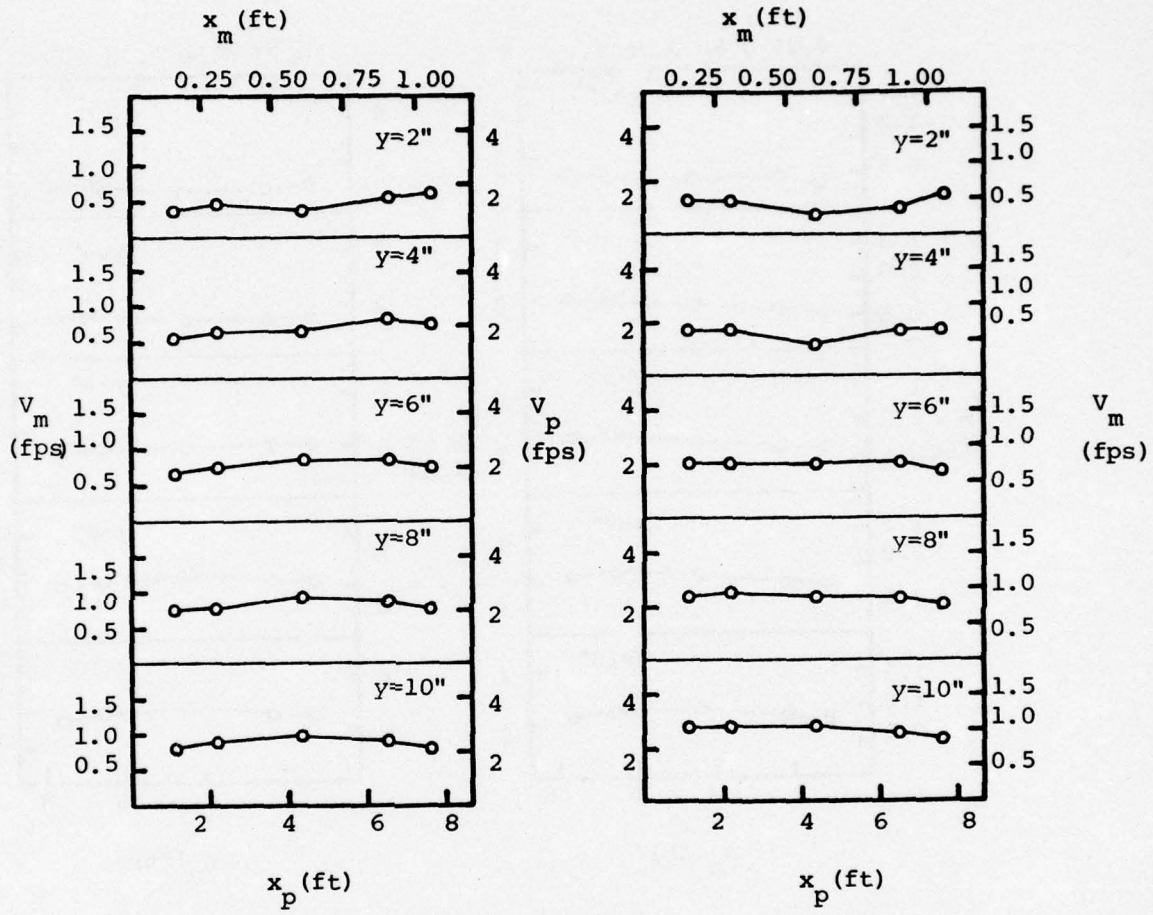

Figure 33.1. Velocity distribution (section A, two-pump operation, model depth = 12", case 12)

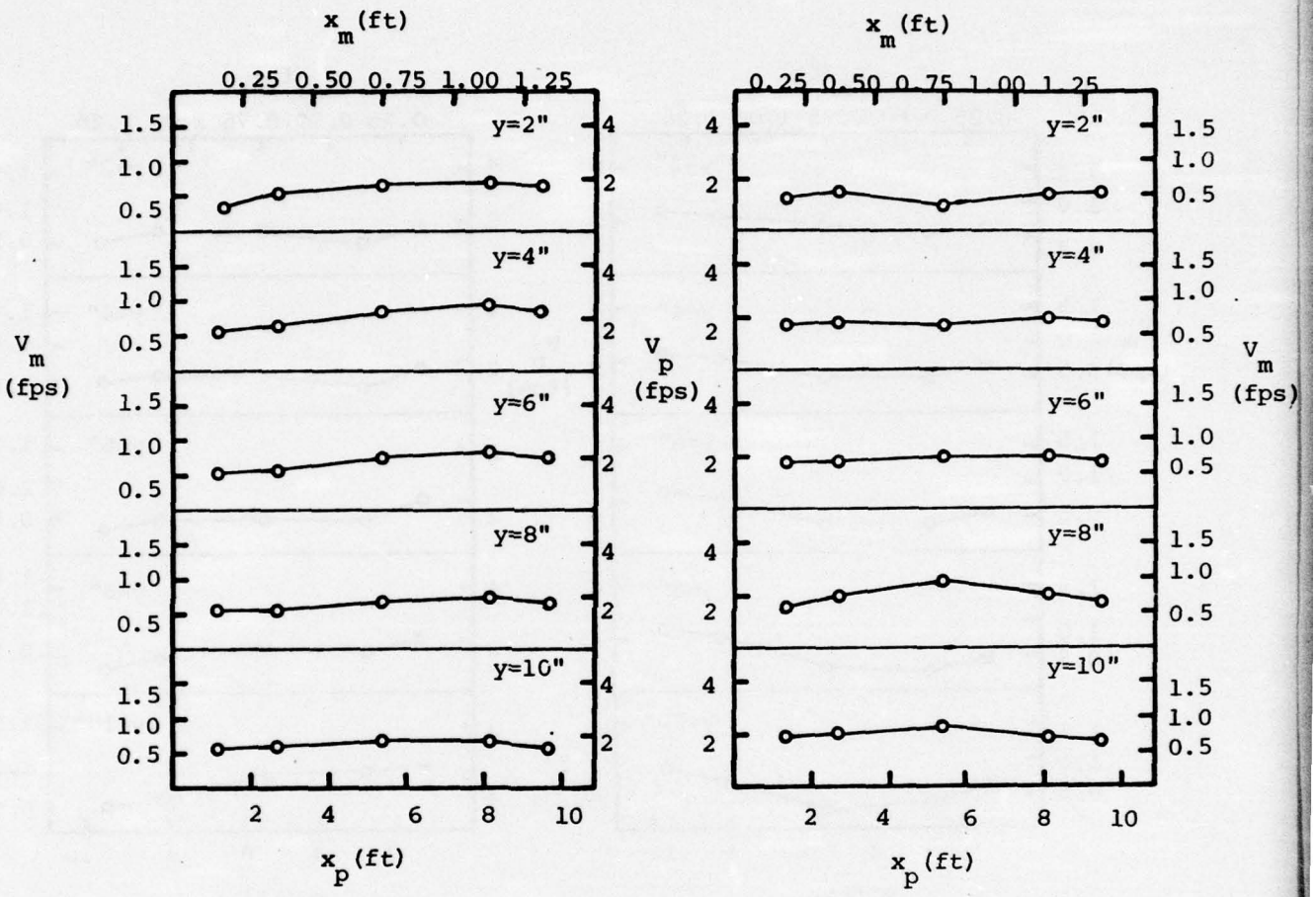

Figure 33.2. Velocity distribution (section B, two-pump operation, model depth = 12", case 12)

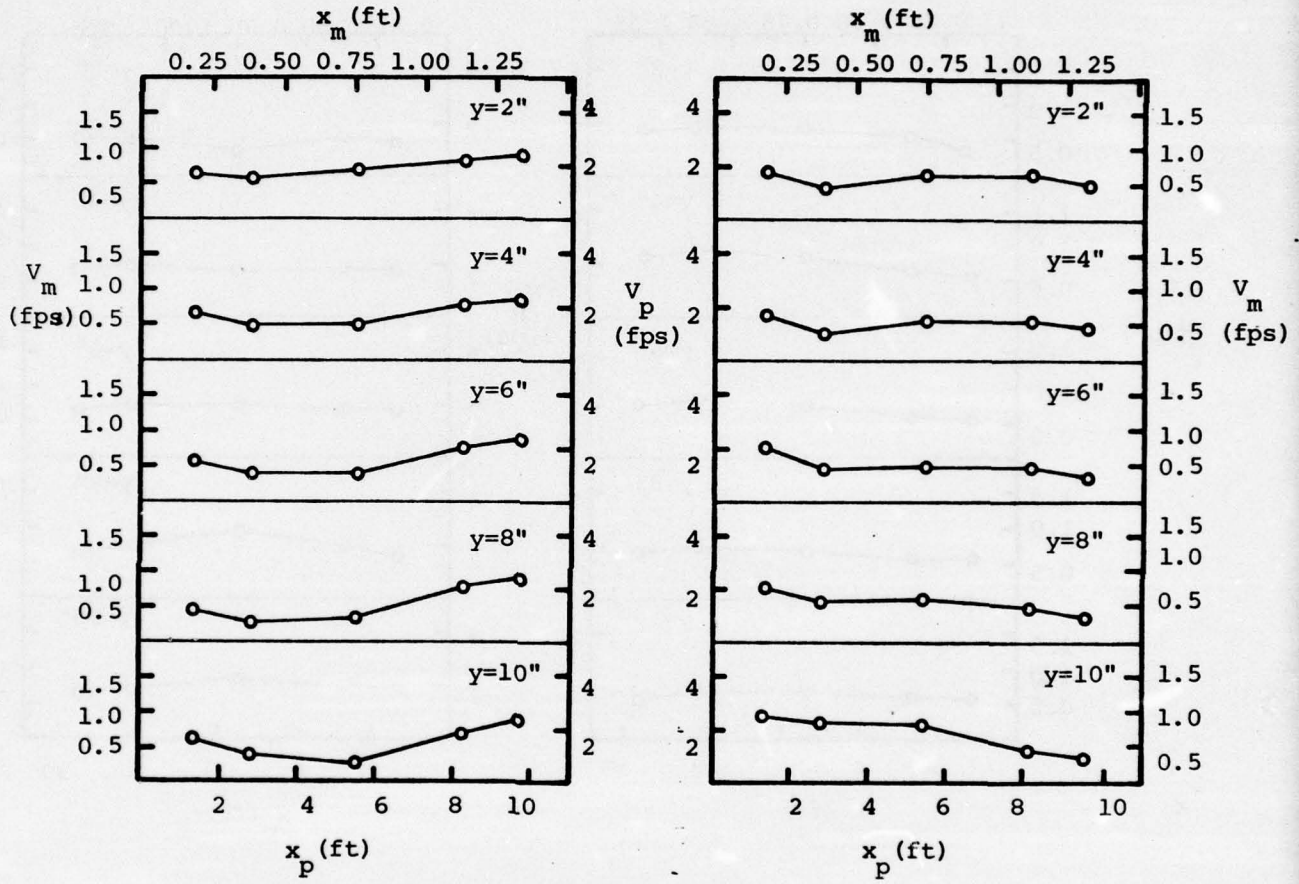

Figure 33.3. Velocity distribution (section C, two-pump operation, model depth = 12", case 12)

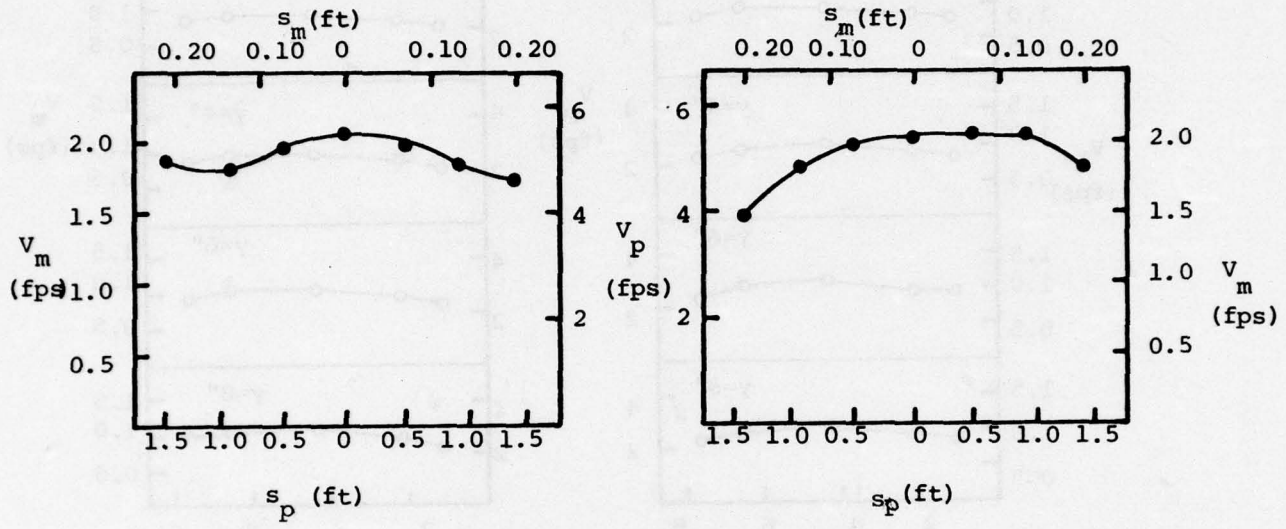

Figure 33.4. Velocity distribution around syphon bell (two-pump operation, model depth = 12", case 12)

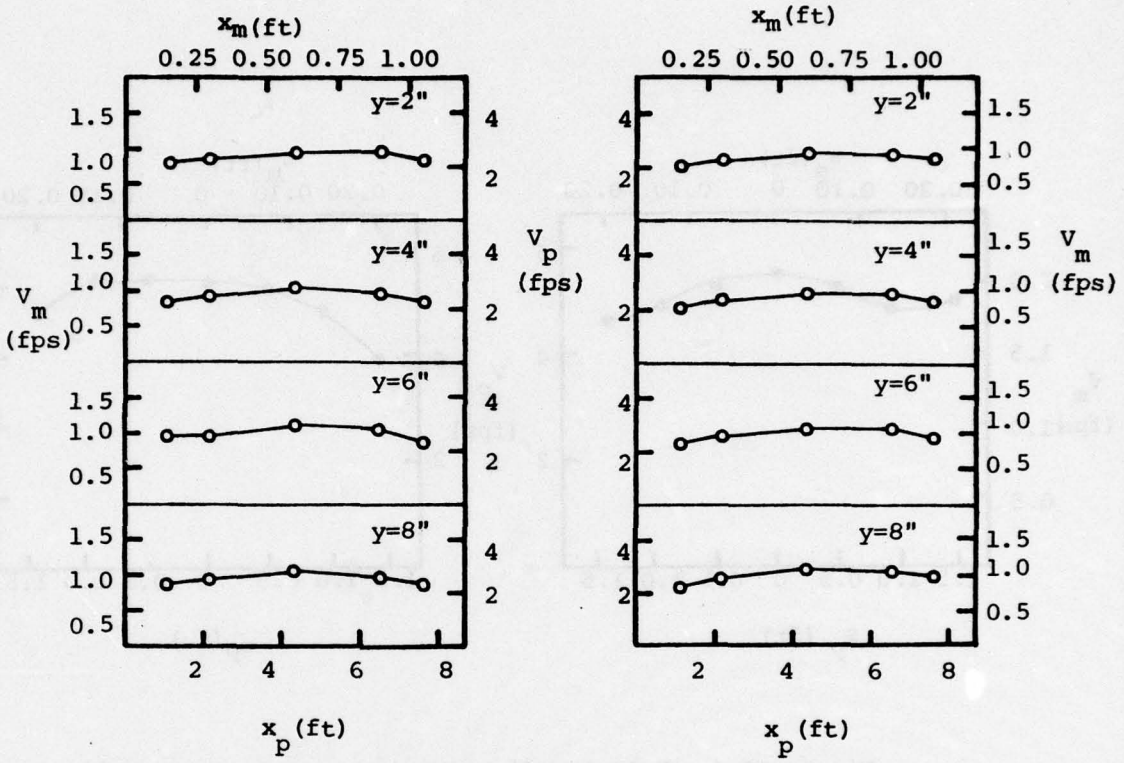

Figure 34.1. Velocity distribution (section A, one-pump operation, model depth = 8.5", case 12)

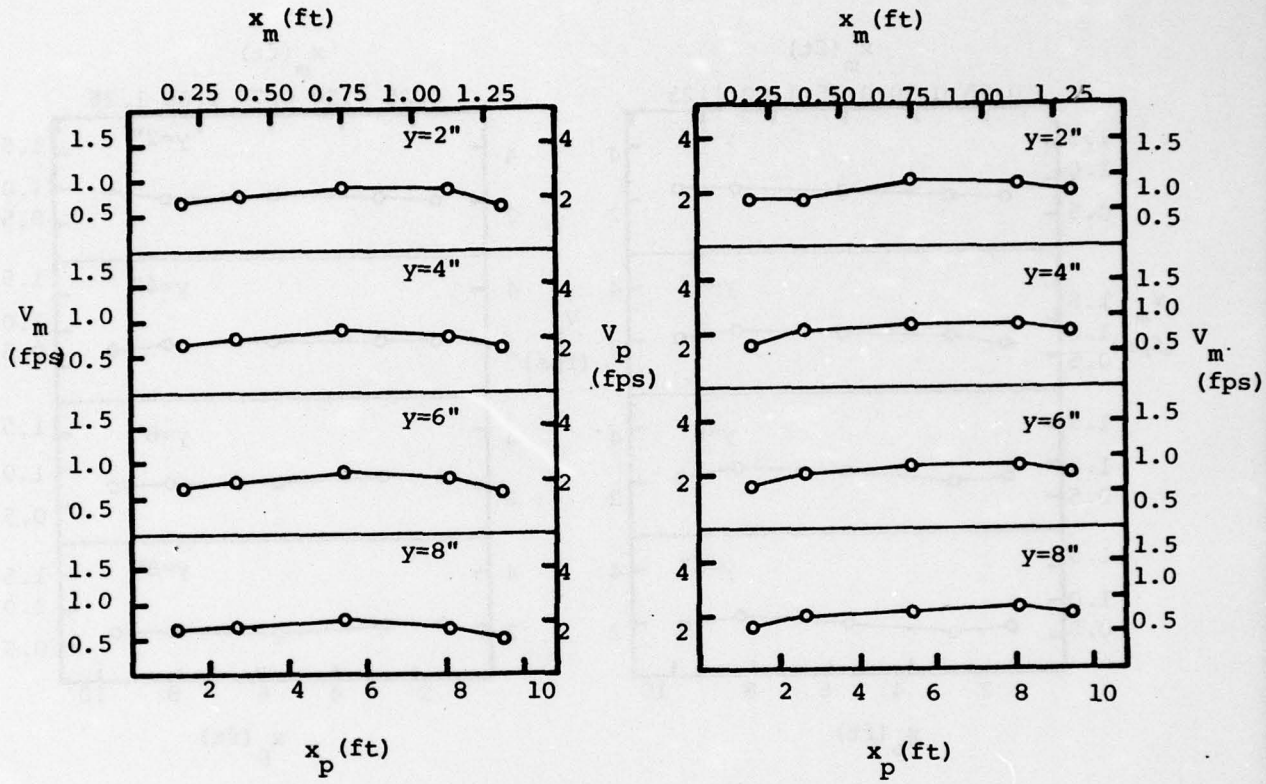

Figure 34.2. Velocity distribution (section B, one-pump operation, model depth = 8.5", case 12)

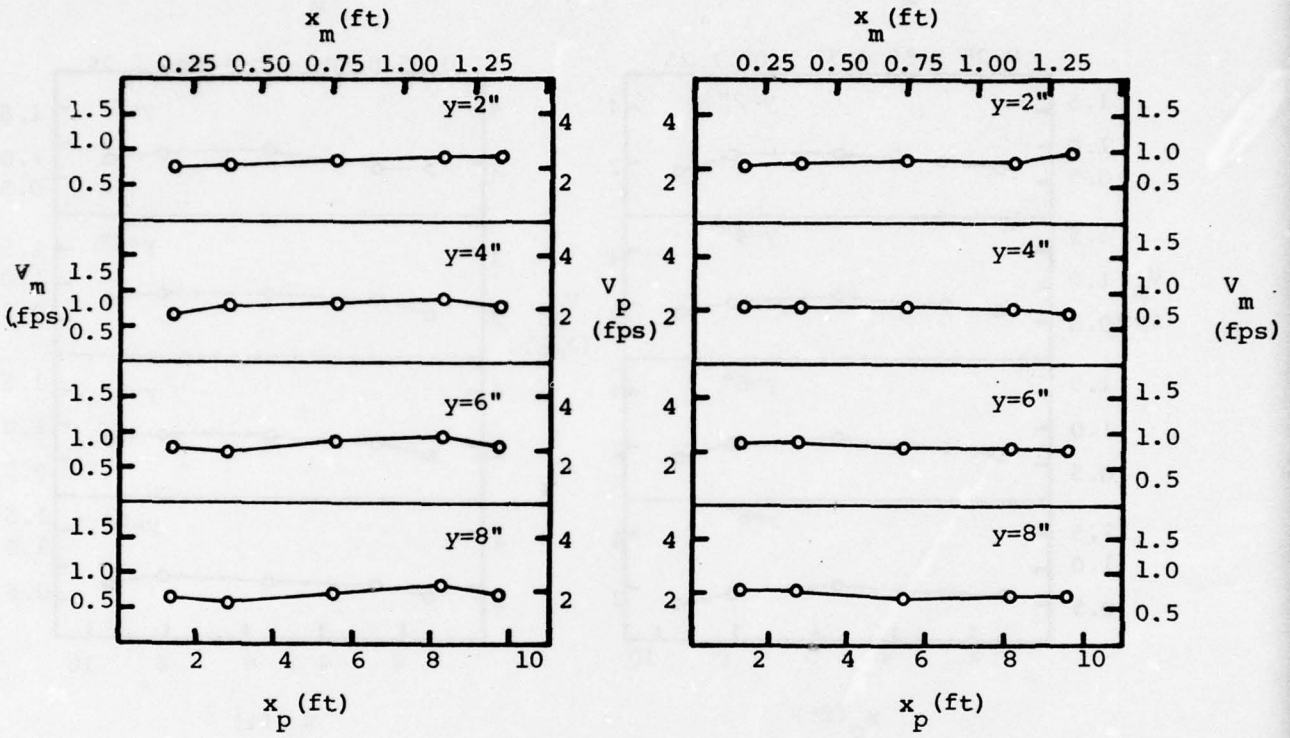

Figure 34.3. Velocity distribution (section C, one-pump operation, model depth = 8.5", case 12)

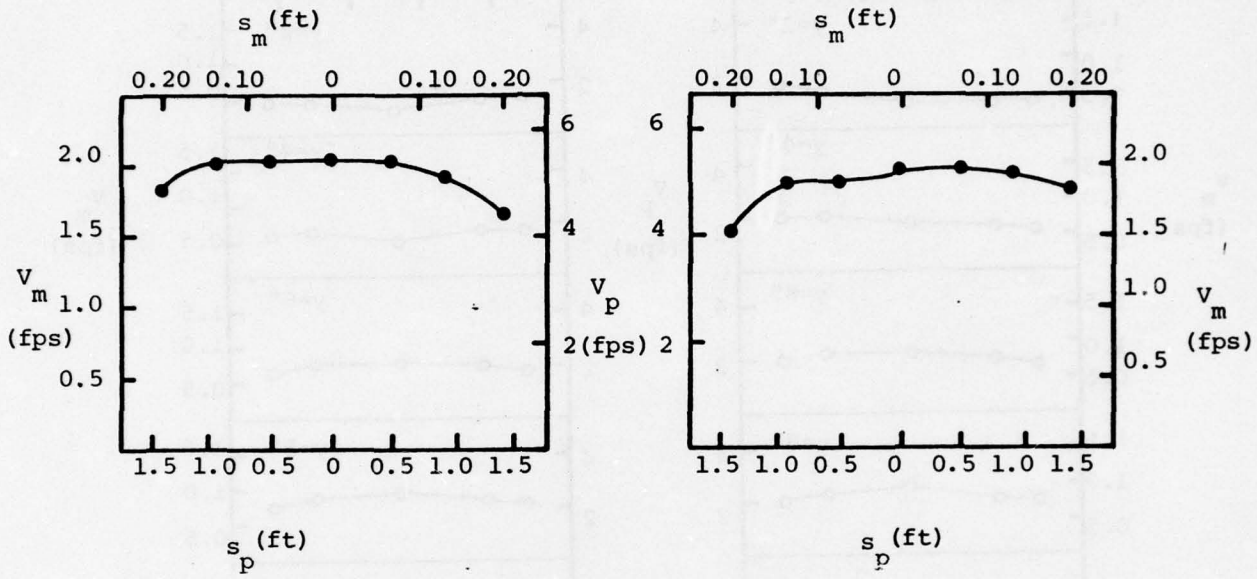

Figure 34.4 Velocity distribution around syphon bell (one-pump operation, model depth = 8.5", case 12)

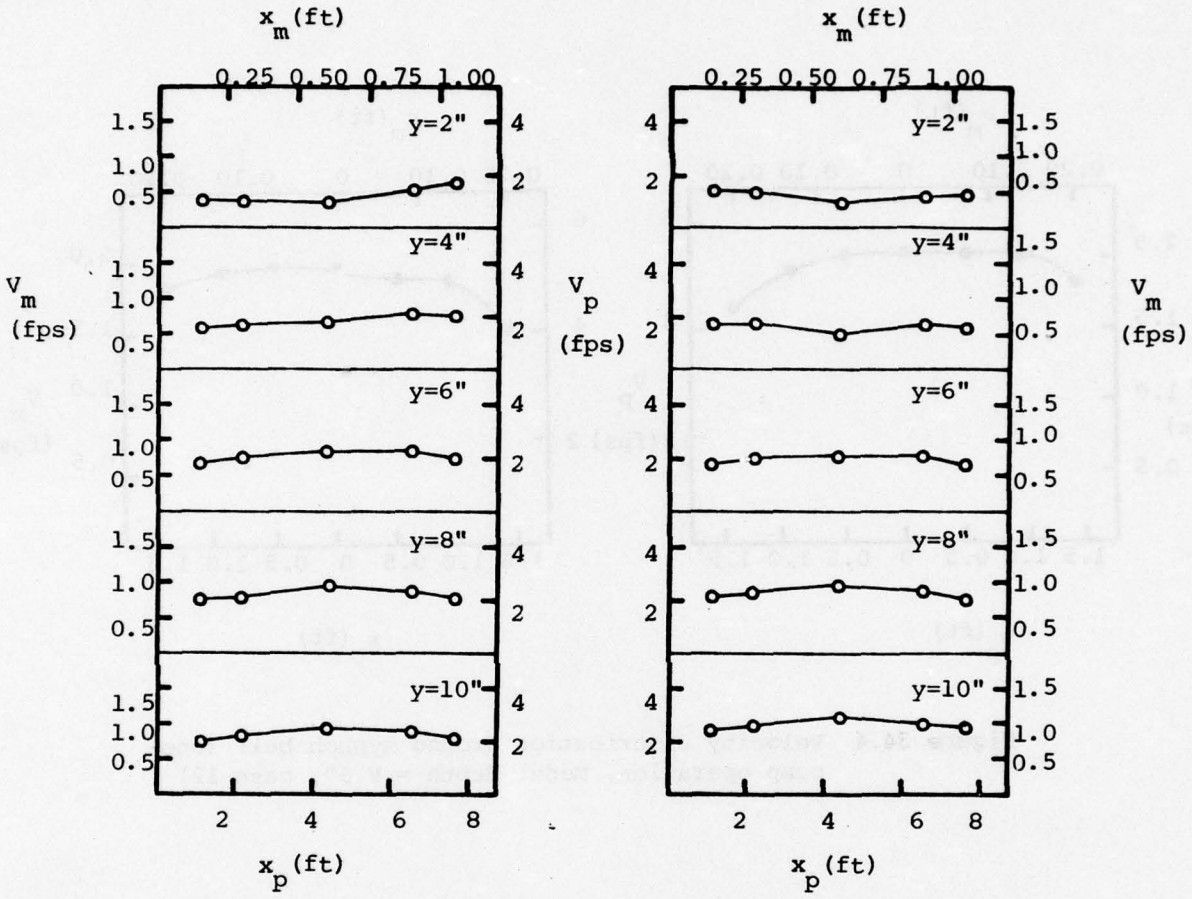

Figure 35.1 Velocity distribution (section A, two-pump operation, model depth = 12", case 13)

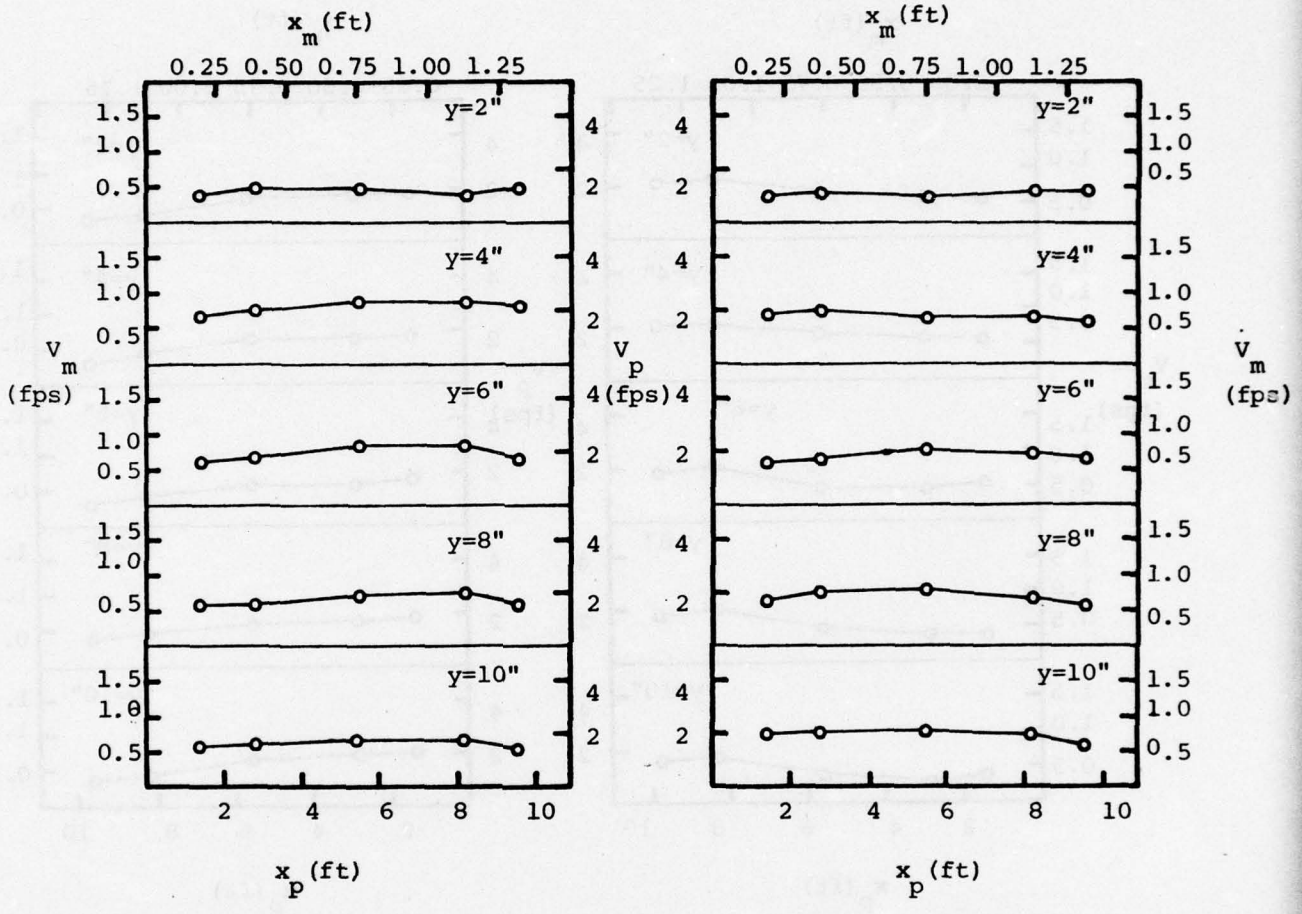

Figure 35.2. Velocity distribution (section B, two-pump operation, model depth = 12", case 13)

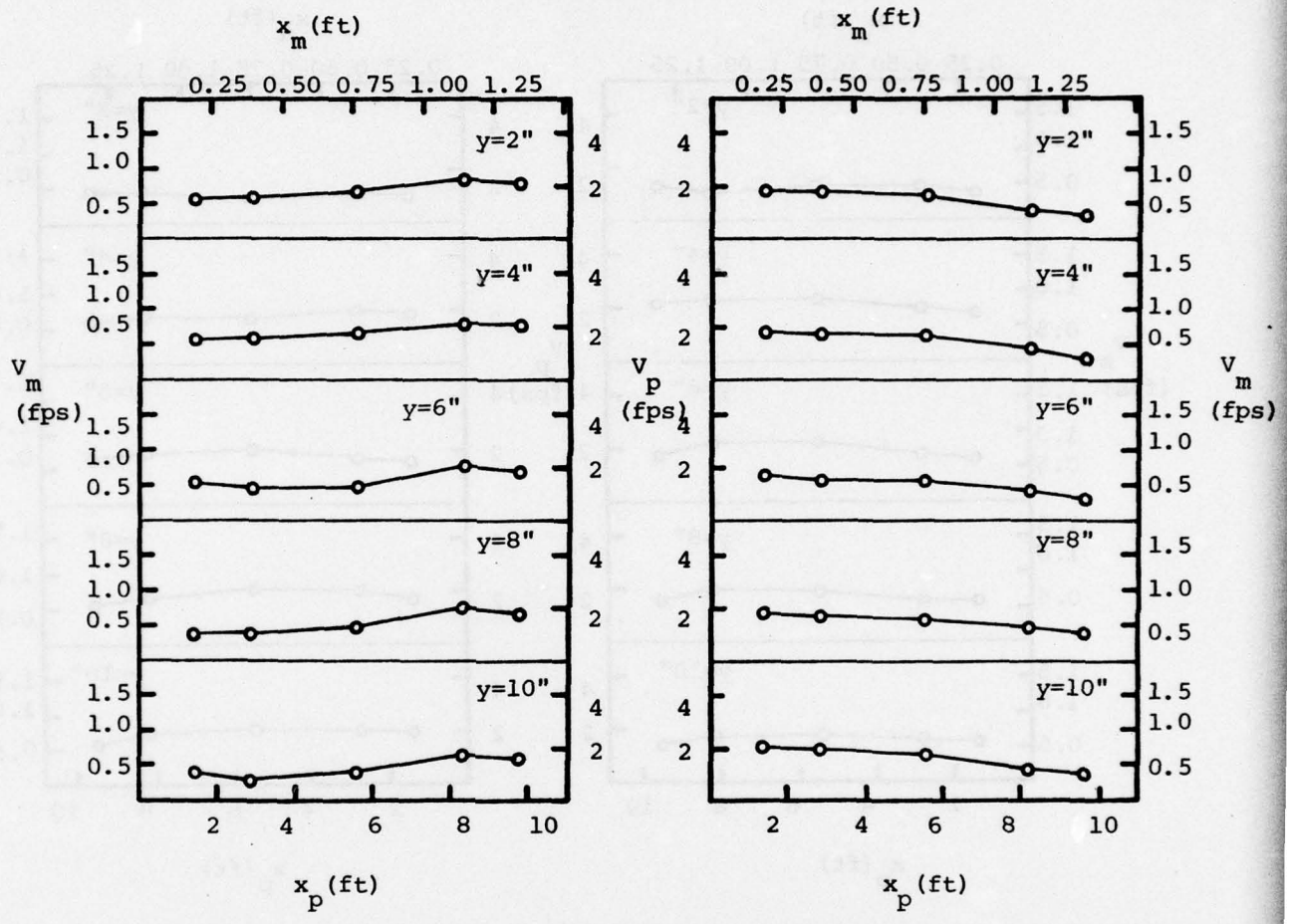

Figure 35.3 Velocity distribution (section C, two-pump operation, model depth = 12", case 13)

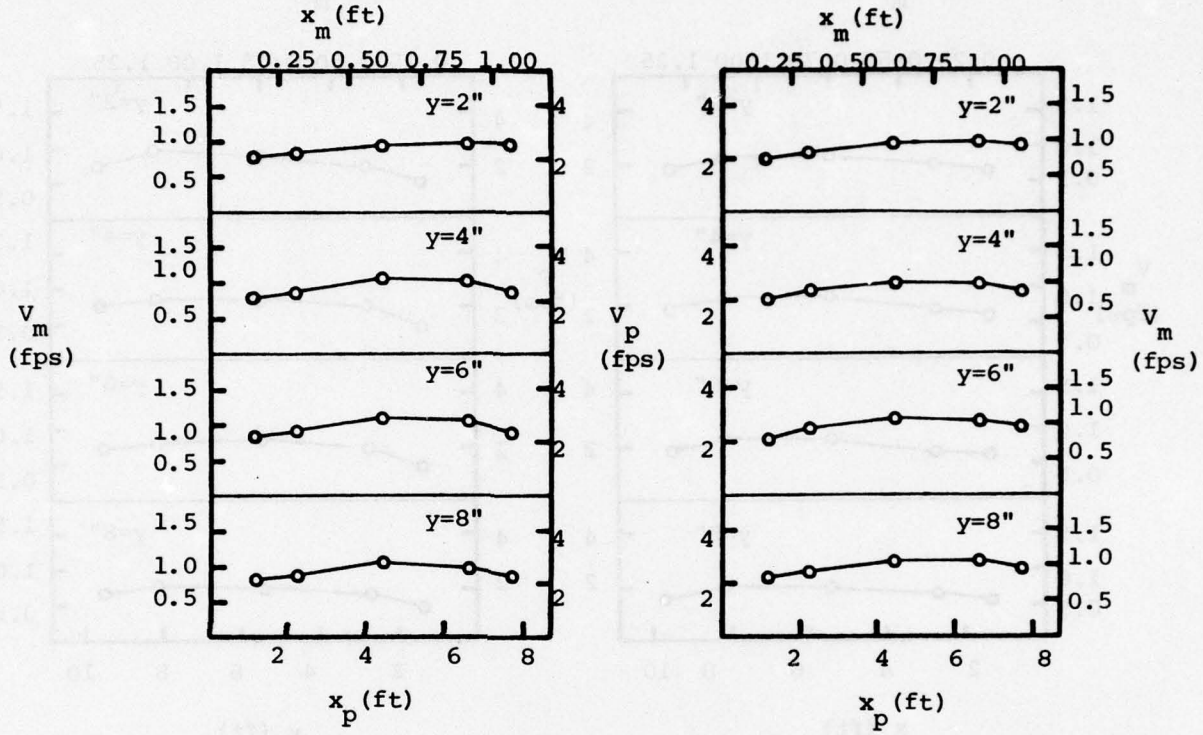

Figure 36.1 Velocity distribution (section A, one-pump operation, model depth = 8.5", case 13)

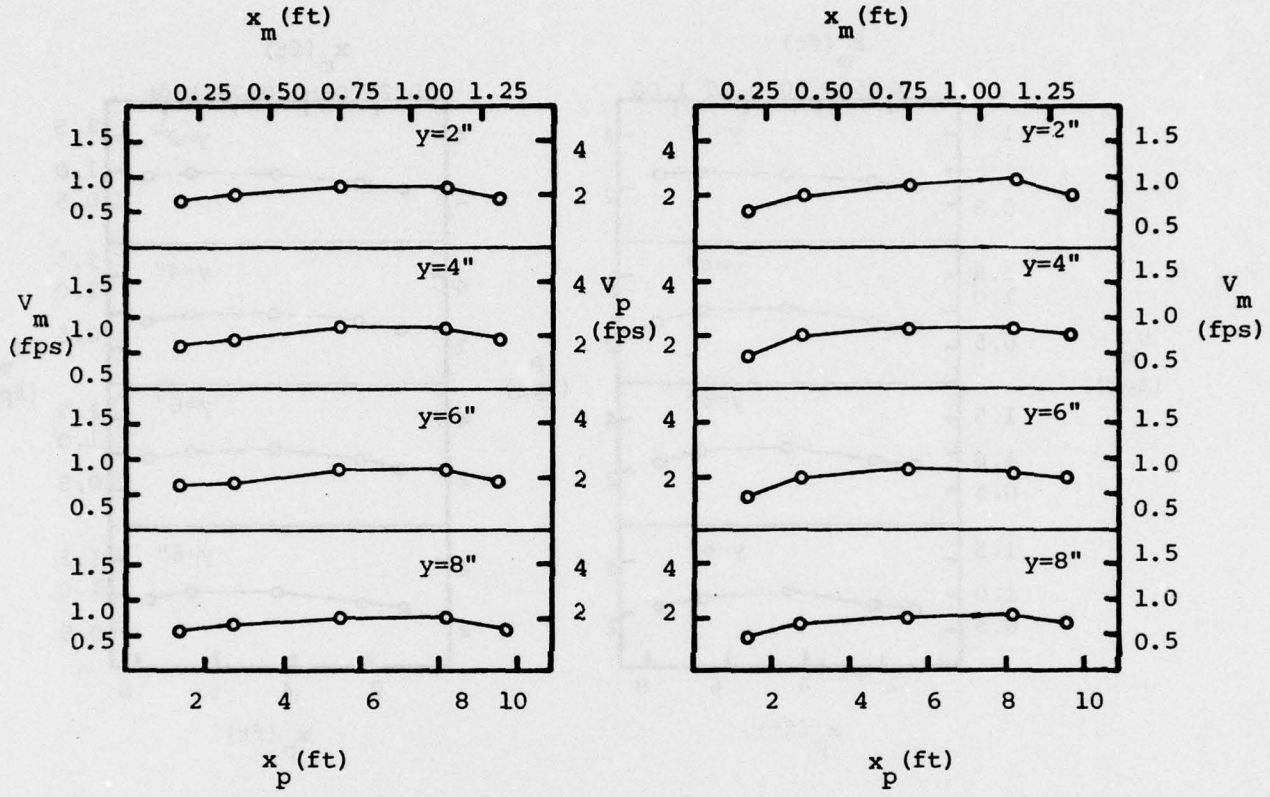

Figure 36.2 Velocity distribution (section B, one-pump operation, model depth = 8.5", case 13)

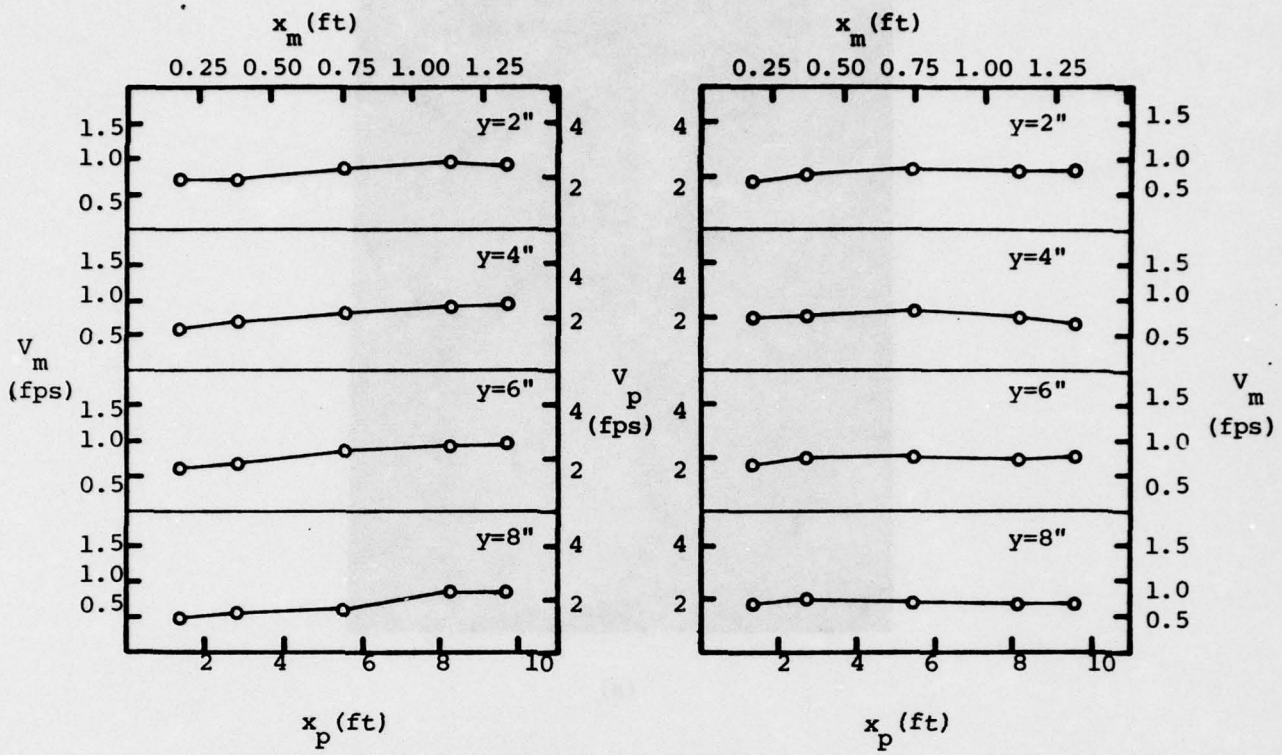

Figure 36.3. Velocity distribution (section C, one-pump operation, model depth = 8.5", case 13)

(a)

(b)

Figure 37. Flow visualization in the forebay. Case 12 baffle arrangement

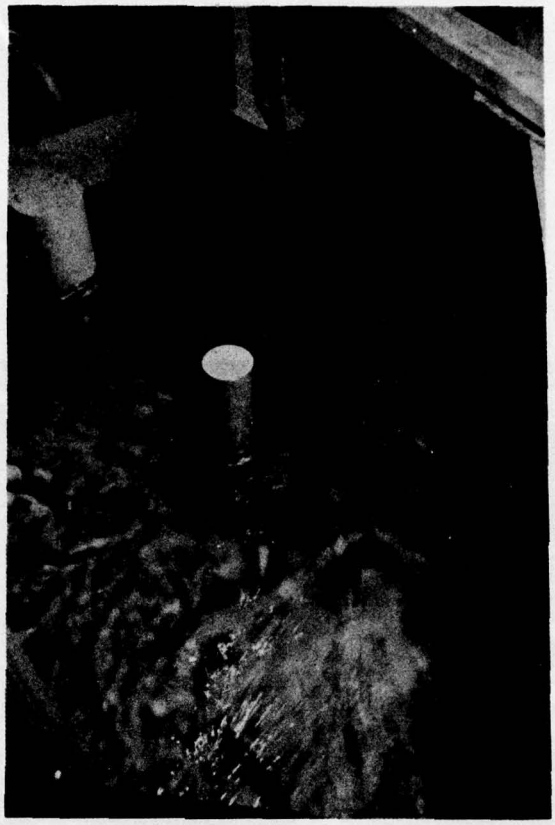

(c)

(d)

Figure 37 (continued)

(e)

Figure 37 (continued)

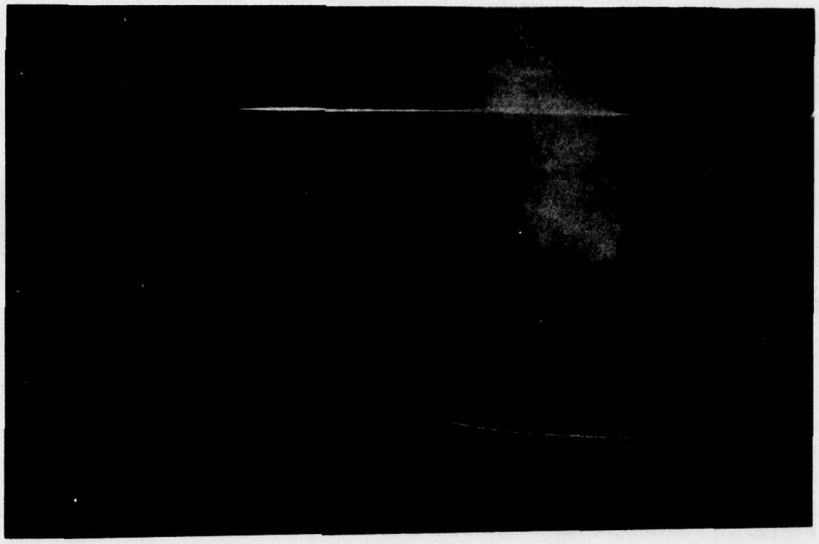

(a)

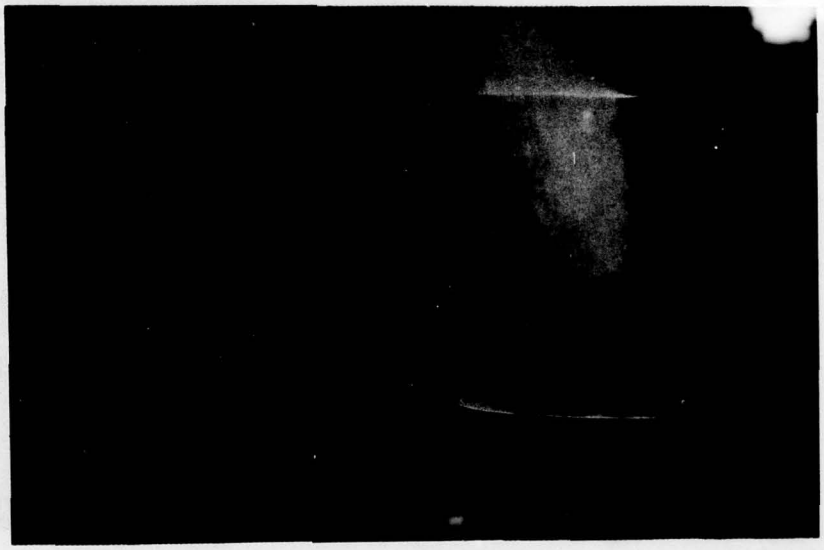

(b)

Figure 38. Visualization of flow into the bell. Dye injection at the centerplane of the sump.

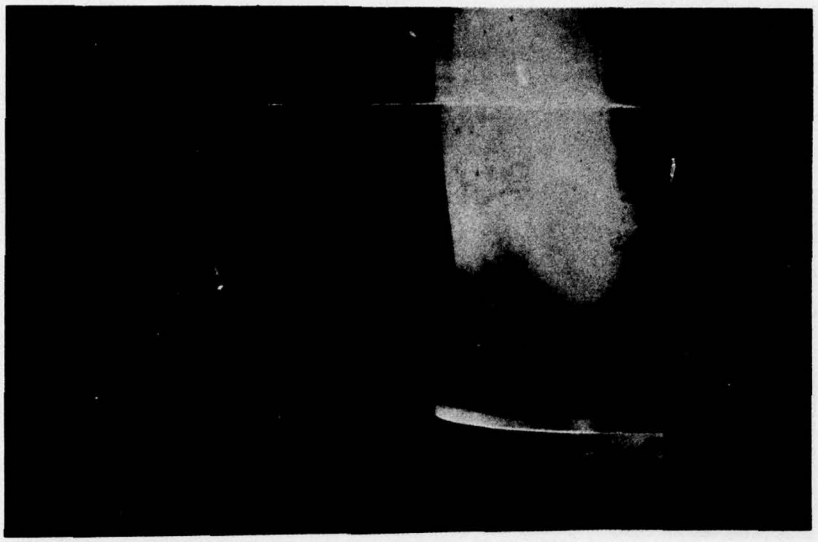

(a)

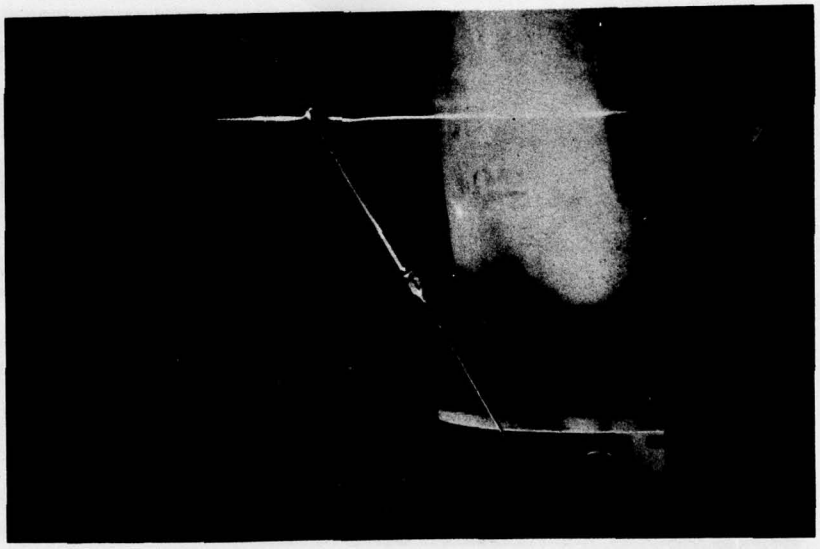

(b)

Figure 39. Visualization of flow into the bell. Dye injection very close to the converging side wall

(a)

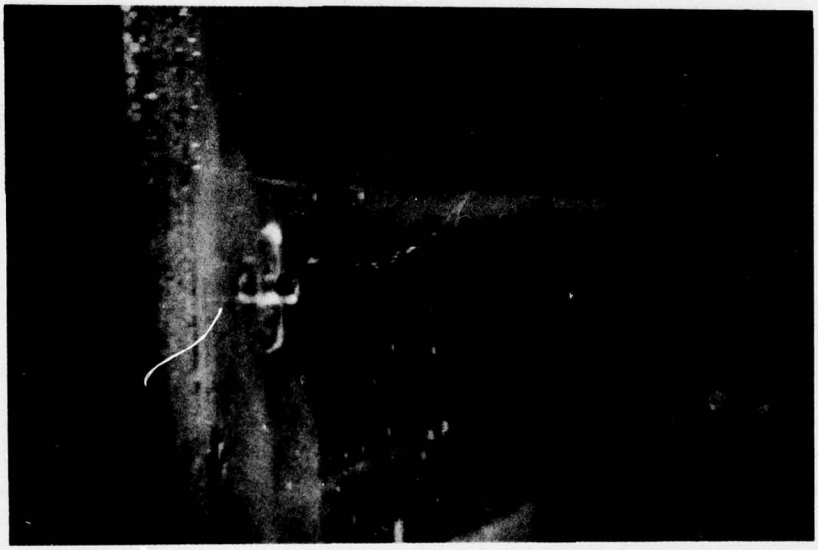

(b)

Figure 40 Visualization of vortex originating at the side wall

AD-A035 343 IOWA INST OF HYDRAULIC RESEARCH IOWA CITY F/G 13/2
MODEL STUDY OF THE INLET AND SUMP OF THE CLINTON FIRST AVENUE P--ETC(U)
NOV 76 C FARELL DACW25-76-C-0017
UNCLASSIFIED IIHR-196 NL

2 OF 2
AD
A035343

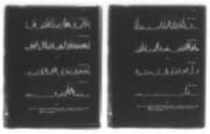

END
DATE
FILMED
3-77

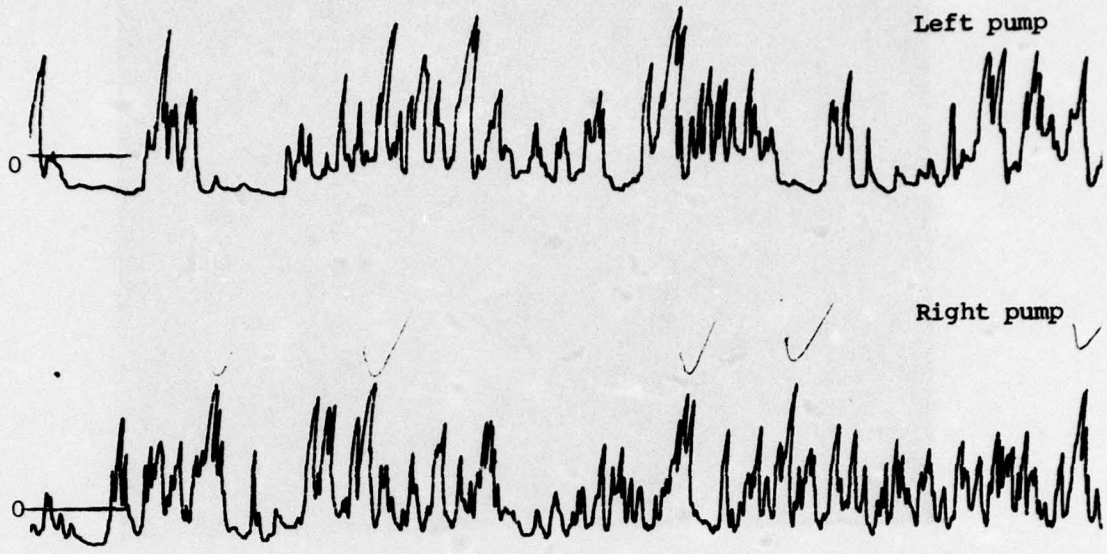

(a)

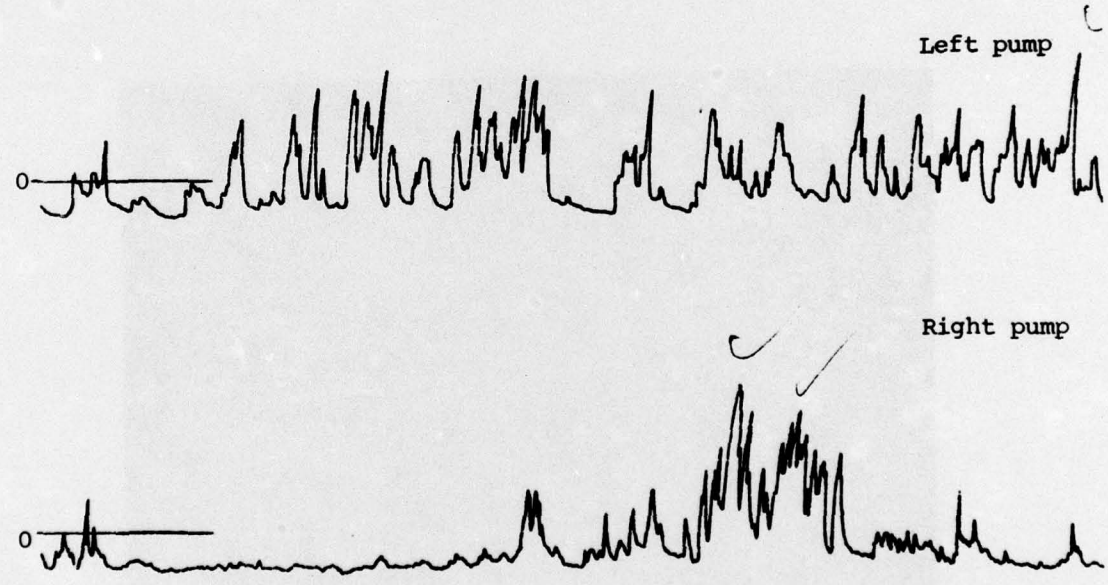

(b)

Figure 41. Pressure fluctuation records. Two-pump operation, model depth = 12 in. a) model without baffles. b) Case 13 baffle arrangement.

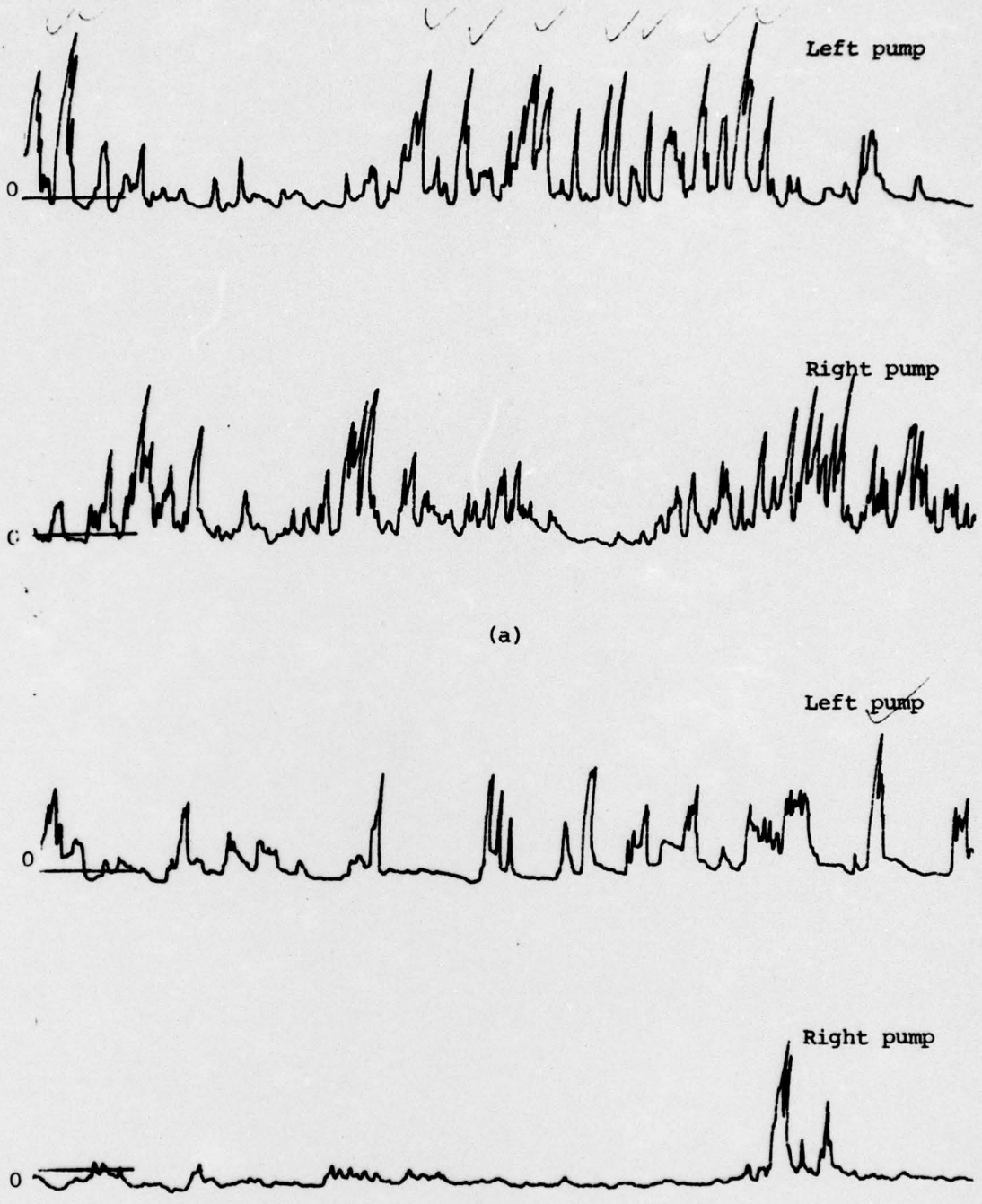

Figure 42. Pressure fluctuations records. One-pump operation, model depth = 8.5 in., a) model without baffles. b) Case 13 baffle arrangement.